

THESIS FOR THE DEGREE OF DOCTOR OF PHILOSOPHY

# ADIPOSE TISSUE HETEROGENEITY

## Development and Application of Nonlinear Microscopy Methods

ALEXANDRA PAUL



Division of Chemical Biology  
Department of Biology and Biological Engineering  
CHALMERS UNIVERSITY OF TECHNOLOGY  
Gothenburg, Sweden 2018

Adipose Tissue Heterogeneity  
- Development and Application of Nonlinear Microscopy Methods  
Alexandra Paul  
ISBN 978-91-7597-674-7

© Alexandra Paul, 2018.

Doktorsavhandlingar vid Chalmers tekniska högskola  
Ny serie nr 4355  
ISSN 0346-718X

Department of Biology and Biological Engineering

Chalmers University of Technology  
SE-412 96 Gothenburg  
Sweden  
Telephone + 46 (0)31-772 1000

Cover:

*Ex vivo* white (left) and brown (right) adipose tissue from mice: lipids (magenta, CARS, 2845  $\text{cm}^{-1}$ ), active mitochondria (green, MPEF, Rhodamine 123), and fibrillar collagen (cyan, SHG). [200  $\mu\text{m}$  x 200  $\mu\text{m}$ ]

Printed by Chalmers Reproservice  
Gothenburg, Sweden 2018

# ADIPOSE TISSUE HETEROGENEITY

## Development and Application of Nonlinear Microscopy Methods

ALEXANDRA PAUL

Department of Biology and Biological Engineering  
CHALMERS UNIVERSITY OF TECHNOLOGY

### Abstract

Although the negative health impacts of obesity have been well documented, the number of overweight and obese patients has and is predicted to continue rising. One of the causal factors of obesity is a constant positive energy balance mainly from excessively high caloric intake from food compared with limited physical activity (caloric expenditure). While this basic concept is well understood, the specific changes that obesity invokes within the body have not been fully uncovered and thus a molecular reversal of obesity has not been achieved to date. Along the way to identify a pharmaceutical target, a new type of fatty tissue, brown adipose tissue (BAT), has moved into the focus with potential therapeutic implications.

In contrast to white adipose tissue (WAT) that serves as long-term fat storage in the form of neutral lipids, BAT uses these molecules as fuel to perform non-shivering thermogenesis, a process seen most commonly in hibernating animals and infants, and used to keep the body core temperature stable. Since BAT function is very different from WAT function, the two tissue types are often studied in conjunction in order to better identify the characteristics and the possibility to increase BAT activity and mass in obese adults (as a way to increase “parasympathetic” caloric expenditure).

This thesis work aims to investigate adipose tissue (AT) physiology on different levels: from interactions of isolated adipose-derived stem cells (ADSC) with matrices to the function of AT in mice. Special focus is directed towards the molecules at the center of adipose tissue physiology: triacylglycerols (TAGs). These are often neglected during analysis due to the difficulty to study them in a cellular context. Classical methods, like gas chromatography, usually rely on extraction of all lipids from a tissue depot requiring extensive sample preparation. Magnetic resonance imaging or matrix-assisted laser desorption/ionization followed by mass spectrometry imaging can be used to visualize lipids in their natural setting but do not offer high enough resolution or require extensive sample preparation. Thus, in this work, I focused on using a label-free chemical imaging approach called coherent anti-Stokes Raman scattering (CARS) microscopy to study TAGs *in situ* at increasing levels of biological complexity. This method requires almost no sample preparation and can visualize sub-micrometer-sized TAG storage depots based on their intrinsic chemistry.

First, CARS microscopy was used to follow ADSC during the early stages of attachment and interaction with an extra cellular matrix (ECM); then CARS was employed to follow lipid accumulation during adipogenic differentiation to study how the ECM structure affects that process. Next, mature adipocytes were studied in *ex vivo* tissue sections. During this study mitochondrial activity was also investigated. In the following studies, not only the volume/number of lipid depots was of interest but also their contents. Therefore, we extended the CARS imaging with a spectral dimension, developing a new method to generate maps of TAG chain length and saturation, which were then be employed to see how high fat diet affects the lipids in BAT and WAT.

**Keywords:** adipose tissue · broadband coherent anti-Stokes Raman scattering · extracellular matrix · least squares decomposition · multivariate spectral analysis · obesity · stem cell adipogenesis





## List of publications

This thesis is based on the work contained in the following publications:

- I. **Micro- and nano-patterned elastin-like polypeptide hydrogels for stem cell culture**  
A. Paul‡, M. Stührenberg‡, S. Chen, D. Rhee, W.-K. Lee, T. W. Odom, S. C. Heilshorn, A. Enejder  
*Soft Matter* (2017), 13(34), 5665-5675. doi.org/10.1039/C7SM00487G
- II. **Increased adipogenesis of human adipose-derived stem cells on polycaprolactone fiber matrices**  
C. Brännmark, A. Paul, D. Ribeiro, B. Magnusson, G. Brolén, A. Enejder, A. Förslow  
*PLOS ONE* (2014), 9(11), e113620. doi.org/10.1371/journal.pone.0113620
- III. **Protein Kinase STK25 Regulates Oxidative Capacity and Metabolic Efficiency in Adipose Tissue**  
S. Sütt‡, E. Cansby‡, A. Paul, M. Amrutkar, E. Nuñez-Durán, J. Laurencikiene, B. W. Howell, S. Enerbäck, M. Mahlapuu  
*submitted*
- IV. **Quantitative mapping of triacylglycerol chain length and saturation *in situ* using hyperspectral CARS microscopy**  
A. Paul, C. Brännmark, M. Bonn, S. H. Parekh  
*manuscript*
- V. **Differential rates of high fat diet-induced changes in oxidative versus lipid storing tissues in mice**  
A. Paul, B. Chanclón C. Brännmark, P. Wittung-Stafshede, C. Olofsson, M. Bonn, I. Wernstedt Asterholm, S. H. Parekh  
*manuscript*

‡ Authors contributed equally to this work.

Additional publications not included in this thesis:

- VI. **Hybrid Elastin-like Polypeptide-Polyethylene Glycol (ELP-PEG) Hydrogels with Improved Transparency and Independent Control of Matrix Mechanics and Cell Ligand Density**  
H. Wang, L. Cai, A. Paul, A. Enejder, S. C. Heilshorn  
*Biomacromolecules* (2014), 15, 3421-8. doi.org/10.1021/bm500969d
- VII. **Covalently Adaptable Elastin-Like Protein–Hyaluronic Acid (ELP–HA) Hybrid Hydrogels with Secondary Thermoresponsive Crosslinking for Injectable Stem Cell Delivery**  
H. Wang, D. Zhu, A. Paul, L. Cai, A. Enejder, F. Yang, S. C. Heilshorn  
*Advanced Functional Materials* (2017), 27, 1605609.  
doi.org/10.1002/adfm.201605609
- VIII. **Mathematical modeling of white adipocyte exocytosis predicts adiponectin secretion and quantifies the rates of vesicle exo- and endocytosis**  
C. Brännmark‡, W. Lövfors‡, A. M. Komai, T. Axelsson, M. F. El Hachmane, S. Musovic, A. Paul, E. Nyman‡, C. S. Olofsson‡  
*Journal of Biological Chemistry* (2017). 292(49), 20032-20043. doi.org/10.1074/jbc.M117.801225.
- IX. **Review: CCN5/WISP2 and metabolic diseases**  
J. R. Grünberg, J. Elvin, A. Paul, S. Hedjayifar, A. Hammarstedt, U. Smith  
*Journal of Cell Communication and Signaling* (2017), doi.org/10.1007/s12079-017-0437-z.
- X. **Tunable Control of ‘Bead-String’ Hydrogel Microstructure from Self-assembly of Elastin-like Protein**  
H. Wang, A. Paul, D. Nguyen, A. Enejder, S. C. Heilshorn  
*submitted*
- XI. **Microstructured Elastomer-PEG Hydrogels via Kinetic Capture of Aqueous Liquid-Liquid Phase Separation**  
H. K. Lau, A. Paul, I. Sidhu, L. Li, C. R. Sabanayagam, S. H. Parekh, K. L. Kiick  
*submitted*

‡ Authors contributed equally to this work.

## Contribution summary

- I. Coordinated the project, performed CARS and cell experiments, analyzed the results, and wrote the paper.
- II. Designed the analysis algorithm for microscopy analysis, performed the microscopy experiments, and helped writing the paper.
- III. Designed the microscopy method including experimental setup and data analysis, performed microscopy experiments, and helped writing the paper.
- IV. Designed the study and analysis algorithm with S.H.P., performed all experiments, analyzed the data, and wrote the paper.
- V. Designed the study with I.W.A. and S.H.P., performed all experiments except sample collection, analyzed the data, and wrote the paper.
- VI. Designed and performed the CARS microscopy experiments, read/edited the paper.
- VII. Designed and performed the CARS microscopy experiments, read/edited the paper.
- VIII. Performed and analyzed experiments to determine lipid volume per cell and cell number, read/edited the paper.
- IX. Contributed the figures, read/edited the paper.
- X. Designed and performed the CARS microscopy experiments, read/edited the paper.
- XI. Designed, performed, and analyzed the BCARS microscopy experiments with S. H. P., helped writing the paper.



## **Preface**

This dissertation is submitted for the partial fulfilment of the degree of doctor of philosophy. It is based on work carried out between January 2014 and February 2018. Experimental work was performed at three different institutions: (i) Division of Chemical Biology, Department of Biology and Biological Engineering, Chalmers University of Technology; (ii) Division of Metabolic Physiology, Sahlgrenska Academy, Department of Neuroscience and Physiology, University of Gothenburg; and (iii) Group of Molecular Imaging, Department of Molecular Spectroscopy, Max Planck Institute for Polymer Research. This project was supervised by Pernilla Wittung Stafshede, Cecilia Brännmark, and Sapun H. Parekh. Funding was provided from the European Union's Seventh Framework program (FP7/2007-2013) under grant agreement n°607842 (FINON ITN), Stiftelsen Wilhelm och Martina Lundgrens Vetenskapsfond, and Kungl. Vetenskaps- och Vitterhets-Samhället.

Alexandra Paul

February 2018



# Contents

<b>1 Introduction .....</b>	<b>3</b>
Structure of the thesis .....	4
<b>2 Adipose Tissue Biology.....</b>	<b>7</b>
Obesity - a threat to health worldwide .....	7
Three types of adipocytes .....	10
Lipid metabolism.....	15
Pathological changes in obesity.....	20
Adipogenic differentiation of stem cells as a model for obesity research.....	21
<b>3 <i>In situ</i> analysis of adipocyte physiology.....</b>	<b>29</b>
An overview of methods .....	29
Toolbox I: Microscopy for LDs and their dynamics .....	29
Nonlinear microscopy.....	30
Nonlinear microscopy of adipocyte physiology (Paper I - III).....	37
Toolbox II: Visualization of LD chemistry .....	41
TAG chain length and saturation maps <i>in situ</i> (Paper IV & V).....	42
<b>4 Adipose Tissue Heterogeneity .....</b>	<b>49</b>
Surface pattern perturbations of <i>in vitro</i> rat and human ADSC (Paper I & II) .....	49
Genetic perturbations of <i>in vivo</i> mouse adipocytes (Paper III) .....	52
Nutritional perturbations of <i>in vivo</i> mouse adipocytes (Paper V) .....	53
<b>5 Concluding Remarks .....</b>	<b>59</b>
<b>Acknowledgements.....</b>	<b>65</b>
<b>References.....</b>	<b>71</b>





## Abbreviations

Related abbreviations in alphabetical order or grouped. Gene/protein names and symbols used in equations are summarized in the next section.

2D		two dimensional
3D		three dimensional
AFM		atomic force microscopy
AR		adrenergic receptor
AT		adipose tissue
	BAT	brown adipose tissue
	WAT	white adipose tissue
	i/sWAT	inguinal/subcutaneous WAT
	g/eWAT	(peri)gonadal/epididymal WAT
ATP		adenosine triphosphate
BF		body fat
BMI		body mass index
(B)CARS		broadband coherent anti-Stokes Raman scattering
(c)AMP		(cyclic) adenosine monophosphate
CD		chow diet
	HFD	high fat diet
CLSM		confocal laser scanning microscopy
DAG		diacylglycerol
	MAG	monoacylglycerol
	TAG	triacylglycerol
DNA		deoxyribonucleic acid
ECM		extracellular matrix
ELP		elastin-like protein (recombinant)
EM		electron microscopy
	TEM	transmission electron microscopy
ER		endoplasmic reticulum
FA		fatty acids
	NEFA	non-esterified fatty acids
FDA		Food and Drug Administration
FDG PET		fluorodesoxyglucose positron emission tomography
G3P		glycerol-3-phosphate
GC		gas chromatography
IBMX		3-isobutyl-1-methylxanthine
LCST		lower critical solution temperature
LD		lipid droplet
LDL		low density lipoprotein
	VLDL	very low density lipoprotein
MALDI-MSI		matrix-assisted laser desorption/ionization mass spectrometry imaging

MPEF		multi photon excited fluorescence
	OEPF	one photon excited fluorescence
MRI		magnetic resonance imaging
NRB		non-resonant background
OECD		Organization for Economic Co-operation and Development
PCL		polycaprolactone
PDMS		poly(dimethylsiloxane)
RGD		amino acid sequence: arginine-glycine-aspartic acid
Rho123		Rhodamine 123
SC		stem cells
	(h/r)ADSC	(human/rat) adipose-tissue derived stem cells
	ESC	embryonic stem cells
	MSC	mesenchymal stem cells
SHG		second harmonic generation
SRS		stimulated Raman scattering
T2D		type II diabetes
TGF		transforming growth factor
THG		third harmonic generation
WHO		world health organization
WT		wild-type
	KO	knock-out
	TG	transgenic

## Genes and Proteins

AGPAT2	1-acylglycerol-3-phosphate-O-acyltransferase
ATGL	adipose triacylglyceride lipase (same as PNPLA2)
BMP7/8B	bone morphogenic protein 7/8B
C/EBPs	CCAAT-enhancer-binding proteins (CCAAT = nucleotide sequence)
CPT1	carnitine palmitoyltransferase 1
DGAT1/2	acyl-coenzyme A (acyl-CoA):diacylglycerol acyltransferase 1/2
EBF2	early B-cell factor 2
ELOVL	fatty acid elongase
FASN	fatty acid synthase
FGF21	fibroblast growth factor 21
GPAM	glycerol-3-phosphate acyltransferase, mitochondrial
GPD1	glycerol-3-phosphate dehydrogenase 1
HSL	hormone-sensitive lipase (same as LIPE)
LIPE	lipase E, hormone-sensitive type
LPL	lipoprotein lipase
MCP1	monocyte chemoattractant protein 1
MYF5	myogenic factor 5
PCK1	phosphoenolpyruvate carboxykinase 1
PGDFRA	platelet-derived growth factor receptor alpha
PNPLA2	patatin like phospholipase domain containing 2 (same as ATGL)
PPAR $\gamma$	peroxisome proliferator-activated receptor gamma
PPARGC1A	PPAR $\gamma$ coactivator 1 alpha
SCD1/2	stearoyl-CoA desaturase 1/2
SREBF1c	sterol regulatory element binding factor 1c
STE20	sterile 20 kinase superfamily
STK25	serine/threonine protein kinase 25
UCP1	uncoupling protein 1
VEGF	vascular endothelial growth factor

Throughout this thesis gene/protein nomenclature for mice is used. With gene names starting with uppercase letters and italicized while proteins are all uppercase and non-italicized.

## Variables

$A$		amplitude of the vibrational mode
$C_{\#C=C}$		component for number of C=C bonds
$C_{chain}$		component for chain length
$C_{protein}$		component for protein
$C_{TAG}$		component for TAG backbone
$\Gamma$		line width of the vibrational mode
$\epsilon_0$		electric permittivity in vacuum
$E^{(n)}$		strength of the applied optical field
$I_0$		intensity of the incident beam
$\lambda$		wavelengths of laser beams
$N$		molecular density
$P^{(n)}$		$n$ th order polarization
$\sigma$		Raman cross section
$\chi^{(n)}$		$n$ th order susceptibility
	$Re \left\{ \chi_R^{(3)} \right\}$	real part of the 3 <sup>rd</sup> order susceptibility
	$Im \left\{ \chi_R^{(3)} \right\}$	imaginary part of the 3 <sup>rd</sup> order susceptibility
$\Omega$		frequency of the vibrational mode
$\omega$		frequencies of laser beams
$z$		length of the sample

# **Chapter 1. Introduction**



# 1 Introduction

Obesity and the associated metabolic syndrome have become some of the most pressing concerns for world health during the 21<sup>st</sup> century. With an estimated 39% of all adults worldwide classified as overweight (13% obese), health care systems face extended challenges to cope with this scenario [1]. Cardiovascular diseases, which obese patients are prone to develop, are the leading cause of death worldwide, especially in developed countries. Concurrently with the development of this health crisis, our understanding of the underlying changes that obesity causes within the body has continued to grow. This includes our insight into the role and function of the main involved tissue during obesity – the fat, or adipose tissue (AT). During the last 15 years, there has not only been a revolution from seeing the AT as inert mass of fat to classifying it as an endocrine organ [2], but also two new types of AT have been described in human adults [3], [4]. This increased awareness has also opened further questions about the basic function and physiology of AT. In order to answer some of these questions, different levels of model systems have had to be established. On the first level are cells: isolated mature adipocytes, stem cells, and cell lines that allow well-defined intervention with known stimulating factors. The second level is studies on a whole organism – murine or human – to see the interaction between ATs and other parts of the metabolism.

However, it is not only crucial to develop model systems mimicking the effects of obesity, but the concurrent advancement of analysis techniques is fundamental to improve our understanding of these systems. So far the focus has been on techniques that analyze whole populations of cells or a whole tissue. Similar to the revolution in personalized medicine, such a holistic analysis could potentially mask the existence of distinct sub-populations, which may hide in the average behavior. Since this has been understood, single-cell analysis techniques have experienced a boost in development [5]. During my doctoral studies I contributed to this field with the development of molecular microscopy tools to study adipogenic differentiation of stem cells (**Paper II**), the metabolic state of AT (**Paper III**), and the chemical investigation of lipid species *in situ* in cells or tissue (**Paper IV**).

In addition to the development of microscopic tools, I also employed these techniques to answer physiological questions about the interaction of stem cells with complex environment *in vitro* (**Paper I & II**), and the impact of kinases or nutrition on lipid composition in ATs (**Paper III & V**).

### Structure of the thesis

Following this brief introduction, **Chapter 2** establishes a deeper background on adipose tissue biology, pathological changes during obesity, and *in vitro* adipogenesis. **Chapter 3** focuses on tools for *in situ* analysis of adipocyte physiology, metabolic activity, and lipid chemistry and the physics of nonlinear microscopy as relevant for this thesis work. In appropriate places the contributions from **Paper I, II, III, & IV** to the analytical methods of AT biology are highlighted. In this way, the applications of nonlinear microscopy methods to biological question are established prior to **Chapter 4**, which focuses on the biological results from **paper I, II, III, & V**. Finally, I present a brief conclusion in **Chapter 5** with an outlook for where my research can lead.



## **Chapter 2. Adipose Tissue Biology**



# 2 Adipose Tissue Biology

## Obesity - a threat to health worldwide

During the past 100 years our daily lives have undergone dramatic changes: the majority of the work force is now employed in an office setting with only light physical activity throughout the day [6] while at the same time the calorie intake has risen markedly [7]. These two factors seem to have played a key role in the increased prevalence of obesity, essentially being overweight to a degree that it causes medical complications, around the world [8]. Other factors causing an imbalance in energy intake vs. expenditure are genetic or medical [9]. Today, more than one in two adults and almost one in six children are classified as overweight or obese in OECD (Organization for Economic Co-operation and Development) countries (**Figure 1A**) [10]. A further increase of the obesity rates is predicted (**Figure 1B**) and social inequalities are a strong risk factor – less-educated women are three times more likely to be overweight than those with higher level of education [10]. Other risk factors are, e.g., poverty, stress, and poor diet [11]. Both the World Health Organization (WHO) and OECD define overweight with a body mass index (BMI,  $\text{weight height}^{-2}$ ) of  $\geq 25 \text{ kg m}^{-2}$  and obesity  $\geq 30 \text{ kg m}^{-2}$ . Other classifications like a body fat (BF) percentage of  $> 25\%$  in men and  $> 35\%$  in women have been suggested [12]. BMI has high specificity but low sensitivity compared to BF-detected obesity, i.e., the identification of true positives is  $>97\%$  while more than 50% of people with excess body fat are wrongly qualified with a non-obese BMI [13], [14].

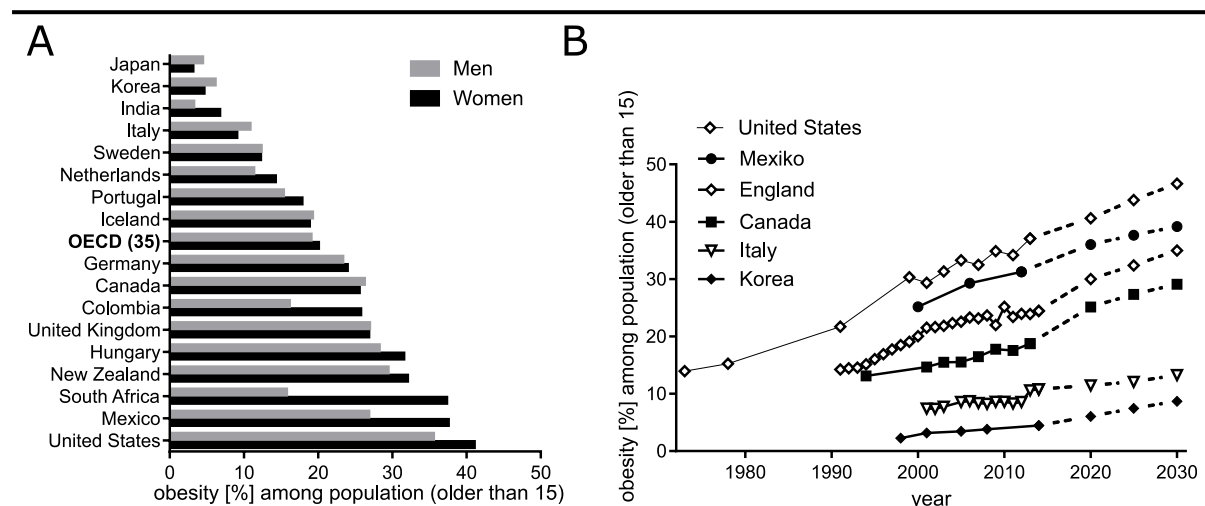


**Figure 1. Obesity worldwide. (A)** Prevalence of obesity among women and men. Data collected by OECD 2012-2015. **(B)** Development of obesity rates during the years with predicted trends for until 2030 assuming a linear increase. Data reproduced with permission from OECD(2017), Obesity Update [10].

Only with the BF definition, patients with normal weight obesity, *i.e.*, those who have a normal BMI but increased body fat and at the same time display metabolic dysregulation, are included [15].

The occurrence of interconnected physiological, biochemical, clinical, and metabolic factors that increase risk of type 2 diabetes (T2D), atherosclerotic cardiovascular disease, and mortality, are summarized as the concept of metabolic syndrome [16]. There are several different combinations of symptoms and risk factors for obesity, although no cohesive view has been agreed upon, as summarized by Kaur [16]. Additionally, the increased risk for morbidity and the rise in obesity also puts a strain on healthcare systems [11].

Much research is devoted to the identification of dietary, environmental, biochemical, and molecular factors contributing to the development and ultimately to the early prevention of obesity. However, there is also strong interest in the changes human bodies undergo en route to obesity development and with that interest, searching for a possible course to revert to better metabolic health in obese individuals. To date the most effective treatment for obesity is weight loss induced by bariatric surgery [17]. If compared to lifestyle intervention, such as exercise plans and dietary changes, the weight loss after surgery is higher and more often sustained. Moreover, surgery resolves the metabolic syndrome more effectively [18]. In T2D patients, one of the major advantages of surgery is the resolution of the insulin dependence after surgery in 82% of all patients, with 62% remaining diabetes free after two years [17]. Other studies have confirmed that bariatric surgery improves patient health for over 10 years [19]. Although the weight loss seems to play a role for the resolution of T2D [17], there are other cases, where T2D clears within days of bariatric surgery [20]–[22], highlighting the interconnection among weight, hormones, and signaling found within the body. The fact that the insulin dependent T2D resolves before the BF can change, demonstrates the complexity of studying disease mechanisms with human patients as an apprehension on top of the ethics limiting the possibility for intervention in humans and with that the search of specific cellular and molecular targets.

In order to study a disease with so many involved tissues, interconnected signaling pathways, and an unclear dominant symptom, it is crucial to work with model systems where specific features can be isolated, while also considering the disease at the whole organism and population level. This allows forming correlative relationships between specific tissues/cells and aspects of obesity and T2D. For example, while the analysis of groups of the human population helps the identification of contributing factors, which could be the basis for potential early intervention programs or nutritional recommendations, it is nearly impossible to isolate specific molecular factors and establish a single line of treatment for all cases due to large heterogeneity between patients. For that purpose, animal models can allow a higher degree of control over, *e.g.*, nutrition and exercise. Mice (*Mus musculus*), and other animals like *Drosophila melanogaster* and *Caenorhabditis elegans*, offer an opportunity to decipher the interplay of different organ systems and what effect lipids or sugars have on a whole organism. Nevertheless, it is still extremely challenging to understand the function of individual tissues or cell types *in vivo* in animal models.

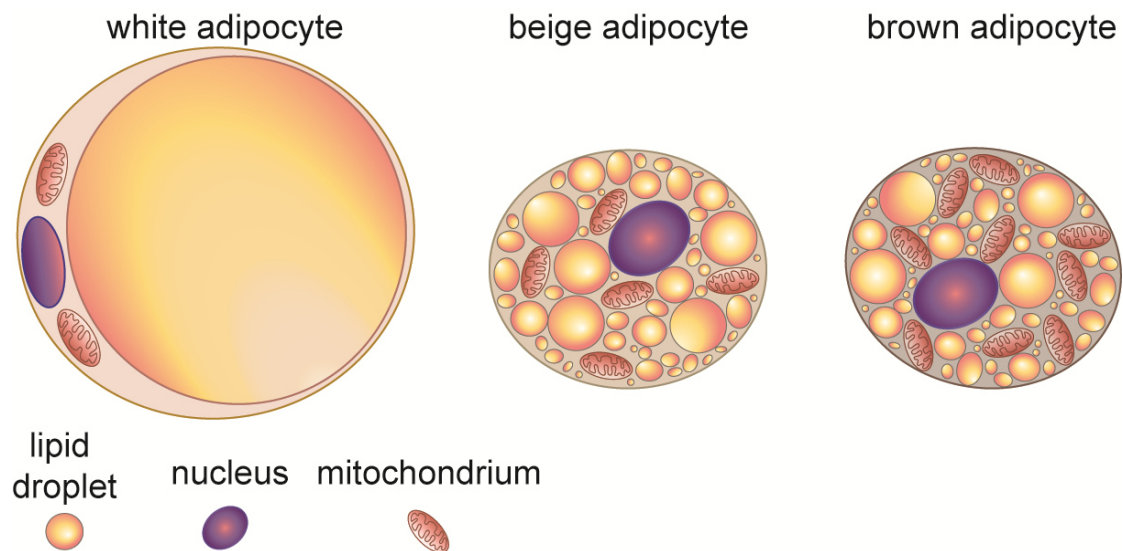


**Figure 2. Three types of adipocytes.** The morphological differences between the three types of adipocytes (from left to right: white, beige, brown) are the number of lipid droplets and mitochondria. They also differ in lineage origin, gene expression, and function.

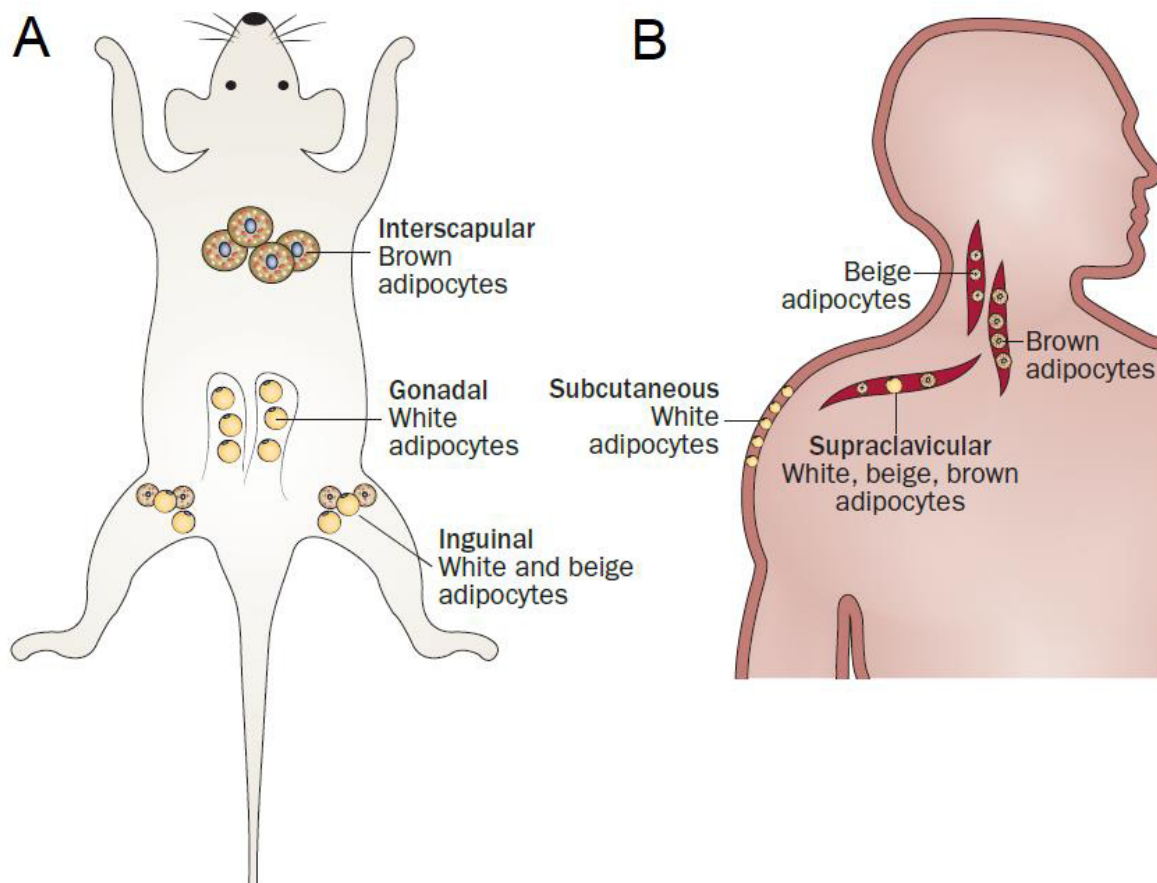


**Figure 3. Adipose tissue depots in mouse and human.** Both mice (**A**) and humans (**B**) have interscapular or cervical depots of brown adipocytes, respectively. Inguinal WAT in mice is comparable to subcutaneous WAT in humans, while gonadal (mice) is similar to visceral (human, not depicted). Reprinted with permission from [23].

For this reason, *in vitro* cell cultures are better suited to establish specific cell-type responses. Given the broad impact and complexity of studying obesity, a combination of data from different model systems is essential to further the molecular and physiological understanding of obesity.

### Three types of adipocytes

Adipose tissue (AT), or fat, with its metabolic pathways and gene products has evolved from invertebrate origins into lower vertebrates to mammals and birds. Fat is present in all mammals and consists of several depots around the body. AT can be fundamentally separated into two types - white (WAT) and brown (BAT) - according to their function for either energy storage or dissipation, respectively. Although there are two fundamental ATs, there are three types of adipocytes as shown in **Figure 2**.

#### White adipose tissue

WAT has its origin in the mesenchymal stem cell (MSC) lineage, which also gives rise to myoblasts, chondroblasts, and osteoblasts [24]. It is the most plastic of the metabolically active tissues, *i.e.*, tissues that generate bioactive molecules and have a high oxygen consumption, and can contribute to 5-60% of the total body weight, depending on the nutritional status [25].

WAT is split into several depots, with some differences in function. The locations of the depots are either below the skin, the so called subcutaneous fat, or deeper in the abdomen, the visceral AT [26]. The most used pre-clinical model to study AT development and pathology are rodents (most often mice and rats); thus, it is important to be aware of similarities and discrepancies between rodents and humans [27]. There are differences in the distribution of the fat depots between mice (and rats) and humans (**Figure 3**), as well as the number of layers that can be found in the subcutaneous AT. Still, the inguinal WAT (iWAT) in mice, spreading from dorsolumbar to gluteal region, is seen as most similar to the gluteoformoral subcutaneous AT in humans. For studies aiming at human visceral AT depots, the mesenteric fat pad, along the intestines in mice, would be best suited but due to larger volume and possibility of surgical manipulation the (peri)gonadal fat pad (gWAT) is used more common [27]. The accumulation of excess visceral AT is known to correlate with the afore-mentioned metabolic syndrome, while subcutaneous AT, especially on the legs, does not seem to raise the risk [28].

Both rodent and human WAT consist of several cell types, including stem cells, adipocytes, T cells, B cells, and stromal-vascular cells (**Figure 4**). Stem cells from WAT have been recognized as an important supply for mesenchymal differentiation lineages *in vitro* [29]–[31].

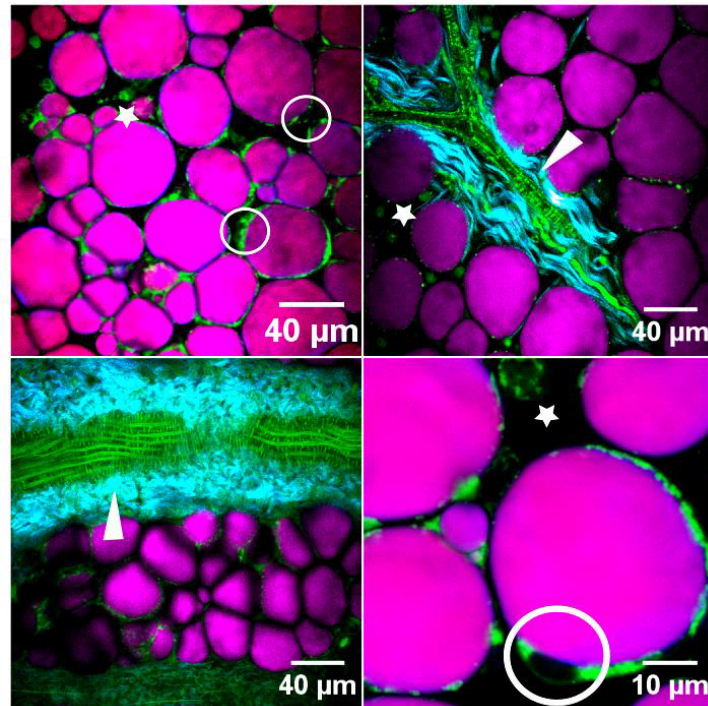


**Figure 4. Inguinal white adipose tissue from mice.** *Ex vivo* iWAT stained for active mitochondria (green, MPEF, Rho123). Lipids (CARS,  $2845\text{ cm}^{-1}$ ) are shown in magenta, fibrillar collagen (SHG) is shown in cyan. Blood vessels are marked with arrow heads, non-adipocyte cells with stars, and nuclei circled. Scale bars: 40 and 10  $\mu\text{m}$ .

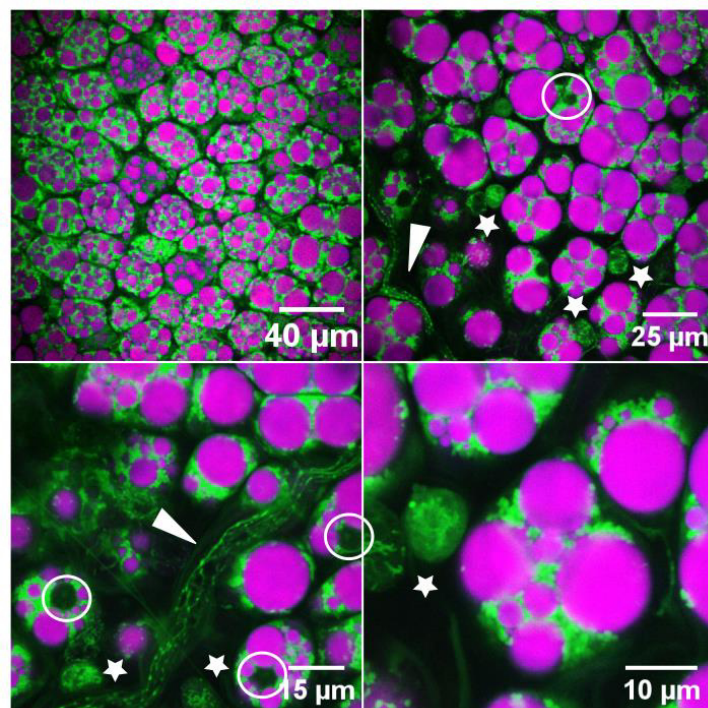


**Figure 5. Interscapular brown adipose tissue from mice.** *Ex vivo* BAT stained for active mitochondria (green, MPEF, Rho123). Lipids (CARS,  $2845\text{ cm}^{-1}$ ) are shown in magenta. Blood vessels are marked with arrow heads, non-adipocyte cells with stars, and nuclei circled. Scale bars: 40, 25, 15, and 10  $\mu\text{m}$ .



They contribute 15-50% of all cells in AT [32]. Mature adipocytes *in vivo* are filled by a single large fat storage compartment called a lipid droplet (LD), occupying ~ 90% of the cell volume and forcing all cellular organelles into close proximity of the plasma membrane (**Figure 2 & 4**) [26]. These LDs are dynamic storages for neutral esters of fatty acids (FAs), which are often toxic to (when non-esterified) but needed to readily supply energy to most cells in the body [33]. WAT acts as a buffer for plasma non-esterified fatty acids (NEFAs) and TAG levels in order to avoid ectopic lipid build-ups (lipotoxicity) [34]. Lipotoxicity is based on the observation that lipid-derived metabolites and the accumulation of LDs in non-lipid storing tissues (ectopic lipids in, *e.g.*, pancreas, heart, blood vessel walls) causes impaired insulin-stimulated glucose transport, diminished insulin secretion, mitochondrial malfunctioning, endoplasmic reticulum (ER) stress, accumulation of reactive oxygen species, and cell death [35], [36]. In contrast to this, it has also been observed that some intramuscular lipid storages (in athletes) can lead to increased insulin sensitivity and these beneficial properties might be linked to changes in lipid composition and turnover [37].

Moreover, as an endocrine organ, WAT is involved in glucose homeostasis and immune response, affecting development of infectious diseases and cancer, through the release of adipokines (cell-signaling proteins) [25]. The expression and secretion of some of these adipokines can be induced by nutrients in both humans and rodents [27]. These proteins regulate diverse processes, *e.g.*, whole-body energy homeostasis, angiogenesis, blood pressure, and hemostasis [38].

### **Brown adipose tissue**

BAT, in contrast to WAT, is a thermogenic organ, found in almost all eutherian (placental) mammals except in, *Sus scrofa domesticus* (domestic pigs) [39], [40]. Other mammal classes, monotremes (egg-laying mammals) and marsupials (pouched mammals), possess no BAT [41]. BAT contributes to almost half of all oxygen consumed in cold-adapted mammals, *i.e.*, animals that have been exposed to low temperatures for a prolonged time frame [42]. BAT has been studied for a long time in rodents, but evidence of its presence in adult humans only emerged in the last 10 years in seminal studies using F-18 FDG PET (Fluorodesoxy positron emission tomography) [43]–[49]. However, not all adults seem to have active BAT; the prevalence rates range from 30-95% depending on the study, as reviewed by Nedergaard, Bengtsson, and Cannon [50]. Within the BAT-positive patient group the thermogenic activity/capacity also varies. Without activation, the main depots for BAT in adult humans are found in the cervical, supraclavicular, axillary, and paravertebral regions, and the areas can be expanded under noradrenergic stimulation [42]. In rodents and human infants the major BAT depot is found in the neck, interscapular region (**Figure 3**), and a smaller depot in the perirenal region. Rodents keep their BAT depots throughout their life [51]. Additionally to the role in non-shivering thermogenesis, it has also been suggested that BAT might have a similar endocrine role as WAT [52]. Moreover, BAT contributes to 50% and 75% of whole-body TAG and glucose clearance from circulation shortly after a meal in mice [53].



Adipocytes in BAT display several small LDs and are packed with mitochondria (**Figure 2 & 5**) in stark contrast to WAT adipocytes. The inner membrane of these mitochondria contains the uncoupling protein 1 (UCP1), which short circuits the ATP production in the respiratory chain by dissipating the proton gradient, thus allowing direct heat production from fatty acid oxidation. The brown adipocyte activity is controlled by nerve fibers and BAT is highly vascularized (**Figure 5**), so the substrate for heat production, oxygen and lipids, can be readily supplied [54]. These capillaries can also carry heat produced in BAT to other parts of the body. Similarly to WAT, BAT also contains stem cells, which play an important role for BAT expansion during increased thermogenic demand. For a long time, a common stem cell source was presumed for brown and white adipocytes, since both cell types contain significant LDs. However, it is now known that brown adipocytes develop from precursor cells expressing *Myf5* and are part of the dermomyotomal lineage, which also give rise to skeletal muscle cells [55]. Consistent with this common precursor, the gene signature [56] and mitochondrial proteome [57] is similar between BAT and skeletal muscle.

The total thermogenic capacity of BAT at any given time is determined by the mitochondrial density and amount of UCP1 in the cells and on cell number, which is in turn controlled by the rates of proliferation and apoptosis. While the amount of UCP1 can be controlled within minutes, the recruitment of new cells needs days/weeks of constant stimulation. The number of brown adipocytes increases after cold stimulus and can also be increased with chemical stimulus such as norepinephrine, the most important and well-studied signaling molecule in BAT [42]. Other factors are FGF21 (secreted by liver, BAT), irisin (muscle), VEGF (blood vessel, BAT),  $T_4$  (Thyroid), natriuretic peptides (heart), BMP8B (BAT), orexin, and BMP7 [55]. The cellular sources for orexin and BMP7 are unknown. Norepinephrine is an endogenous signaling mediator in the autonomous nervous system that interacts with three types of adrenergic receptors (AR) of which the most significant in rodents is the  $\beta_3$ -AR stimulation. In humans, the  $\beta_3$ -AR is found in WAT, BAT, gallbladder, and to a much lower extent in the colon [58]. Thus, efforts have been made to target this receptor specifically and develop anti-obesity drugs by exploiting the localization of the receptor [59], [60]. Due to low oral bioavailability and undesirable cardiovascular effects that stem from cross-reactivity with  $\beta_1$ -AR, none of the tested drugs so far have made it past clinical trials. However, now there is a promising candidate drug, which has been approved for treatment of an overactive bladder [61].

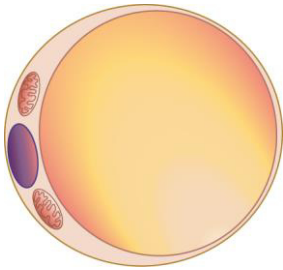
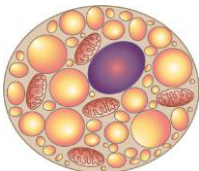
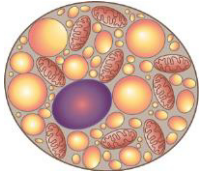
Another way to stimulate brown adipocyte recruitment is chronic cold exposure to temperatures below “the lower critical temperature of the thermoneutral zone”, which for most mammals lies close to 30°C [42]. During short-term cold exposure the body core temperature can be kept constant with shivering, but if the cold exposure becomes chronic non-shivering thermogenesis in BAT takes over. This leads to an activation of PPARGC1A (PPAR $\gamma$  coactivator 1 alpha), which leads to the induction of genes involved in UCP1 dependent thermogenesis and to mitochondrial biosynthesis [62]. Nedergaard, Bengtsson, and Cannon hypothesize that this activation could be used as anti-obesity treatment and that rising room temperatures and availability of warm clothes could have contributed to the increase in obesity rates [50]. In connection with investigation of cold activation on BAT, it could also

be established that BAT activity correlates negatively with age, BMI, and yearly season: there is generally less BAT in older subjects, BAT-positive subjects were more likely to have a low BMI, and reduced BAT activity would occur in summer [63]. Some studies indicate that there might be more BAT in females than in males. However, Nedergaard, Bengtsson, and Cannon speculate that this might be due to a difference in temperature perception of women vs. men, and thus different levels of BAT activation during clinical evaluation of BAT mass [50].

### Beige adipocytes

There is a population of adipocytes in WAT, which can express *Ucp1*, and show increased UCP1 protein levels, upon stimulation, and hence acquire brown-like features [64], [65]. During the recent years, this cell type have been set apart from classical brown adipocytes and termed “recruitable”, “brite” (brown in white), or beige adipocytes [4]. The latter term is more common than the others and will be used exclusively throughout the rest of this thesis. These cells have an appearance similar to brown adipocytes, with multiple LDs and high mitochondrial activity [66].

**Table 1.** Differences and similarities of the three types of adipocytes [67], [68].

	 <b>White</b>	 <b>Beige</b>	 <b>Brown</b>
<b>Origin</b>	MSC-derived white precursors	MSC-derived beige precursors ( <i>Ebf2</i> <sup>+</sup> , <i>Pgdfr</i> <sup>+</sup> )	dermomyotomal ( <i>Myf5</i> <sup>+</sup> )
<b>Location</b>	<i>human</i> : subcutaneous, visceral <i>mice</i> : inguinal, gonadal, mesenteric	<i>human</i> : subcutaneous, supraclavicular <i>mice</i> : interspersed with WAT (inguinal > gonadal)	<i>human</i> : cervical, supraclavicular, axillary, paravertebral <i>mice</i> : interscapular, perirenal
<b>Function</b>	Energy storage (TAGs), endocrine signalling, immune response	Adaptive Thermogenesis	Energy dissipation, endocrine signalling (?)
<b>Morphology</b>	Unilocular LD, few mitochondria	Multilocular LDs, few mitochondria (increase upon stimulation)	Multilocular LDs, abundant mitochondria, highly vascularized/innervated
<b>UCP1</b>	undetectable/low	induced after stimulation	high
<b>Activation</b>	Food intake, thiazolidinediones	Cold, $\beta$ 3-AR stimulation, PPAR $\gamma$ agonists, thyroid hormones, catecholamines	Cold, $\beta$ 3-AR stimulation, PPAR $\gamma$ agonists, thyroid hormones

However, they do not originate from *Myf5* positive progenitors [69]. Equivalently to white precursors, beige precursors originate from mesodermal stem cells [51].

In contrast to brown adipocytes, which are separated from WAT by a layer of connective tissue, in cases where the depots are in close proximity, beige adipocytes are interspersed with white adipocytes [70], [71]. All three types of adipocytes display unique genetic profiles [51], [67]. Beige adipocytes can be found in WAT depots upon cold-stimulation, long-term treatment with PPAR $\gamma$  (*e.g.*, rosiglitazone) or  $\beta_3$ -AR agonist (*e.g.*, CL-316,243), or upregulation of intracellular cyclic AMP [3], [72], [73]. The features of the three adipocytes types are compared in **Figure 2** and **Table 1**. Chronic stimulation to recruit beige adipocytes is often referred to as ‘browning’ of WAT (**Figure 6**), while they also increase BAT activity at the same time. There is an ongoing speculation if this browning response only triggers the differentiation of beige precursors in WAT or if it is possible for white precursors or even mature white adipocytes to transdifferentiate into beige adipocytes [51], [68]. Two observations speak for transdifferentiation: the DNA content or adipocyte number does not change during ‘browning’ [74] and beige adipocytes are derived from non-dividing cells [64], [72], [75]. From genetic marker studies, it has been suggested that only interscapular BAT depots in human infants express classic brown genotypes [70] while supraclavicular BAT depots in human infants and adults are actually more comparable to rodent beige adipocytes [3], [51], [70], [76]. These beige-like properties are in line with studies showing the possibility of recruitment, as typically seen for beige cells, of human adult BAT to previously BAT-negative patients [77]–[79].

## Lipid metabolism

Clearly, lipids play a major role in all three types of adipocytes. Moreover, in organisms without dedicated AT, *e.g.*, *Caenorhabditis elegans*, *Drosophila melanogaster*, and *Saccharomyces cerevisiae*, lipids still play a large role in chemical energy storage [80]–[82]. In fact, virtually all eukaryotic cells have the ability to form LDs, in varying numbers and sizes, containing neutral, *i.e.*, uncharged, lipids, especially upon exposure to high levels of nutritional NEFAs. An average non-obese person stores around 500 000 kJ of chemical energy in adipocyte TAGs, enough for ~30 marathons [83]. This is 200-fold more energy than is contained in the liver- and skeletal muscle-stored glycogen, the multibranched polysaccharide that serves as main fuel for muscles [83]. When lipids are needed for energy, they are packed into lipoprotein and released into the plasma. Lipoprotein particles are built from a single phospholipid layer, with embedded apolipoproteins, and a TAG/cholesterol core and can vary in size and density. Due to their analogous architectures, lipoprotein particles can be viewed as miniature LDs [83].

In contrast to earlier understanding, LDs are not only inert lipid storages but rather contribute to diverse cellular functions, including signaling, temporary protein storage, and protein degradation [84]–[86].

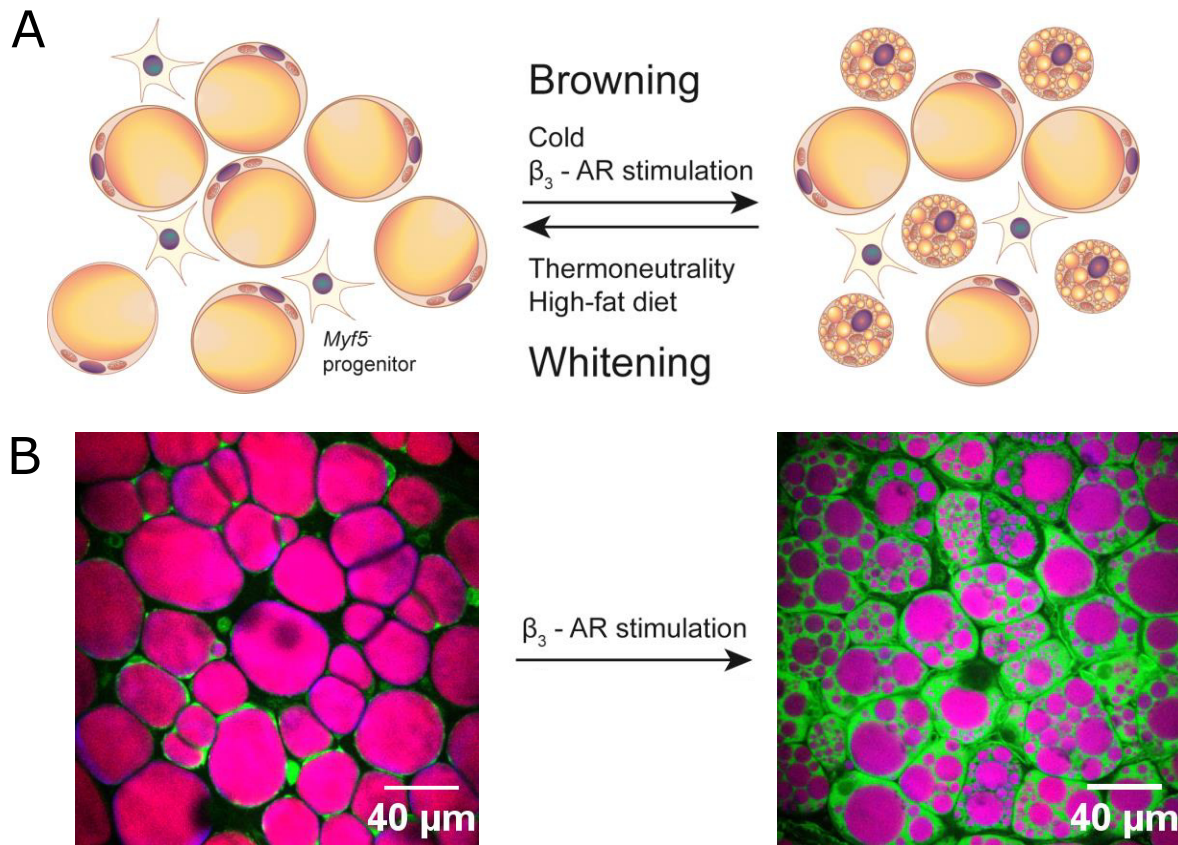


**Figure 6. Browning/Whitening of WAT.** (A) The number of beige adipocytes in WAT can be increased with cold temperature or  $\beta_3$ -AR stimulation (browning), while the number decreases with thermoneutrality or high-fat diet/obesity (whitening). Both white and beige adipocytes are derived from MSCs. There has also been speculation about transdifferentiation of adult white adipocytes. Adapted from [23]. (B) left: iWAT from 9 week old C57/BL6 mice, right: after 10 day injection with  $\beta_3$ -AR agonist (CL316,243, 1  $\mu\text{g/g}$ ). Lipids are shown in magenta (CARS, 2845  $\text{cm}^{-1}$ ), mitochondria in green (MPEF, Rho123). Scale bar: 40  $\mu\text{m}$ .

Despite being a way to deal with toxicity of NEFAs for most cells [33], the occurrence of LDs has also proven detrimental to certain cell types, *e.g.*, pancreatic  $\beta$ -cells, where excess lipid accumulation interferes with insulin secretion and can lead to apoptosis [87], [88]. In addition to the presence of LDs as disease indicators, the TAG chemical composition, *i.e.*, the length of the chains and the number of C=C bonds, can be of importance. For example, the chain length of NEFAs in blood correlates with stimulated insulin secretion [89], while saturation levels of lipids found in skeletal muscle cells are linked to insulin resistance [90]. It has also been shown that there are hepatic inter- and intra-cellular differences in LD composition as possible mechanism to reduce lipotoxicity [91], [92]. LDs can grow or shrink within hours upon changes in the nutrient source [93]. One of example where LDs change dramatically is adipogenic differentiation of stem cells.

In mammalian adipocytes, LDs consist mainly of TAGs and to lesser extent of sterol esters and diacylglycerols (DAG) [94]. LD size can vary by three orders of magnitude from 100 nm to 100  $\mu\text{m}$ . The hydrophobic droplets are covered with an emulsifying monolayer of

phospholipids that contain a specific subset of proteins (**Figure 7**), such as the perilipin protein family [95], [96]. Some of the proteins on the LD surface are also found in the endoplasmic reticulum (ER) membrane, suggesting that LD biogenesis could have its origins there [94]. TAGs for storage in LDs can be produced from two different pathways: (i) *de novo* lipogenesis of NEFAs from products of glycolysis and esterification, or (ii) uptake and direct esterification of NEFAs from plasma. Although there are typically many enzymes involved in these pathways, the following paragraphs will focus on important reporter enzymes that are relevant for the work in **Paper V**.

### **De novo lipogenesis**

WAT *de novo* FA lipogenesis can account for up to 40% of whole-body lipogenesis in humans [97]. Besides that, liver and the mammary glands (during lactation) are the main sites for FA synthesis, and often liver is the key contributor [98], [99]. In AT, this pathway is only active, if carbohydrate intake exceeds energy demand, and has been estimated to contribute to approximately 10% of AT TAGs [100]. Glucose, the fuel for *de novo* lipogenesis can either be supplied from carbohydrate sources in the diet or generated *de novo* in gluconeogenesis. The latter process occurs mainly in the liver [101] and *Pck1* (cytosolic phosphoenolpyruvate carboxykinase) is the main regulator [102]. One of the first steps in *de novo* lipogenesis is carried out by the multi-enzyme complex fatty acid synthase (FASN), which is indirectly controlled by insulin [103]. Desaturases (SCD) and elongases (ELOVL) are employed to adjust number of double bonds and chain length of FAs to cellular needs. The main FAs found in mammalian LDs are C16 and C18, both saturated and mono-unsaturated [94]. SREBF1c (sterol regulatory element binding factor) is a transcription factor that is linked with activation of *Fasn* and *Scd1* [104]. Another gene involved is *Agpat2* (1-acylglycerol-3-phosphate-O-acyltransferase), which generates precursors, phosphatidic acid, for both TAGs and phospholipids and is crucial for adipocyte differentiation [105].

### **FA esterification**

Most of the TAGs in WAT are produced from circulating TAGs and FAs, packed with lipoproteins, derived from nutrition or *de novo* lipogenesis in liver. Lipids absorbed *via* the small intestine are packed in chylomicrons and lipids produced in the liver travel in the blood packed as very low density lipoprotein (VLDL). They are freed from their protein packing in the extracellular space by lipoprotein lipase (LPL), secreted from adipocytes. Exactly how the FAs gets into the adipocytes is not fully understood [106].

Inside the cell, one of the key molecules required for the esterification of FAs is glycerol-3-phosphate (G3P), which can be formed from: (i) glucose *via* the glycolytic pathway, (ii) glycerol (employing glycerol kinase), and (iii) other precursors [25]. In WAT glyceroneogenesis (pathway iii) is preferred [107], [108], while BAT depends on glycerol kinase [109]. The main enzymes for TAG synthesis in mammalian cells are acyl-coenzyme A (acyl-CoA):diacylglycerol acyltransferase (DGAT1 & DGAT2); they add a third acyl chain to DAG molecules.



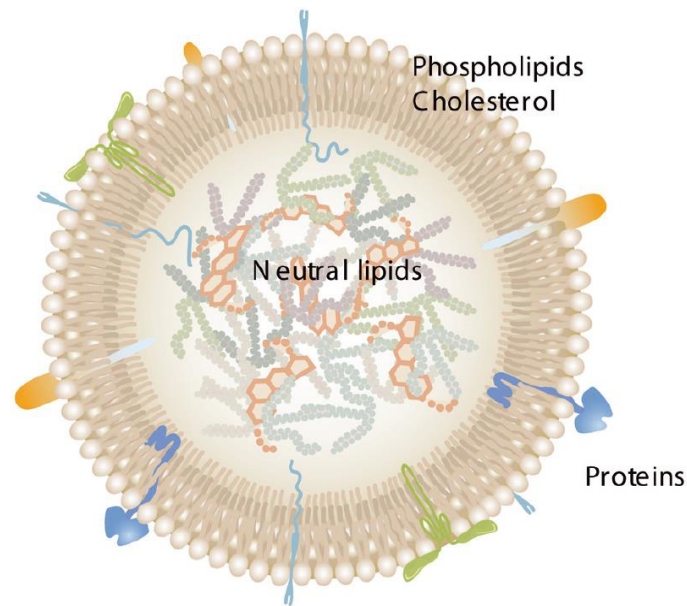


**Figure 7. Lipid droplet.** The LD is filled with neutral lipids (TAGs and cholesterol) and surrounded by a phospholipid monolayer with cholesterol and different proteins embedded. Reprinted with permission from [110].

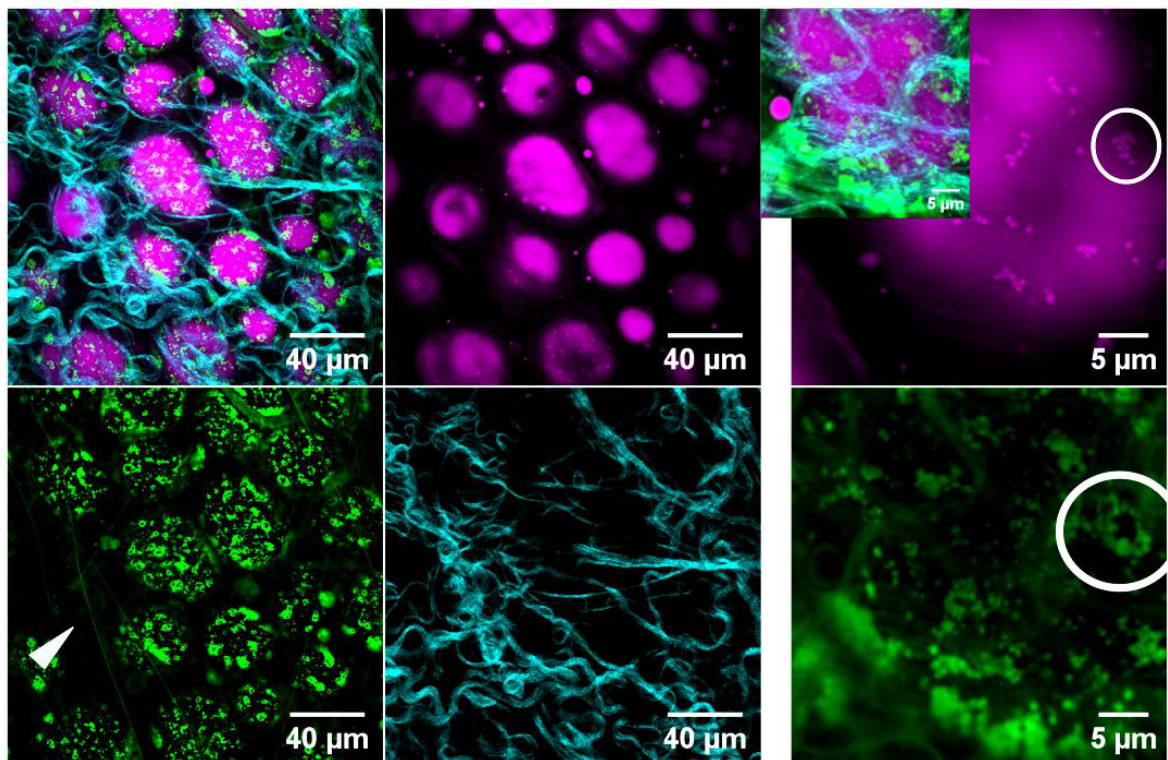


**Figure 8. Lipolysis in WAT.** Small LDs (magenta, CARS,  $2845\text{ cm}^{-1}$ ) on the surface of white adipocytes (circle top row) are surrounded by active mitochondria (green, MPEF, Rho123, circle bottom row). White adipocytes are embedded by fibrillar collagen (cyan, SHG) and elastin (green, MPEF, arrow head). Scale bars: 40 and 5  $\mu\text{m}$ .

DGAT1 localizes in the ER, while DGAT2 localizes with the LD and mitochondria [111], [112]. The expression ratio between the two depends on the tissue, with typically lower levels of *Dgat1* than *Dgat2* in liver and AT [113], [114]. Only DGAT2 is essential for survival [37]. The substrates for the DGATs are generated from G3P and FAs. GPD1 (glycerol-3-phosphate dehydrogenase) catalyzes the production of G3P, and GPAM (glycerol-3-phosphate acyltransferase) adds the first acyl chain [115].

### Lipolysis and FA utilization

When lipids are needed for energy or membrane lipid synthesis, FAs are mobilized from TAGs *via* lipolysis governed by adipose triacylglyceride lipase (ATGL) and hormone-sensitive lipase (HSL) [116]. The hydrolyzed lipids in AT are then either re-esterified to TAGs, used for mitochondrial long chain  $\beta$ -oxidation, which is crucial for BAT thermogenesis, or shuttled to other tissues for consumption there. In white adipocytes it can also be noted that lipolysis seems to occur in proximity to mitochondria (**Figure 8**). A complex trafficking system is set up inside cells to ensure maximum oxidative metabolism and avoid FA toxicity [117]. FAs can induce UCP1-dependent thermogenesis both in WAT [118], [119] and BAT [120]–[122] with carnitine palmitoyltransferase 1 (CPT1) as rate-limiting enzyme. The re-esterification rate after lipolysis increases upon fasting reaching almost 60% in 60 h starved humans [123]. It is commonly assumed that this re-esterification, which ‘costs’  $\sim 3\%$  of the energy content of one TAG molecule, is due to insufficient sensitivity in the regulation of lipolysis [107]. TAG has an energy density of 30 kJ/g while glycogen has 17 kJ/g as free molecule and 4 kJ/g in the hydrated form [124]. Since there is a constant release of NEFAs from the LDs in WAT their half-life is estimated at 250 days. However, this is a long time compared to oxidative tissues like muscle or liver, inside which the LD half-life is 24 and 100 h, respectively [124].

### Supply of NEFAs to other tissues

The majority of lipids that are released from WAT or liver are supplied to other tissues in a controlled way. The flow of NEFAs between organs depends on the nutritional state. After a meal (postprandial), due to increased plasma insulin concentrations, more NEFAs are stored as TAGs in WAT, compared to the fasting state. LPL, the enzyme that hydrolyses TAGs in lipoproteins, to allow NEFAs uptake into adipocytes, is upregulated [59]. At the same time lipolysis is suppressed by insulin, along with VLDL-TAG release from the liver. This means that while there is a high amount of circulating lipids (from food), FAs are not produced by *de novo* lipogenesis. During fasting, the liver and AT release NEFAs to support metabolism in other cells, *e.g.*, skeletal muscle and heart [124]. This differential response of stopping lipolysis postprandial and subsequent resumption is important to keep plasma FA levels within a healthy range [125]. All in all, WAT in symbiosis with liver and muscles acts as buffer organ for lipid flux, switching between lipid storage and release, similar to the role of liver in buffering glucose levels. Non-esterified FAs and chylomicron-TAGs (lipoprotein packed TAGs from food) have half-lives of only 3 and 5 minutes in plasma before they are taken up by cells, while non-chylomicron-TAGs, *e.g.*, VLDL-TAGs stay in the plasma for approximately 120 minutes [34].

Since BAT relies on FAs to fuel thermogenesis, it might not be surprising that BAT has a role in postprandial TAG clearance especially when activated. The majority of TAGs in BAT is extracted from circulation lipoproteins, which depends on LPL activity. In this process, the signal for production/release of LPL is norephedrine [126], [127]. Norepinephrine release leads to an accelerated plasma TAG clearance already after short-term cold exposure, 4 – 24 h, in mice [53]. In unstimulated BAT, TAGs originate mainly from *de novo* lipogenesis using glucose [42].

## Pathological changes in obesity

### Tissue morphology

The hallmark of obesity is the excess volume of AT, which is also the single identifying marker visible from the outside of the patient. The clinical definition of obesity is set to a BF% where the excess lipid storage causes health problems leading to increased mortality. It has been suggested that the definition should be changed to include the metabolic dysfunction that diminishes the ability of AT to protect other tissues from lipotoxicity [128].

Obesity usually develops slowly due to a long term positive energy balance causing the body to store this excess energy in the form of TAGs that slowly fill the capacity of AT. There are two ways AT attempts to handle the increased amount of circulating lipids under constant overfeeding: (i) enlargement of existing adipocytes, hypertrophy, or (ii) increase of adipocyte numbers, hyperplasia. Both adaptations occur in gWAT, while in iWAT only hypertrophy has been found [129]. However, if the AT cannot store all the lipids and the circulating NEFAs reach a concentration which is toxic to most cells [33], lipid depots are eventually formed in other tissues, *e.g.*, skeletal muscle and liver [110].

In contrast, BAT mass decreases during long-term positive energy balance and thus during obesity [44]. Additionally, in obesity, through the control of TGF- $\beta$  signaling, beige adipocyte differentiation is suppressed, hence leading to fewer beige adipocytes in WAT [51]. It is not fully understood if diet leads to changes in number of beige and brown adipocytes directly and/or indirectly *via* organs involved in stimulation of non-shivering thermogenesis, *e.g.*, liver (FGF21 signaling), skeletal muscle (Irisin signaling), hypothalamus (norephedrine) [23].

It has also been found that not all AT depots behave equally under prolonged surplus of energy. Expansion of visceral AT (deep in the abdomen and around the organs) has been especially linked to many of the adverse health effects obese patients face, such as hypertension, dyslipidemia, and T2D [28], [32]. Subcutaneous WAT expansion has not been similarly linked to adverse health effect, due to its ability to act as a buffer for lipid influx, thus preventing ectopic built-up of lipids [27] and the secretion of more beneficial adipokines [130]. For example, non-obese patients with high visceral-to-subcutaneous fat ratio are more likely to be insulin resistant [131]. In both WAT depots, smaller adipocytes are more insulin



sensitive than larger ones [132], and the presence of larger adipocytes in subcutaneous WAT have been linked to an increased risk for T2D [133]. To summarize, it is fair to say that increased subcutaneous AT is rather “metabolically healthy” whereas excess visceral AT is more “metabolically unhealthy”.

### **AT inflammation and insulin resistance**

With an increase in adiposity, somehow the endocrine function of adipocytes gets dysregulated, which is key in obesity-related insulin resistance. FA plasma levels are elevated in obese patients, in parallel to the increase in fat mass. These FAs, together with several other metabolites, have been thought to impact intracellular kinases, which in turn can impair insulin signaling [134], [135]. Some of the factors secreted from AT, like monocyte chemoattractant protein-1 (MCP1), are linked to the increased macrophage infiltration found in obese mice [136] and humans [137]. The presence of macrophages increases from 5-10% to 50% of all cells in AT during obesity [137]. This increase in macrophage numbers in AT has been linked to insulin resistance in skeletal muscle, *via* macrophage secreted cytokines that trigger increased lipolysis and decreased TAG synthesis in adipocytes [138]. However, at the same time, it has been shown that AT inflammation is crucial for tissue expansion, which if disrupted leads to increased ectopic lipid depositions [139]. Ectopic lipid depositions become especially visible in liver, which under normal conditions contains 1-10% lipids by weight, but can increase significantly and lead to non-alcoholic fatty liver disease [124]. Thus there is clearly a balance between “normal” AT expansion and metabolic abnormalities.

## **Adipogenic differentiation of stem cells as a model for obesity research**

In order to study adipocyte function, *in vitro* models have been established [140]. Besides stable cell lines, one of the promising approaches is the differentiation of adipose-derived stem cells (ADSC) or MSC into cells of adipocyte lineage. For both stem cell types, a beige or beige/brown differentiation protocol, in addition to a white adipocyte commitment, has been developed [140], [141]. The following sections will focus on white adipogenesis which is relevant for **Paper II**.

### **Stem cell niches in AT**

AT contains ADSC to be able to regenerate and regulate its cell number. These stem cells are part of the stromal population in AT together with microvascular endothelial cells and smooth muscle cells. The stem cell fate is not only regulated by intrinsic factors, but also by the interaction with its environment. Every cell in the body is in contact with extra cellular matrix (ECM) proteins at some point (**Figure 9**), which conveys a number physical and biochemical cues that can alter differentiation programs. Cells react to ECM mechanical cues in a complicated process known as mechanotransduction [142]. This mechanosensitivity of adipocytes has been observed *in vivo* and *in vitro* [143].

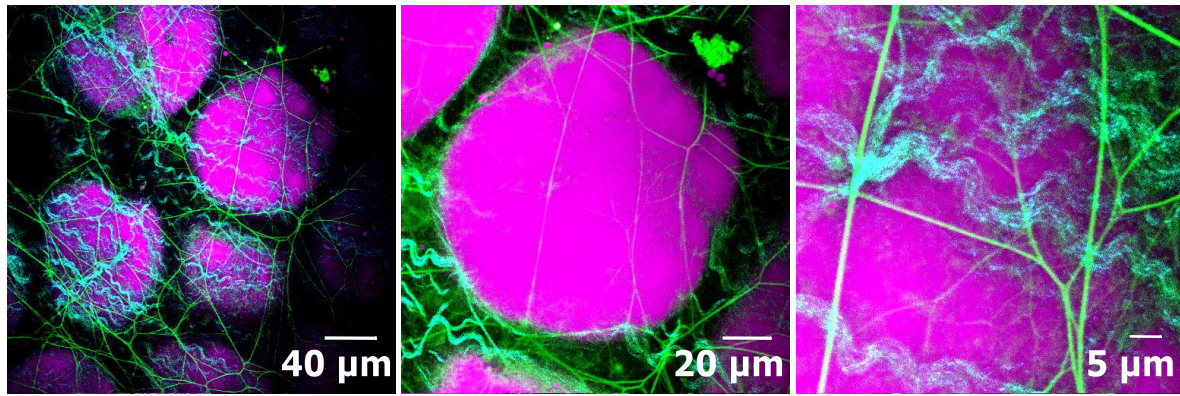


**Figure 9. ECM in gWAT of mice.** Adult and precursor cells are in close contact with the ECM in gWAT. Lipids (magenta, CARS,  $2845\text{ cm}^{-1}$ ), fibrillar collagen (cyan, SHG), elastin (green ‘strings’, MPEF). Scale bars: 40, 20, and 5  $\mu\text{m}$ .

In connective tissue, like WAT or cartilage, cells are completely surrounded by the ECM, to which they adhere *via* different surface proteins, which can also modulate cell fate [130].

During the development of AT in the embryo it is presumed that AT starts out as a loose connective tissue with sparse population of mesenchymal cells. Those cells are further expanded and blood vessels are formed. Subsequently, the cells start to accumulate small lipid depots, which later transform into the large LD in mature adipocytes. This final step of differentiation is accomplished after birth [144]. Stem cells in formed tissues reside in specialized niches and it is believed that mechanical cues in those niches can help to decide over a proliferation or differentiation pathway [145]. Human ADSC localize into a perivascular niche during early AT development as well as in mature tissue [144]. AT is dynamic and contains a vast mixture of mature adipocytes, precursor cells, extracellular vesicles, immune cells, fibroblasts and extracellular matrix. Adipocyte precursor cells, like mesenchymal cells, can remodel their own ECM during their development; they change both structure and composition of the ECM during this process. It has been found *in vitro*, that collagen IV and laminin expression is upregulated, while fibronectin expression decreases during differentiation [146]. This suggests that the differentiation matrix for hADSC is more laminar than fibrillar, which accommodates for cell size expansion. Additionally, many degrading enzymes are active during the differentiation process facilitating tissue remodeling. During obesity, AT is in a state of chronic tissue inflammation, which is also characterized by increased fibrosis of the tissue. Consequently, more fibrous collagen is found in AT of obese patients, which makes it stiffer [147]. Macrophages, which are recruited during inflammation, contributes further to the ECM production [144] and are key-initiators of the matrix remodeling during obesity [148].

#### **Adipocyte differentiation *in vivo***

Adipocytes develop, *in vivo*, from mesenchymal stem cells in the AT. The vast majority of adipocytes are developed during late gestation. In the adult tissue, on the other hand, differentiation events occur in order to keep a constant cell number [149]. Stem cells are usually kept in a state, where pro- and anti-adipogenic *Wnt* signaling pathways keep each

other stalled, resulting in maintenance of stem cell features [150]. A signal from outside the stem cell is needed to disrupt this balance and initiate differentiation [150]. Gene expression during differentiation is tightly controlled and first initiates a determination phase, where the stem cell commits towards adipocyte lineage and can no longer differentiate to any other cell type (**Figure 10**). At this point, the cells reach growth arrest and withdraw from the cell cycle, in order to allow adipose conversion. In the second phase, the termination, lipid transport and synthesis, and insulin sensitivity are established. Additionally, secretion of adipocyte-specific proteins is commenced. This signaling cascade can be started by intrinsic factors, cell-cell contact, cell-ECM contact, or cell shape [150]. Two important genes in this signaling cascade are the nuclear peroxisome proliferator-activator receptor  $\gamma$  (PPAR $\gamma$ ) and CCAAT-enhancer-binding proteins (C/EBPs). PPAR $\gamma$  is needed to initiate and maintain adipocyte differentiation. Several C/EBPs participate during adipogenesis and these proteins cannot function efficiently without PPAR $\gamma$  [149]. However, some of the steps in this signaling pathway remain obscure. Investigating signaling pathways controlling *in vivo* differentiation is complex. Murine knockout models are used to understand the role of individual genes in development.

Yet, knockout or upregulation of relevant genes might lead to high frequencies of life impairing diseases and initiation of compensatory mechanisms. Thus, many conclusions about *in vivo* differentiation are drawn from *in vitro* studies, with cell lines or stem cells. A problem with such systems is that all stem cell lineages do not behave in the same way, leading to difficulties in understanding and relating gene expressions. Sometimes, *in vivo* and *in vitro* findings even contradict each other, for example, sterol regulatory element binding factor 1c (SREBF1c) as a transcription factor [149]. *In vitro* SREBF1c seems to be crucial for lipid PPAR $\gamma$  expression [151], while *in vivo*, mice lacking SREBF1c display normal fat pads [152].

There are more than a hundred reported transcription factors expressed in adipocytes, of which many affect differentiation. Not all factors bind to DNA, protein-protein interactions can also affect gene expression by forming for example co-activator or co-repressor complexes.

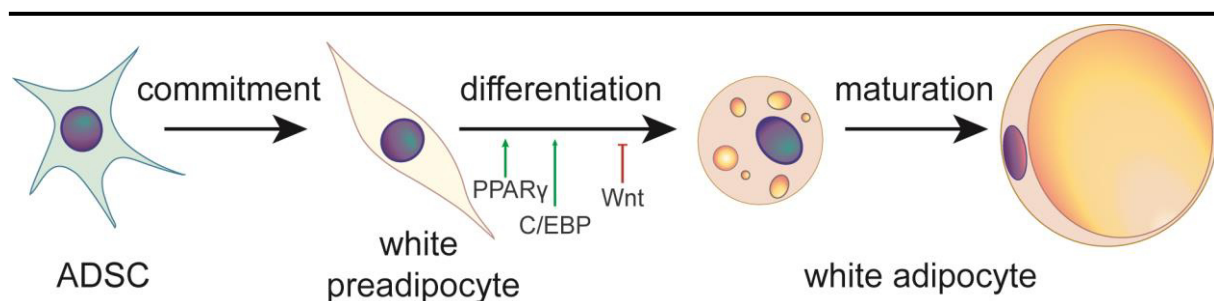


**Figure 10. *In vivo* adipogenesis of ADSC.** The differentiation of ADSC occurs in stages. First, the multipotent stem cell, which can give rise to osteoblasts, chondroblasts, adipocytes, commits towards a lineage. In this case the commitment is towards a white preadipocyte lineage. From there adipogenesis occurs with enhancing ( $\uparrow$ ) and inhibiting ( $\downarrow$ ) factors. After initial differentiation the adipocyte matures and the unilocular lipid droplet forms.

Many evolutionary highly conserved pathways are important for adipocyte differentiation. Activity in a *Wnt* signaling pathway and a hedgehog pathway seem to inhibit adipocyte differentiation *in vitro*, while *in vivo*, involvement of the same pathways is likely to increase differentiation [149], [150]. Although many involved factors in the adipocyte differentiation are identified, both *in vivo* and *in vitro*, it has been difficult to design an *in vitro* differentiation protocol, which offers all stimuli present in the *in vivo* AT. On top of that, some signaling molecules which have been identified in mature adipocytes, inhibit differentiation if added in the determination phase during *in vitro* differentiation. These are some of the difficulties of replicating the perfect timing of the natural signaling cascade in an *in vitro* setup.

### **ADSC differentiation *in vitro***

The stromal-vascular fraction in AT can enzymatically be isolated from the tissue and separated from the mature adipocytes *via* centrifugation. Subsequent passaging of the cells leads to a more homogenous cell population, which is then termed ADSC. ADSC have the ability to extensively proliferate and commit to multiple lineages derived from mesenchymal cells, towards adipocytes, osteoblasts, or chondrocytes. They are therefore part of a superior population (MSCs) [31]. ADSC and bone-marrow MSC, among others, can be used to obtain adipocytes in *in vitro* cultures. However, so far no fully functional adipocyte-phenotype could be achieved using *in vitro* differentiation.

During the differentiation of ADSC several compounds and hormones are added to the culture medium. The four main ones are pioglitazone, dexamethasone, 3-isobutyl-1-methylxanthine (IBMX), and insulin. Some of these compounds can be replaced with chemically similar molecules, which will induce the same effects. Pioglitazone is originally an antidiabetic drug, which enhances insulin sensitivity. Drugs in this group are activators of PPAR $\gamma$ , thus increasing the transcription of insulin-responsive genes [153]. Dexamethasone is a glucocorticoid agonist, typically used to maintain organ transplants and to manage chronic inflammations. Glucocorticoid expression upregulates also transcription of a class of PPAR $\gamma$  and C/EBP [154]. IBMX raises intracellular cAMP levels by inhibition of phosphodiesterase [155]. Insulin is important for the differentiation of adipocytes and there are at least four points of interference in the gene expression cascade [149].

Although there are many similarities between *in vitro* differentiated adipocytes and freshly isolated mature adipocytes, *e.g.*, lipolysis, insulin stimulated glucose uptake, secretion of adipokines [156]–[158]; the *in vitro* adipocytes contain multilocular LDs (**Figure 11**), show different levels of maximal lipolysis [159] and of secretion of VEGF and bFGF [160].

In order to improve *in vitro* differentiation, the need of mechanic cues like response to cell stretching, compression, and shear stress from fluid flow, has been explored. This opens up the possibility using materials that can support and/or enhance adipocyte differentiation *in vitro*. Such materials can for instance be designed to mimic AT. Therefore, it is desired that they are soft, but also stable and support stretching of cells as well as allowing the cells to



round up when they have differentiated further. It has even been shown that micro- and nano-patterns can influence cell fate [161].

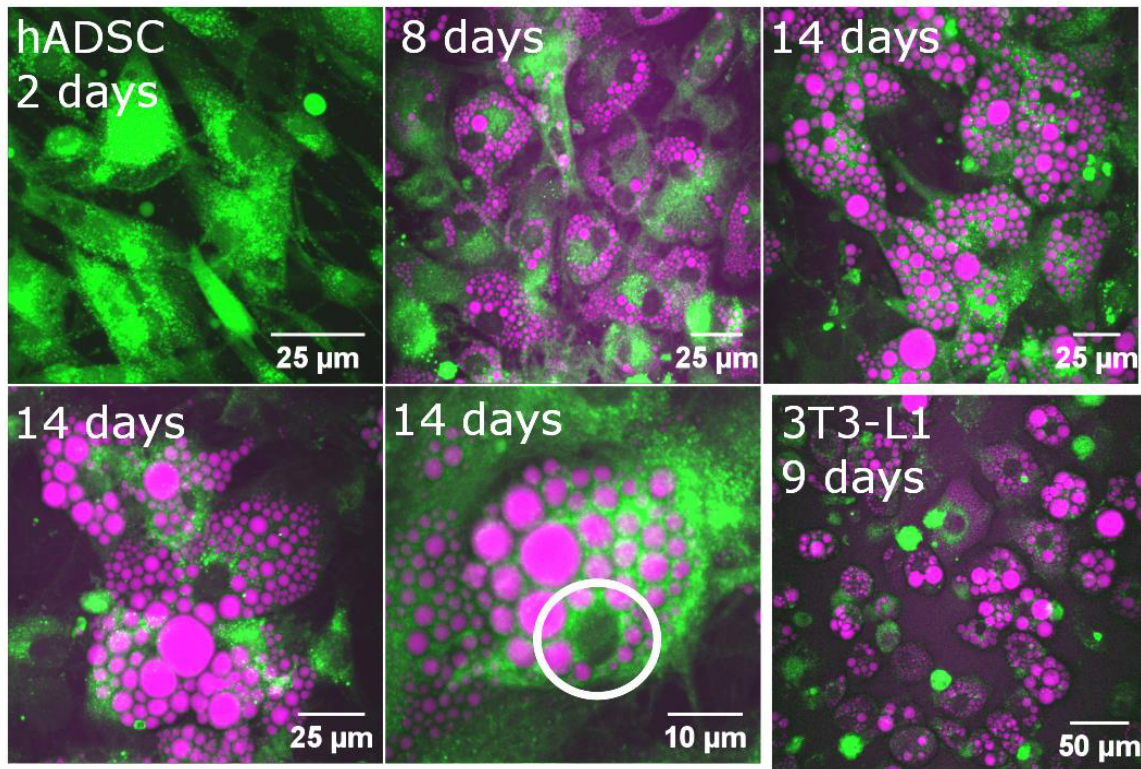


**Figure 11. *In vitro* adipogenesis of progenitor cells.** hADSC accumulate LDs (magenta, CARS,  $2845\text{ cm}^{-1}$ ) over the course of 14 days differentiation *in vitro* on cell culture treated plastic. The LDs in the cells remain multilocular. Intrinsic cellular fluorescence (green, MPEF) shows the cytosol and outlines of the cells. Nuclei are seen as an absence of signal (circle). 3T3-L1, a mouse fibroblast cell line, can also be differentiated into adipocytes (bottom right). Scale bars: 25, 10, and 50  $\mu\text{m}$ .



## **Chapter 3. *In situ* analysis of adipocyte physiology**





# 3 *In situ* analysis of adipocyte physiology

## An overview of methods

Standard histological images of LD-containing tissues are known to show empty shells where the droplets used to be. The lipids inside these LDs are lost during embedding in paraffin and dehydration. Small LDs ( $< 2\ \mu\text{m}$ ) are challenging to identify from sections prepared in this way. Only with advances in optical and electron microscopy has the presence of LDs in nearly all cell types been confirmed. Still, there are short-comings to current methods leaving many fundamental questions in LD biology open [162].

There are two principal areas of LD physiology that need further research and development: (i) imaging LD morphology, dynamics, and interaction with other molecules/organelles, and (ii) revealing the chemistry of the molecules that make up LDs. These two areas require somewhat different experimental approaches, and this chapter will focus on the methods developed and employed that are part of this PhD thesis.

## Toolbox I: Microscopy for LDs and their dynamics

When considering cell dynamics, different time scales can be of interest. Cells migrate over hours, organelles move within minutes, and molecular interactions form within seconds or less, while adaptations of *in vivo* tissue to external influences or differentiation of stem cells can take days to months. Additionally, LDs can range in size from several nm to  $100\ \mu\text{m}$ , similarly to lipoproteins. Ohsaki, Suzuki, and Fujimoto speculate that even the density and protein content in LDs varies analogous to that of lipoproteins [162]. This large heterogeneity among LDs is not likely to be captured by a single technique. Three main techniques can be employed to visualize LDs *in vitro*: electron, fluorescence, and nonlinear microscopy, which are briefly introduced and compared below.

LDs, but not their phospholipid membrane, are visible using osmium tetroxide as stain for transmission electron microscopy (TEM). Due to limits in contrast, LDs below  $50\ \text{nm}$  diameter have proved challenging using this technique [163]. Yet, a more integral challenge is the sample preparation. Aldehydes, which are routinely used in TEM sample preparation, do not react with lipids; osmium tetroxide and uranyl acetate bind lipids albeit not uniformly [162]. Both lipid-binding cross linkers react mainly with C=C bonds in the acyl chains, thus the image contrast can be modulated by lipid saturation level in an unknown way. Cryo-,

freeze fracture, and deep-etch EM allow direct observation of LDs without crosslinking. These techniques can be used to visualize the phospholipid monolayer on isolated LDs [164], gold-nanoparticle labeled proteins on the surface of (and even inside) LDs from fractured cells [164], [165], and LDs in, *e.g.*, macrophages [164]. TEM offers the highest theoretical resolution of the techniques compared with  $\sim 50$  pm [166]. Cryo-EM has lower resolution at  $\sim 300$  pm, withal gaining the feasibility to map 3D structures [167]. Nevertheless, the mapping of crowded cellular spaces is challenging, it is not possible to follow biological processes in real-time, and no quantitative differentiation between lipid chemical species can be made using EM.

For that purpose, fluorescence microscopy is better suited. Especially with recent advances in super-resolution microscopy allowing the visualization of biological molecules *in situ* with  $\sim 20$  nm resolution [168]. Hell *et al.* summarize advances in super-resolution techniques as well as challenges faced [169]. One of the major trends in this field is the move towards live-cell, 3D imaging [168]. With the development of new dyes combined with structured illumination microscopy, the possibilities to achieve sufficient resolution in 3D are within reach [168]. There is now a multitude of dyes available for imaging lipids with conventional confocal laser scanning microscopy (CLSM), with  $\sim 180$  nm resolution [170]. The main drawback here is that these dyes might interfere with LD motility [171], label LDs unevenly due to changes in composition [92], or get excreted over time by intracellular transporters [172].

Nonlinear microscopy, a collection of several techniques allows, in addition to fluorescence, the possibility to visualize lipids and other biological molecules **without** external labeling. The resolution here is limited at  $\sim 300$  nm [173], [174]. As the focus of this thesis is on nonlinear microscopic lipid visualization, I will primarily describe coherent Raman scattering (CRS) and briefly third harmonic generation (THG), which have been extensively used to visualize lipids in cells, tissues, and even organisms. These two techniques can be readily combined with other nonlinear microscopy techniques such as second harmonic generation (SHG), visualizing fibrillar collagen or dendrites in nerve cells, or multi-photon excited fluorescence (MPEF).

## Nonlinear microscopy

### Basic principles

The theoretical basis for non-linear microscopy was established in 1931 by Maria Göppert-Mayer, who mathematically showed the possibility for two-photon adsorption and its quadratic dependency on the intensity of light [175] (English translation: [176]). In 1977, with the development of more powerful light sources, this process could be utilized for image generation [177]. Along with the construction of pulsed lasers with high peak-powers, more nonlinear processes could be explored and employed.

Nonlinear optics as a discipline is set apart from linear optics, the class of light-matter interactions behind everyday effects like rainbows, cameras, or telescopes that is also the basis of epifluorescence microscopy and CLSM. These interactions occur with natural, low

light intensities and physical parameters describing them depend linearly on the incident light electric field amplitude (and therefore intensity). A much higher light intensity is needed to trigger light-matter interactions classified as nonlinear. In such processes, the induced polarization in a material with caused by the incident electric field (light) is no longer linearly dependent on the field amplitude.

The theory behind nonlinear optics in general, and specifically coherent Raman scattering has been described in detail in textbooks [178], [179]. Briefly, the induced macroscopic polarization  $P(t)$  of the electric dipoles in a material depends on the strength of the applied optical field  $E(t)$ . For weak electric fields (compared to the fields binding electrons to the nucleus), this relation can be formulated in a linear dependence as:

$$P(t) = \varepsilon_0 \chi^{(1)} E(t) \quad \text{eq. 1}$$

where  $\varepsilon_0$  is the electric permittivity in vacuum and  $\chi^{(1)}$  the linear susceptibility of the material. For stronger fields,  $P(t)$  can be expanded as a power series:

$$\begin{aligned} P(t) &= \varepsilon_0 [\chi^{(1)} E(t) + \chi^{(2)} E^2(t) + \chi^{(3)} E^3(t) + \dots] \\ &= P^{(1)}(t) + P^{(2)}(t) + P^{(3)}(t) + \dots \end{aligned} \quad \text{eq. 2}$$

where  $\chi^{(n)}$  is the  $n$ th order susceptibility.  $P^{(n)}$  is the  $n$ th order polarization. The physical processes occurring as result of the second-order polarization differ from the third-order polarization. There is a multitude of processes that can occur in the nonlinear regime. The following sections focus on processes originating due to  $P^{(2)}$  or  $P^{(3)}$  as they commonly occur in biological samples. Due to the applied nature of this thesis the mathematics behind solutions for the prediction of  $P^{(2)}$  or  $P^{(3)}$  are omitted.

### Coherent Raman scattering (CRS)

Raman scattering describes a light-matter interaction, where the response of the interaction between incident light and matter contains information about molecular oscillations of chemically bound nuclei. Typically the main portion of the incident light with the frequency  $\omega_1$  undergoes Rayleigh (elastic) scattering, meaning the same light frequency (energy) is scattered (**Figure 12A, B**). However, a relatively small fraction of scattering results in light with discrete frequencies above or below that of the incident light. This spontaneous Raman (inelastic) scattering is called Stokes Raman or anti-Stokes Raman, depending on if the emitted light frequency is lower ( $\omega_1 - \omega_v$ ) or higher ( $\omega_1 + \omega_v$ ) than the incident light frequency  $\omega_1$  (**Figure 12A, B**).  $\omega_v$  denotes the nuclear resonance frequency. Although it is the electrons that are set in motion by the light field, this motion is perturbed by the presence of the nucleus position and hence the electronic polarizability depends on  $\omega_v$ . The change in polarizability depends on the symmetry of the nuclear modes, and this forms the basis for selection rules in Raman spectroscopy. A mode is only Raman active if the change in polarizability with nuclear motion is not zero [180].

For spontaneous scattering, each molecule carries out an independent spontaneous oscillation, which radiates a field that is not correlated in phase with any other molecule; there is no synchronization of the process. In practice, Raman scattering efficiency can be formulated with a cross section  $\sigma$ , analogous to (but different in physical origin from) the Lambert-Beer law for absorption. The total Stokes contribution of the scattered Raman-shifted light can be formulated as:

$$I(\omega_s) = N z \sigma(\omega_s) I_0 \quad \text{eq. 3}$$

where  $N$  is the molecular density,  $z$  the length of the sample, and  $I_0$  the intensity of the incident beam. Spontaneous Raman scattering is a weak process that is linear in molecular density and intensity of the incident beam. The anti-Stokes components are typically orders of magnitude lower in intensity compared to the Stokes components, since anti-Stokes transitions occur from excited vibrational states which are not as frequently populated at thermal equilibrium.

The possibility of Raman transitions can be increased in a nonlinear way when a combination of intense laser sources is used with appropriately chosen energies. The resulting process is denoted as coherent Raman scattering (CRS) [181]. CRS is a third-order nonlinear process where a pump ( $\omega_p$ ) and Stokes ( $\omega_s$ ) stimulate a specific transition. This process is enhanced if  $\omega_p - \omega_s$  is in resonance with a vibrational (or rotational) transition of the probed molecule. In this case, one type of signal called stimulated Raman scattering (SRS) can be detected as a modulation of the intensities of the incident Stokes and pump beam *via* the coupling of the light fields with molecule. With improvements laser technology, modulation of one of the laser fields, and lock-in detection, this process can be employed for real-time label-free biomedical imaging [182], [183].

The stimulated Raman process also occurs concurrently with so-called coherent anti-Stokes Raman scattering (CARS). In this process, the molecular coupling induced by the interaction of the two light fields ( $\omega_p$  and  $\omega_s$ ) is probed by scattering a third (probe) light field off the driven molecular oscillation. The scattered field gains energy from the driven oscillation (at  $\Omega = \omega_p - \omega_s$ ) so light at a new frequency is created and can be detected (**Figure 12C, D**). The new frequencies are in principle:  $\Omega + \omega_p$ ,  $\Omega + \omega_{\text{Stokes}}$ , and  $\Omega + \omega_{\text{probe}}$ . In CARS as implemented in this work and nearly all other examples, the pump and probe light fields are the same and the light at frequency  $\Omega + \omega_p$  is detected. The whole process can be summarized as:

$$\omega_{\text{CARS}} = \omega_p - \omega_s + \omega_{pr} = 2\omega_p - \omega_s \quad \text{eq. 4}$$

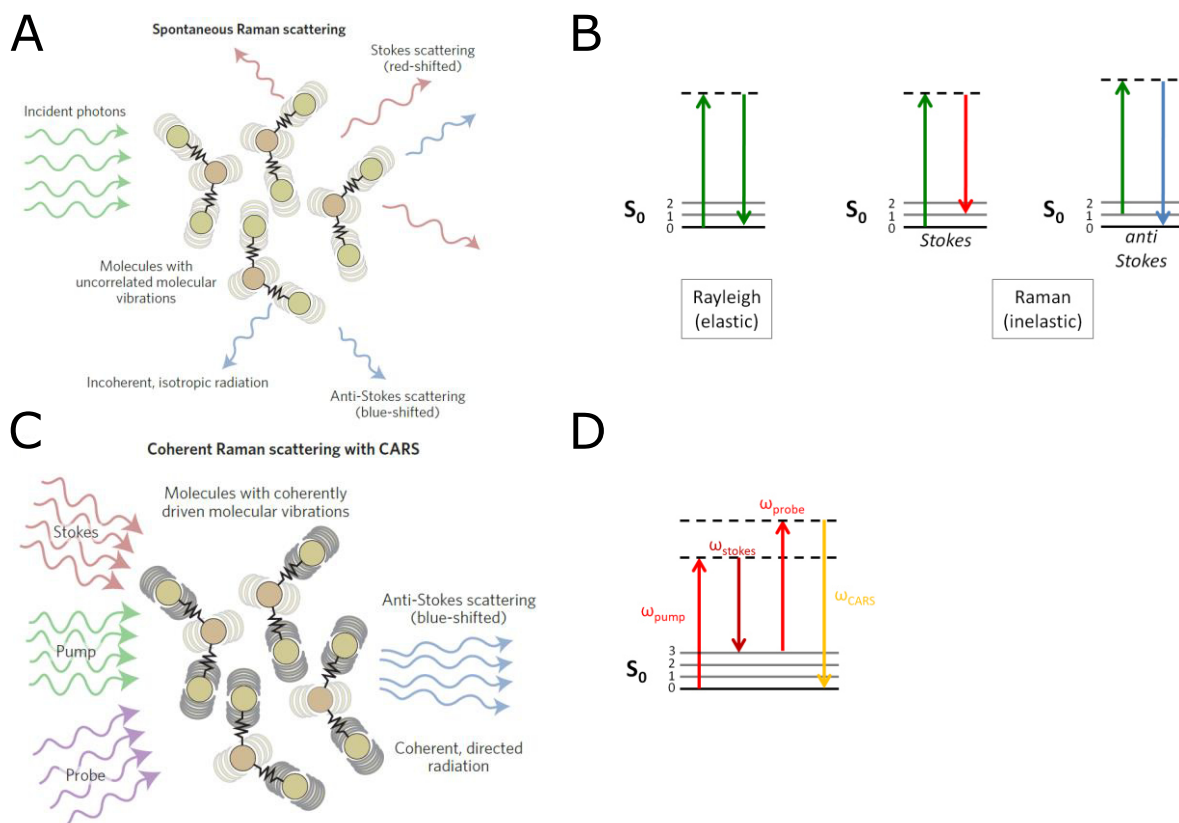


**Figure 12. Spontaneous Raman scattering and CARS.** (A) Spontaneous scattering results in incoherent photons. (B) Jablonski energy diagrams: The scattered photons can either be scattered with the same energy (Rayleigh), transfer some of their incident energy to the matter (Stokes Raman), or increase their incident energy upon interaction with matter in an excited vibrational state (anti-Stokes Raman). (C) CARS is coherently driven process, where three incident photons interact simultaneously to generate anti-Stokes scattering. (D) The CARS process begins and ends in the electronic and vibrational ground state (\$S\_0, v=0\$). \$S\_0\$ electronic ground state, \$v=0-3\$ vibrational states, dashed lines denote virtual states. (A, C) reprinted with permission from [184].

Importantly, in CRS, vibrations, are coherently driven by the beat field at  $\Omega$ , making all molecules vibrate in phase, which is a major reason why these techniques strongly enhance the Raman process compared to (spontaneous) linear Raman scattering. By tuning the difference between  $\omega_p - \omega_s$  ( $\Omega$ ), different molecular vibrations can be driven and measured. In order for this process to occur, additional technical conditions must be fulfilled including phase matching, *i.e.*, momentum conservation for the four light fields, which would necessitate specific angles between the incident and CARS beams. However, in a microscope when the incident light fields are focused in the sample through a high numerical aperture objective, this condition can be relaxed [174]. CARS is a parametric process, *i.e.*, the energy of the matter does not change before and after the interaction.

CARS was first observed in 1964 [185] and employed for microscopy in 1982 [186]. However, with the use of visible light sources the technique was rendered ineffective by two-photon enhanced background signals. As recently as in 1999, with implementation of tight focusing conditions, which relaxes the phase matching, and near IR light, reducing photo damage and enhancing sensitivity, CARS microscopy became applicable to perform 3D scans on a vast array of different samples [174]. Although this implementation improved CARS

sensitivity, the method is not background-free due to oscillating electron clouds that can also cause radiation at detected CARS frequency yet have nothing to do with molecular vibrations. This can be seen by writing the relationship between the intensity of the CARS signal and induced polarization:

$$\begin{aligned}
 I_{CARS} &\propto |\chi^{(3)}|^2 & \text{eq. 5} \\
 &\propto |\chi_R^{(3)} + \chi_{NR}^{(3)}|^2 \\
 &\propto |\chi_R^{(3)}|^2 + |\chi_{NR}^{(3)}|^2 + 2 \chi_{NR}^{(3)} \text{Re} \{ \chi_R^{(3)} \}
 \end{aligned}$$

where the third order susceptibility  $\chi^{(3)}$  is a complex sum of resonant ( $\chi_R^{(3)}$ ) and non-resonant  $\chi_{NR}^{(3)}$  contributions. The non-resonant term leads not only to a spectrally flat background, but also to a crossed term that introduces spectra distortions to CARS spectra when compared to spontaneous Raman spectra. This results in a red-shifted peak, compared to spontaneous Raman peaks, with a dip at the blue end of the peak [179], [187]. Different techniques to reduce the contribution of the non-resonant background (NRB) have been demonstrated, *e.g.*, frequency modulation [188], or epi [189], heterodyne [190], or time-resolved detection [191]. The latter approach has been employed for **Paper I-III**. With time-resolved detection, for instantaneous decaying signals like SHG, and fast decaying signals like CARS a thresholding window is placed to collect only photons arriving within the instrument response time. This reduces the contribution of slower decaying signals like MPEF.

#### **CARS microscopy**

Due to the increased sensitivity of CARS microscopy compared to spontaneous Raman microscopy, integration times for image scanning have been drastically reduced and facilitated video-rate imaging [192]. Moreover, due to the need of high laser intensities, supplied by pulsed laser sources ( $> 70$  MHz) and tight focus, the CARS signal is only generated near the focal plane, thus no additional instrumentation is needed to generate 3D images. The use of near infra-red laser sources reduces scattering in biological samples and allows the imaging of intact tissues with  $\sim 400$   $\mu\text{m}$  penetration depth [187]. Additionally, the use of picosecond-pulsed lasers with wavelengths above 800 nm further reduces the photo damage [192], [193]. To address single frequencies, picosecond-pulsed laser sources are preferred over femtosecond, as often used for other nonlinear techniques, due to a typical Raman linewidth of  $10\text{-}20$   $\text{cm}^{-1}$ ; femtosecond-pulsed lasers have a linewidth of  $150$   $\text{cm}^{-1}$  for 100 fs pulses [187].

The coherent nature of the signal causes the dependence of the far-field radiation pattern on more parameters than for incoherent signals, like fluorescence or spontaneous Raman. The pattern depends on the nonlinear susceptibility, size and shape of the scatterer, and the local sample environment. That can result in differences between forward and epi (or backward)-

detected CARS signals [194]. While a single dipole would generate the same signal in both directions, bulk materials show interferences that typically lead to stronger signal in forward direction. However, epi signals can be stronger for very small objects ( $\frac{\lambda_p}{3}$ ), samples with a high number of local changes in refractive index, or if the forward signal is backscattered by a turbid sample [187]. These differences can be employed for samples, where a bulk substance, like water, conflates the sample response in the forward direction [189] or when epi- and forward direction contain complementary information [194].

### SHG, THG, and MPEF

In this section, I will describe the other nonlinear microscopy techniques used in my PhD work. Second harmonic generation (SHG, **Figure 13A**) is a second order parametric process, which only is non-resonant (does not probe any specific molecular states) but rather molecular asymmetry. Being fully non-resonant, this process can be conceptualized through so-called virtual states. Virtual states are superpositions of states but not true *eigenstates* of the molecule. Transitions involving virtual states are essentially instantaneous and occur synchronously with the excitation pulse. In SHG, the input laser frequency doubled and the output signal is fully coherent. SHG can only occur in highly polarizable materials with non-centrosymmetric molecular organization. Thus, the most common molecules investigated in biological samples are collagen, tubulin, and actomyosin complexes [195].

When three non-resonant fields instead of two are combined, then the process is referred to as third harmonic generation (THG, **Figure 13B**). For a homogenous medium at the focal point, the THG waves interfere destructively resulting in net zero signal [178]. If there is an interface within the focus, the symmetry along the optical axis is broken and the THG signal becomes measurable [196]. This is especially useful for imaging of LDs due to their high refractive index compared to the cellular cytosol [197].

In contrast to the non-resonant polarization that is the basis for SHG and THG, multi-photon excited fluorescence (MPEF, **Figure 13C**) stems from absorption by and electronic excitation of a fluorophore. It resembles one-photon excited fluorescence (OPEF, **Figure 13C**), except that two or three lower energetic photons have to be absorbed at once to bridge the energy gap between ground ( $S_0$ ) and excited electronic state ( $S_1$ ). However the selection rules differ between OPEF and MPEF. A two-photon absorption is only allowed between states with the same parity, while one photon transitions can occur between opposite parity [198]. The emission occurs from the lowest vibrational state in  $S_1$  for both processes. The band shapes of  $S_0$  and  $S_1$  energy manifolds determine the width and wavelength of the emission spectrum. The emission is incoherent (just like OPEF), meaning that we can again linearly add the detected intensities unlike for CARS, SHG, and THG [199]. Since this process involves electron transitions, the life time of the excited state is of order ns and thus longer than for other nonlinear processes (including resonant CARS). Some of the fluorophores developed for OPEF can also be excited with near-infrared light and are thus accessible for MPEF. Additionally, intrinsic biological molecules in cells and tissues can be multi-photon excited [200].

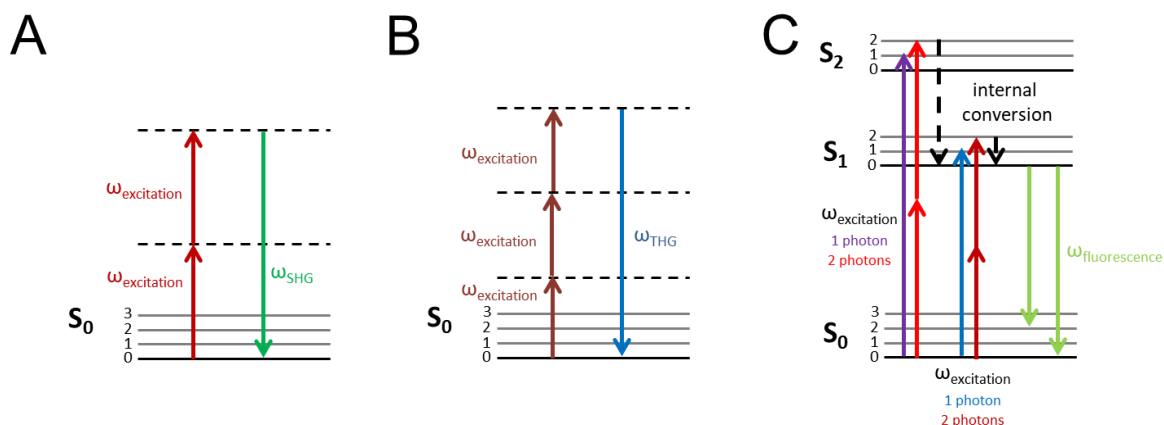


**Figure 13. SHG, THG, and O/MPEF.** Jablonski energy diagrams: **(A)** In SHG active, *i.e.*, non-centrosymmetric, materials, two infra-red photons can combine into one visible photon under frequency doubling. **(B)** In THG active materials, *i.e.*, at interfaces with different refractive indices, three infra-red photons can combine into one visible photon under frequency tripling. **(C)** One photon or two photon absorption can lead to electronic excitation from  $S_0$  to  $S_1/S_2$  in fluorophores. After internal conversion the emission occurs from the vibrational ground state of the first excited state.  $S_0$  electronic ground state,  $S_1/S_2$  electronic excited states,  $v=0-3$  vibrational states, dashed lines denote virtual states.

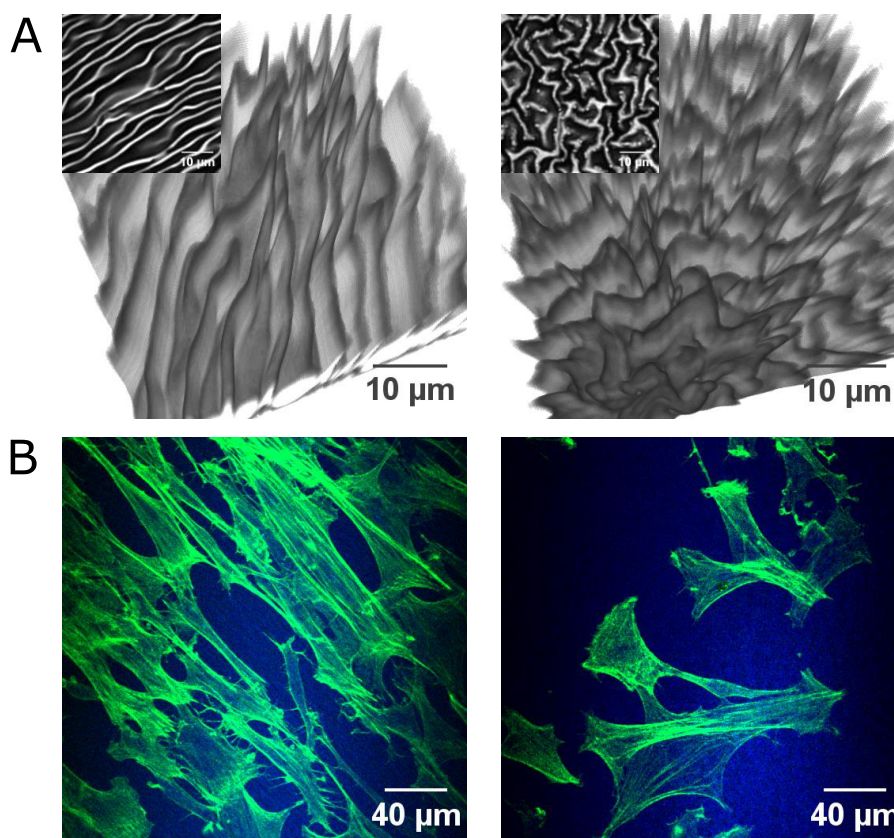


**Figure 14. rADSC on patterned ELP hydrogels.** **(A)** Dried ELP hydrogels containing cell adhesion motifs are either imprinted with aligned (left) or unaligned (right) patterns that vary in spacing (wavelength) and height. The 3D structures of the patterns can be visualized with CARS (grey,  $2930\text{ cm}^{-1}$ ); however techniques with higher spatial resolution, *i.e.*, AFM are better suited to quantitatively extract wavelength and height. **(B)** rADSC align their cytoskeleton (green, MPEF, Alexa488-Phalloidin for F-actin) with the pattern direction (left) or remain randomly oriented (right) on the hydrated gels (blue, CARS,  $2930\text{ cm}^{-1}$ ). Scale bar: 10 and 40  $\mu\text{m}$ .



## Nonlinear microscopy of adipocyte physiology (Paper I - III)

CARS microscopy targeting a single vibrational frequency, *e.g.*,  $2845\text{ cm}^{-1}$  for lipids, has been extensively employed for different lipid-containing samples: *in vitro* in lipid vesicles [201], lipid bilayers [202], [203], plant cell walls [204], intact skin [205], and hepatocytes [206], and *in vivo* in *c. elegans* [207] and mice [192]. Most of these studies have been proof-of-concept due to the novelty and complexity of CARS microscopy. Thus, the aim for **Paper I – III** was to connect established methods in the fields of tissue engineering and *in vivo* biology with nonlinear microscopy to explore both applications and limitations.

### CARS microscopy for AT engineering (Paper I – II)

Tissue engineering is an expanding field of *in vitro* biology, based on the idea that in order to generate functional cell models *in vitro* or to support tissue regeneration *in vivo*, not only chemical stimulation but also mechanical scaffolds are needed. Thus, cells are either placed on a surface with stimuli or embedded in a 3D environment. The biological reasons behind this and the findings from the **Paper I & II** will be further discussed in **Chapter 4**. The enhanced complexity of the samples increases the demands for analytical methods.

In **Paper I**, ADSC were placed on patterned hydrogels, while in **Paper II** they were added to electrospun polycaprolactone (PCL) fibers that strongly resemble the native ECM in terms of size and shape. Hydrogels have been used for a multitude of biomedical applications as reviewed by Hoffman [206]. Their great appeal is the high water content, which is important for transport of nutrients to cells inside the gels.

EM calls for either a conductive coating to be applied or drying of the samples. Moreover, the samples need to withstand handling in vacuum and at low temperatures for sectioning. Such harsh sample preparations can change existing morphologies or introduce new structures into the hydrogel. Thus, less invasive methods like atomic force microscopy (AFM) or optical techniques are better suited. Label-free methods are preferred since especially in hydrogels unspecific accumulations of hydrophobic fluorescence or absorbance dyes with the proteins can occur [206].

In **Paper I**, micro molding was used to imprint soft hydrogels from recombinant elastin-like protein (ELP) with aligned or unaligned patterns with different periodicities and consequently the response of rat ADSC to these patterns is explored (**Figure 14**). Since the hydrogels were made of protein, the  $\text{CH}_3$  vibration at  $2930\text{ cm}^{-1}$  was used for CARS imaging. In order to test the response of stem cells to the surfaces, either the cellular cytoskeleton, here F-actin, or the full cytosol were labelled and probed with MPEF concurrently with CARS for lipids and CARS for the ELP scaffold. The MPEF signals were readily separated from the CARS signals using both dichroic mirrors and filters, and with time-gated signal collection. In addition, the near infrared lasers facilitate the excitation of the fluorophores on top of the 50 – 100  $\mu\text{m}$  thick gels.

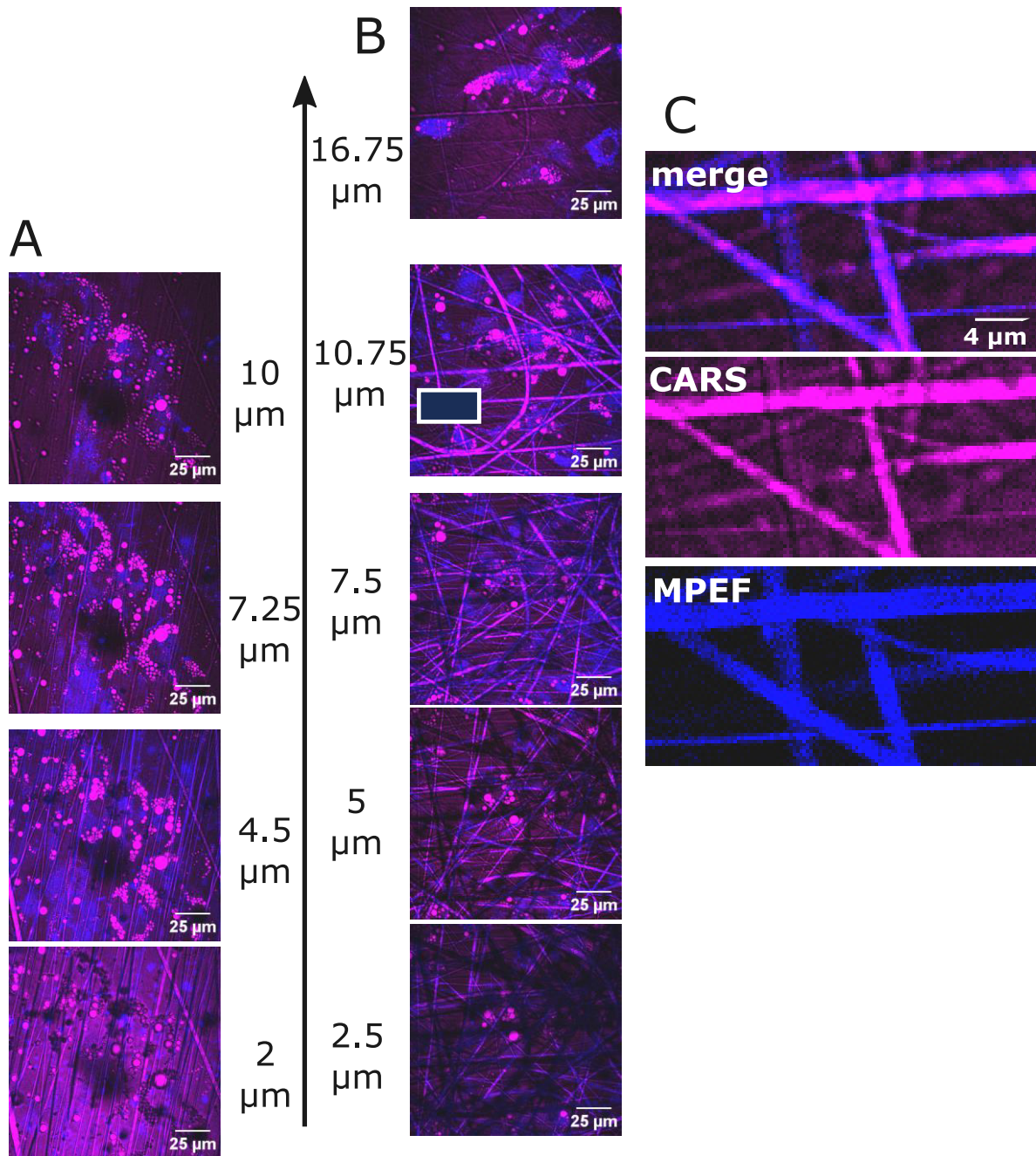


**Figure 15. hADSC on PCL fibers.** hADSC were differentiated towards adipocytes on a matrix of electrospun PCL fibers for 8 days. The fibers in the matrices were either **(A)** aligned or **(B)** random. The aligned matrix is approximately 7  $\mu\text{m}$  in thickness consisting of one layer of fibers, while the random matrix is 14  $\mu\text{m}$  thick with two layers of fibers as estimated from the average depth of CARS (magenta,  $2845\text{ cm}^{-1}$ )/MPEF (blue) z-stacks. Distance above the bottom is indicated with numbers. It can be seen (from the presence of LDs and cytosolic fluorescence) that in the random matrix few cells are at 5-7  $\mu\text{m}$  within the matrix. Most cells are on the surface of the matrix similar to the cells on top of the aligned fibers. Cells can be located from the LDs and cytosolic fluorescence. **(C)** However, the PCL matrix itself also shows both CARS and MPEF (zoom in from the white rectangle in B). The zoomed in images also demonstrate the difference in background for CARS and MPEF. CARS shows NRB over the full image, while for MPEF the majority of the signal comes from the fiber. Scale bars: 25 and 4  $\mu\text{m}$ .

This allowed both the study of cell-material interaction, as well as the response of the cytoskeleton inside the cell, showing that aligned wrinkles on the hydrogel can induce an alignment of the stem cells after 24h. The insights from this analysis are detailed in **Chapter 4**.

In **Paper II**, human ADSC were challenged with patterned surfaces. In this work, a commercial electrospun PCL matrix was used. The variation of the surfaces is only in the alignment of the fibers, not in their diameter or distance between them. Undifferentiated ADSC are solely identified *via* their intrinsic fluorescence. Here, time-gating of the signal is of special importance since the fibers display both a CARS signal at  $2845\text{ cm}^{-1}$  and intrinsic fluorescence. The contribution of the latter can be reduced if only photons that arrive within the instrument response time are considered. Using such time-dependent signal discrimination allows separation of signals from cells and fibers. Thereby, we found that the cells only minimally sink into the matrix (**Figure 15**). Thus, most cells are found on top of the fibers and not between them. Next, we differentiated the cells towards white adipocytes and followed the differentiation *via* the accumulation of LDs. These contribute a strong CARS signal at  $2845\text{ cm}^{-1}$ . For classical lipid stains, like Oil-Red-O, the hydrophobic nature of the fibers lead to unspecific binding of the dye and the separation of fiber and lipid signals during the estimation of the differentiation became more challenging. Due to the ability to generate optical sections with CARS and with the help of the intrinsic MPEF the cell area could be determined, then the CARS signal of the lipids could be thresholded to estimate the diameter of the formed droplets with an adapted voxel analysis as used by Lynn *et al.* [208]. We found that the ADSC differentiated on the aligned nanofiber matrices resembled extracted mature adipocytes most in functionality, albeit not in morphology. Qualitative investigations of adipogenic differentiation with CARS microscopy have also been employed by other groups [171], [209], [210].

#### **CARS microscopy to investigate the metabolic state of *ex vivo* AT (Paper III)**

Whole tissue samples add an additional complexity compared to cells on top of matrices. Since CARS microscopy does not need thin samples, the utilization of living *ex vivo* tissues, as applied in **Paper III**, is possible (**Figure 16A, B**). Especially for lipid containing tissues, this poses the advantage that the lipids remain within the cells and thus allows the estimation of cellular morphology as found *in vivo*. Explanted AT can be cultured for a limited time (several hours) before functionality and gene expression change and apoptosis starts [211]. Thus, fluorescent staining which relies on active cellular metabolism, *e.g.*, rhodamine123 for mitochondrial membrane potential, can be employed for MPEF measurements [212], [213]. This can be combined with SHG imaging for fibrillar collagens, as found in the tissue ECM, and CARS at  $2845\text{ cm}^{-1}$  for the lipids (**Figure 16C**).

Then, the metabolic state of AT can be compared by measuring mitochondrial activity and lipid volume per cell (**Figure 17**). For the purpose of this analysis the central plane of each cell is determined, and then the cell area is measured from the MPEF image with increased contrast settings.

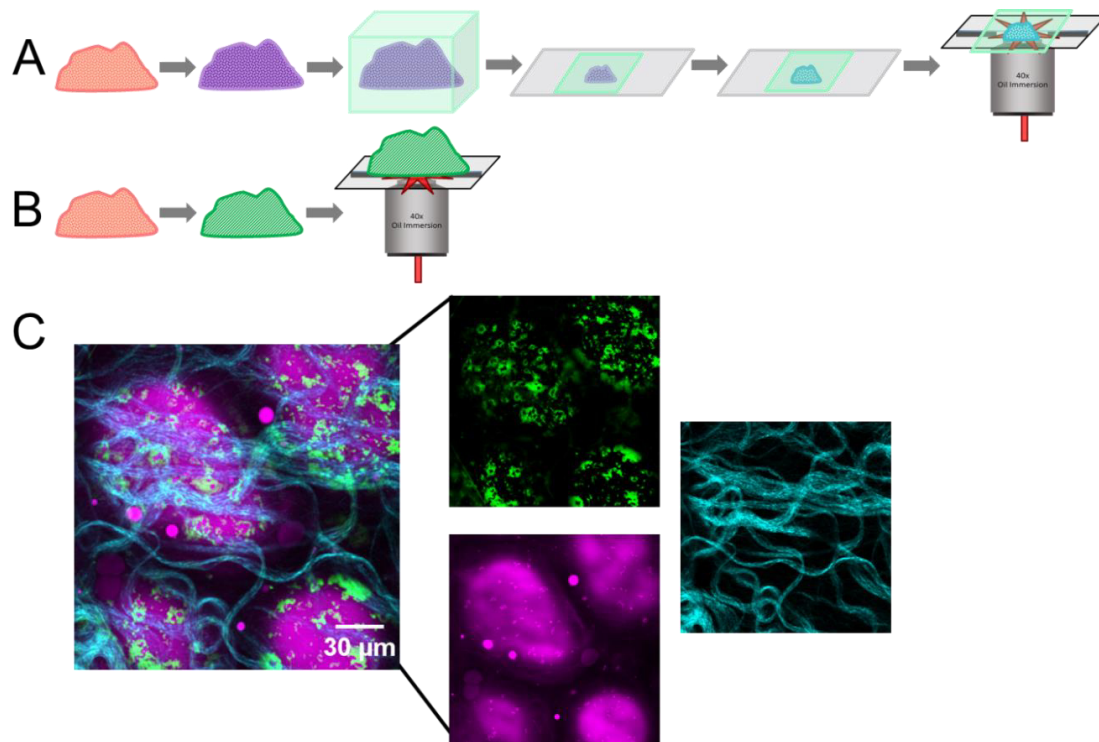


**Figure 16. Nonlinear microscopy for *ex vivo* living tissue.** (A) For CLSM tissue samples are fixed/snap-frozen, embedded, cut into slices, stained/fixed, and visualized. (B) For nonlinear microscopy of AT, staining is done for full *ex vivo* tissue pieces (if required), the full tissue piece is visualized within one hour of extraction and kept at 37°C on the microscope stage. (C) CARS (lipids, 2845  $\text{cm}^{-1}$ , magenta), MPEF (active mitochondria, green, Rho123), and SHG (fibrillar collagen, cyan) Scale bar: 30  $\mu\text{m}$ .

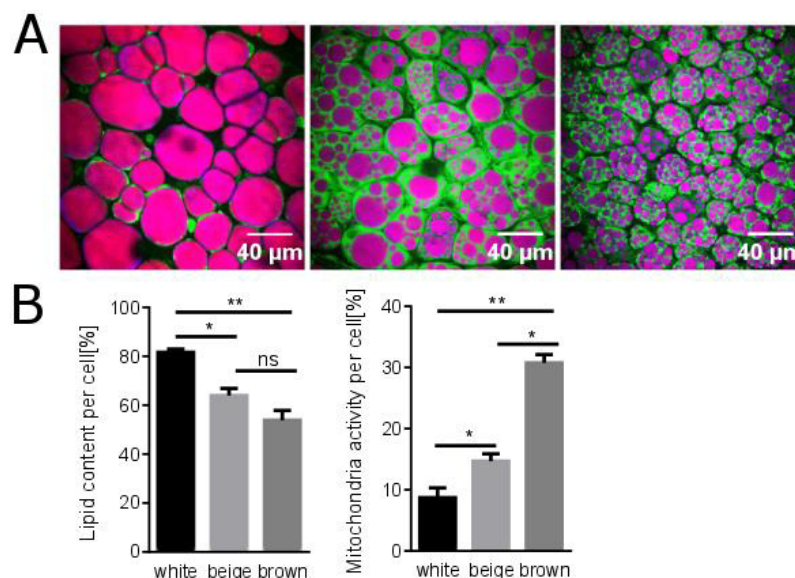


**Figure 17. Lipids and mitochondria in the three adipocyte shades.** (A) White, beige, and brown adipocytes in *ex vivo* mouse tissue. Left: iWAT from 9 week old C57/BL6 mice, middle: after 10 day injection with  $\beta_3$  AR agonist (CL316,243, 1  $\mu\text{g/g}$ ), right: interscapular BAT. Lipids are shown in magenta (CARS), mitochondria in green (MPEF, Rho123). Scale bar: 40  $\mu\text{m}$ . (B) For each cell a lipid content and mitochondria activity can be determined, allowing a ranking of the metabolic state of the AT. Brown as the most active tissue, has the lowest lipid content and highest mitochondria activity.  $N = 5$  mice. Mean  $\pm$  SEM. Multiple two-tailed, unpaired Mann-Whitney tests. P values were ranked  $P > 0.05$  (ns, not significant),  $P \leq 0.05$  (\*),  $P \leq 0.01$  (\*\*).

Afterwards, automated thresholding is performed to determine lipid area and the area covered by the brightest, *i.e.*, most active, mitochondria. Both are set into relation with the cell area thus giving a percentage quantity. The comparison of percentages instead of absolute fluorescence intensity allows the correlation of mitochondrial activity between different measurement days, since fluctuations in the fluorescence emission can occur due to minor changes in beam shape and/or overlap, or staining efficiency. This is especially useful for mixed tissues, like beige AT, where beige adipocytes can be analyzed separated from unilocular white adipocytes. However, it is also useful for the comparison of genetic effects on BAT and WAT, as shown in **Paper III**.

## Toolbox II: Visualization of LD chemistry

While in some cases the morphology is a good indicator for metabolic changes in cells, it can be of equal importance to know cellular contents. In the case of LDs, changes in carbon saturation and chain length can be linked to diseases [89], [90].

The most common analysis method to characterize TAG chain length and saturation relies on sample destruction and extraction of all lipids that are then derivatized and separated with gas chromatography [214]. In order to couple this chemical to spatial information, three techniques can be employed: (i) magnetic resonance imaging (MRI), (ii) matrix-assisted laser desorption/ionization mass spectrometry imaging (MALDI-MSI), and (iii) Raman microspectroscopy or broadband CARS (BCARS) microscopy. MRI can be applied in variant samples *in vivo* [215], [216] although the resolution of 10  $\mu\text{m}$  (xy) and 100  $\mu\text{m}$  (z) limits it to the investigation of bigger lipid depots [217]. Both MALDI-MSI and BCARS rely on fixed samples. For BCARS, these are then cut into thin sections (as done in **Paper V**), while MADI-MSI relies the embedding in a complex matrix. The highest resolution achieved with the latter technique has been 1.4  $\mu\text{m}$  in mouse brain [218]. The resolution BCARS is in principle limited by the diffraction limit at  $\sim 300\text{ nm}$  [184].

### BCARS microscopy

Spectral CARS has been proposed shortly after the development of single frequency CARS microscopy [219]–[222]. After data processing the resulting spectra are similar to spontaneous Raman spectra, which can generate a chemical fingerprint based on unique vibrations found in each molecule and has been used for biological samples [223]. However, due to the low signal intensities even in good scatterers, like lipids, it takes around 0.5 s to acquire a single spectrum [224]. With the BCARS setup used in **Paper IV & V**, the collection time per pixel can be reduced to 5 ms to acquire a full spectrum between 600 and 3400  $\text{cm}^{-1}$ .

In order to probe a full BCARS spectrum, typically a broadband Stokes beam is employed [225]. The broadband supercontinuum can be generated inside a photonic crystal fiber [226]. Often a charge-coupled device (CCD) detector is used, where vertical binning generates a linear array of non-negative integers, *i.e.*, signal intensities per wavenumber [179]. A single

spectrum is collected in each image point and sample scanning can be performed to acquire a spectral map.

Although the collection of BCARS images is faster than spontaneous Raman spectral images, the read out is more challenging due to the contribution of the non-resonant background. This non-resonant component is non-frequency dependent and entirely real, while the resonant component that contains the chemical information can be divided into a real and imaginary part. The imaginary part is directly comparable to spontaneous Raman signals [227]. Both display a linear dependence on molecular concentration [179]:

$$\begin{aligned} \text{Im}\{\chi_R^{(3)}\} &= \frac{N A \Gamma}{\left(\Omega - (\omega_p - \omega_s)\right)^2 + \Gamma^2} \\ I_{\text{Raman}} &\propto \frac{N A \Gamma}{(\Omega - \omega_0)^2 + \Gamma^2} \end{aligned} \quad \text{eq. 6}$$

$N$  is here the number of scatterers,  $A$ ,  $\Omega$ ,  $\Gamma$  amplitude, frequency, and line width of the vibrational mode.

In order to obtain the imaginary part of  $\chi_R^{(3)}$  from raw BCARS spectra, the convolution of the resonant and non-resonant components has to be overcome.  $\text{Im}\{\chi_R^{(3)}\}$  can be extracted if the spectral phase is known, which can be achieved with a modified Kramers-Kronig relation [228]. However, this analysis is technically only applicable to data covering an infinite frequency range. In order to extrapolate the data, one method can be the use of a Fourier transformation, replacing the negative time domain with a frequency dependent non-resonant response, and transforming back to the frequency domain. The relevant mathematical basis to this method has been established by Liu, Lee, and Cicerone [229] and is not within the scope of this thesis work. For **Paper IV & V**, the estimation of the frequency dependent non-resonant response is done either in glass or medium surrounding the samples. Error phase correction was achieved either with (i) an iterative noise-maintaining approach [230] modified to be model-free with the use of a Savitzky-Golay smoothing filter or (ii) an iterative fourth-order polynomial function. Resulting spectra are referred to as Raman-like [231].

#### **TAG chain length and saturation maps *in situ* (Paper IV & V)**

TAG saturation can be mapped in differentiated 3T3-L1 adipocytes from BCARS spectra using the ratio of  $1650 \text{ cm}^{-1} / 1450 \text{ cm}^{-1}$  [232]. Di Napoli *et al.* show further that this ratio can be used both on phase-retrieved spectra and from raw CARS images along with  $2930 \text{ cm}^{-1} / 2885 \text{ cm}^{-1}$  and  $3010 \text{ cm}^{-1} / 2855 \text{ cm}^{-1}$  [233]. Additionally, the same group has shown that an unsupervised factorization approach to decompose chemical components from the Raman-like spectra generated from BCARS data delivers a lipid spectrum, where the same ratios are correlated with the number of double bonds [234]. The disadvantage of this ratio is that only one quantity for TAG chemistry, the number of double bonds, is determined while the chain length is not taken into consideration. In algae, it has been shown that the  $1650 \text{ cm}^{-1} / 1450$

$\text{cm}^{-1}$  from spontaneous Raman spectra can be correlated with number of double bonds and  $N_{\text{C}=\text{C}}/N_{\text{CH}_2}$ . This allows then the calculation of the chain length [235]. However, since the data is collected with spontaneous Raman spectroscopy, the measurements are slow causing low throughput. More promising are methods that employ the full spectrum to obtain information about the lipid species. The use of more than two peaks makes the method more robust for interferences of other cellular components like protein or nucleic acids. Schie *et al.* tested different least square decomposition of spontaneous Raman spectra for this purpose in an hepatic cell line [236]. However, they limit their analysis to oleic and palmitic acid. While these two lipid species belong to the most common chains found in AT, the limitation of the analysis of only two fatty acids, leaves no room to monitor changes such as the increase of chain length and mono-unsaturation that are found in connection with obesity and insulin resistance [237].

Therefore, **Paper IV** aims to generate a spectral decomposition method that employs the full spectral range, but does not make any assumptions about the chains found in the TAGs. First, a matrix is generated containing the known spectra of pure TAGs and a generic protein coupled to the information about their lipid content, chain length, number of C=C bonds, and protein content. The constraint matrix is a 7x4 matrix, which makes the problem overdetermined. Thus, the following equation is used for the decomposition:

$$\text{Minimize } \|\text{Standards} - \text{Constraints } X\| \quad \text{eq. 7}$$

In order to solve the equation, an iterative QR factorization of a constrained least square problem is employed (MatrixLLS in Igor Wavemetrics). In that way four components can be generated of which three represent TAG properties and one the independent protein component. The TAG components do not have to be real spectral features, *i.e.*, non-negative, since they stem from the same chemical species and are thus expected to have peaks in the same locations. Rather, the first component is a general lipid spectrum, while the chain length and #C=C components represent spectral changes in defined locations, which can either be positive and negative.

Once the four components have been determined, unknown spectra can be decomposed with the following equation:

$$\begin{aligned} \text{Meas}(f) = & a * C_{\text{TAG}}(f - f_0) + b * C_{\#C=C}(f - f_0) + c * C_{\#CH_2}(f - f_0) \\ & + d * C_{\text{protein}}(f - f_1) + m * f + e \end{aligned} \quad \text{eq. 8}$$

$a$ ,  $b$ ,  $c$ , and  $d$  are weights of the four components,  $f$  is the Raman shift, and  $f_0$  or  $f_1$  respectively allow for slight shifts of lipid and protein components in the measured data (*Meas*). The residual is minimalized with a Levenberg-Marquardt least-squares method during the curve fitting.



In **Paper IV**, this method was verified for accurate calculation of average TAG chain length and #C=C for pure TAGs, their mixtures, and food oils. For the collection of a BCARS map, less than 1  $\mu\text{l}$  sample is required, while for GC separation  $\sim 500 \mu\text{l}$  are used. Thus, the BCARS method allows a fast estimation of TAG content in liquids, although it does not offer the chemical species resolution as obtained with GC and coupled detection, *e.g.*, flame ionization detection or mass spectrometry.

However, a second advantage of this methods is the possibility to explore differences in TAG chain length and #C=C in space, as in cells (**Figure 18**). Here, we found that the error increases due to the geometry of the droplets and the difference in refractive index with the surrounding aqueous medium ( $n_{\text{oil}} = 1.46$ ,  $n_{\text{water}} = 1.33$ ) [238]. This affects the outer shell of the LD, where typically longer chain lengths are found and the number of C=C differs up to 10% from the center of the droplet. We also noted, that the root mean square error increases in biological samples compared to pure oils, which is due to increased samples complexity. In conclusion, we found the method to be most suitable for organisms with  $> 1 \mu\text{m}$  LDs as found in differentiated adipocytes. Thus, this technique is most applicable in mammalian cell cultures, tissue sections, plant physiology, and food emulsions.

The technique developed and characterized in this way was then applied to WAT, BAT, and liver slices in **Paper V**. In order to balance optimal signal strength and avoid sample damage, adipose tissue was sliced at lower temperatures than liver ( $-39^{\circ}\text{C}$  *vs.*  $-14^{\circ}\text{C}$ ) and the proteins were crosslinked during thawing to avoid disturbances of the cellular morphology (**Figure 19**). This allowed the observation that BAT lipids, similar to liver lipids, assume a composition closer to the diet after one week, while iWAT adapts after four weeks.



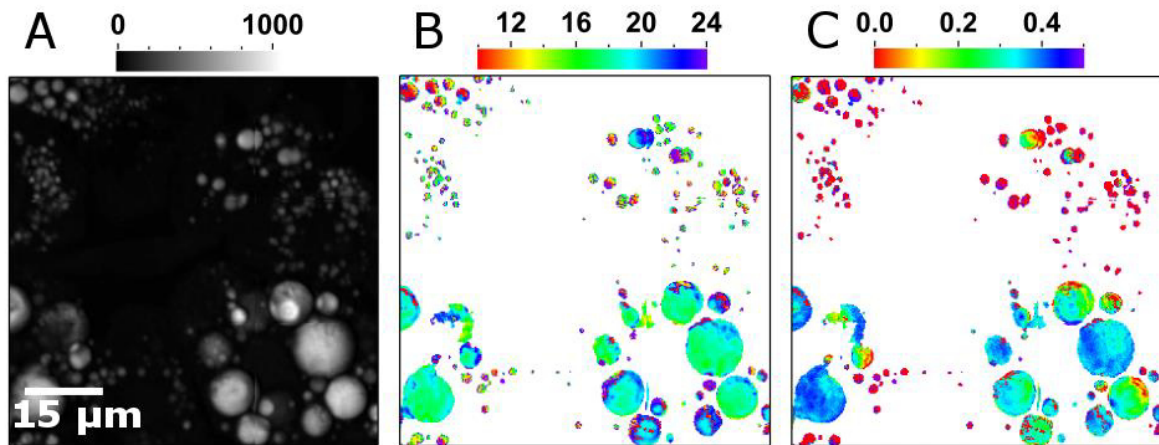


**Figure 18. TAG chain length and C=C maps.** (A) Integrated symmetric  $\text{CH}_2$  stretching vibration intensity ( $2845\text{ cm}^{-1}$ ) to show LDs in differentiated 3T3-L1 adipocytes. (B) Spatial map of TAG chain length and (C) number of C=C bonds. Scale bar:  $40\text{ }\mu\text{m}$ .

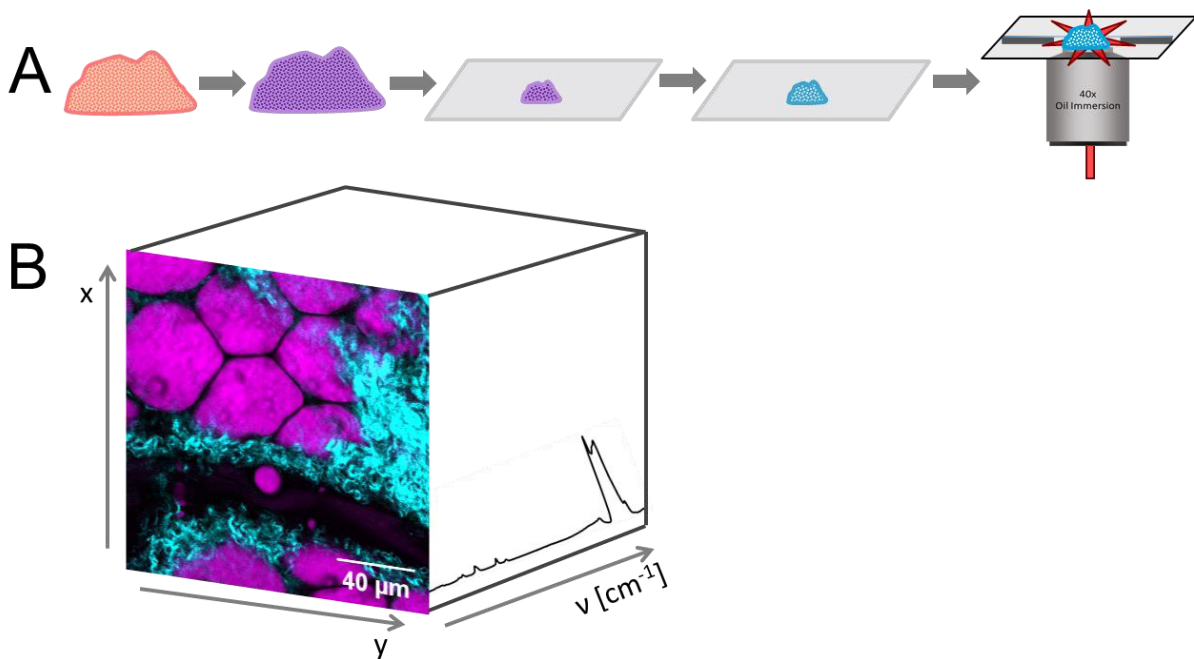


**Figure 19. BCARS for sliced tissue.** (A) For BCARS measurements, the tissue was snap-frozen, sliced ( $20\text{ }\mu\text{m}$ , at  $-39^\circ\text{C}$ ), fixed (4% para formaldehyde, 150 mM sucrose,  $4^\circ\text{C}$ ), and then visualized. (B) BCARS images contain a third dimension of information, the spectral dimension, where each image pixel contains a full BCARS spectrum. From there single wavelengths can be used to visualize, e.g., all lipids (magenta,  $2845\text{ cm}^{-1}$ ). BCARS microscopy can be combined with other methods, e.g., SHG (fibrillar collagen, cyan). Scale bar:  $40\text{ }\mu\text{m}$ .



# **Chapter 4. Adipose Tissue Heterogeneity**



# 4 Adipose Tissue Heterogeneity

## Surface pattern perturbations of *in vitro* rat and human ADSC (Paper I & II)

*In vivo*, stem cells get important cues from both the extra-cellular matrix (ECM) and soluble chemical factors that decide, *e.g.*, if they will undergo proliferation, differentiation or apoptosis [142], [145], [239], [240]. Due to the intricacy of the natural cellular environment these factors remain intertwined and the investigation of these processes *in vivo* is intrinsically circuitous. An impressive amount of materials have been used in an attempt to mimic the natural ECM and to influence stem cell fate in both conventional two-dimensional (2D) as well as three-dimensional (3D) culture systems as reviewed for example by Dawson *et al.* [241]. With the use of such advanced materials for cell culture, it has been shown that not only surface chemistry in both 2D [242], [243] and 3D [244] cell cultures, but also physical properties like the elastic modulus [245] or surface topography on nano- [246]–[248] and microscale [249]–[251] play an important role in driving cell fate. While much attention is devoted to the influence of the matrix on osteogenic differentiation, it has also been shown that ADSC need ECM stimulus for soft tissue differentiations towards, *e.g.*, adipocytes [252]–[256].

In order to fully understand how individual factors influence stem cells in 3D cell cultures, it is desirable to work with materials which allow for the independent tunability of biological relevant factors, *i.e.*, cell adhesion, matrix stiffness, and matrix topography. Protein hydrogels, particularly those made from elastin like peptides (ELPs), offer such control over protein properties combined with effective cytocompatibility. ELPs have been inspired by the amino acid sequence of elastin, one of the major components of the ECM especially in connective tissues [257]. Additionally, bioactive properties can be included into the engineered amino acid sequence, *i.e.*, sites for enzymatic degradation [258] and integrin specific adhesion [259], *e.g.*, the tripeptide RGD, which is present in fibronectin and other ECM matrices [260]. A plasmid equipped with the appropriate sequence allows the production of ELP, with desired properties, in bacterial cultures using standard laboratory techniques. This results in high batch-to-batch reproducibility, in comparison to natural extracted ECM materials, *e.g.*, matrigel, collagen, or alginate, and straightforward scalability. Furthermore, ELPs can be formed into hydrogels for cell encapsulation using a chemical crosslinked [261]–[265]. My work focused on exploring how features on nano- and microscale in soft hydrogels influence adipogenesis of ADSC.

In order to explore the limitations for surface patterns on ELP hydrogels, in **Paper I**, we used a micro molding approach. The patterns, *i.e.*, 1D and 2D wrinkles, were generated with reactive ion edging in polystyrene with wavelengths and depths spanning nano- to micro-

range [266]. For the transferal of the pattern, an intermediate polydimethylsiloxane (PDMS) stamp was used. We could show that on ELP patterns down to  $0.37\ \mu\text{m}$  wavelength (pattern width:  $250 \pm 50\ \text{nm}$ , height:  $50 \pm 30\ \text{nm}$ ) could be imprinted. While smaller patterns could be found on the stiffer PDMS (3 MPa [267]) the pattern formation ELP is not only limited by the softness (400 kPa) but also by the formation of ELP-rich domains. These domains form due to lower-critical solution temperature (LCST) behavior of ELP by transitions above  $33^\circ\text{C}$  and are  $\sim 124 - 180\ \text{nm}$ .

In a next step, rat ADSC were subjected to the patterned surfaces and their initial attachment was observed. Cell movement and attachment to natural patterned surfaces are especially important for cancer cell migration [268], angiogenesis [269], and mechanotransduction [270]. The ADSC placed on the aligned scaffolds, start off loosely adherent and move to form contact, both with the matrix and with other cells. Such contacts were shown to be important for osteogenic [271] and adipogenic [272] differentiation. While the cells adhere loosely, they keep their round cell shape and form long cytosolic protrusions to interact with the matrix and other cells. However after 12 hours, the cells spread onto the hydrogel surface and start to align with the pattern. They still show active migration that is not confined by the direction of the pattern. Nevertheless, the pattern direction does initiate the majority of cells to orient accordingly, as seen from the alignment of F-actin inside the cytosol after 24 hours (**Figure 20**). The alignment according to the surface topography has been shown with similar patterns on PDMS with embryonic stem cells (ESC) [273] and smooth muscle cells [274]. Similarly to the smooth muscle cells on PDMS, we found that there is a limit for ADSC to sense the surface topography of ELP and align their cytoskeleton. In our case, that limit were wrinkles with  $0.37\ \mu\text{m}$  wavelength with heights of  $50 \pm 30\ \text{nm}$ , while for the smooth muscle cells on PDMS the limit was  $0.1\ \mu\text{m}$  wavelength with  $20\ \text{nm}$  height. The fact that higher/wider wrinkles could not be recognized on ELP might be due to the nano-features on the wrinkles caused by the ELP-rich aggregates and the large swelling of ELP after hydration.

In **Paper II**, I went further to investigate the effect aligned or unaligned substrates on the adipogenic differentiation of human ADSC. For the purpose of this study, electrospun PCL fibers were selected as cell culture matrix due to their ideal prerequisite for diffusion of nutrients and oxygen, possibility to trap some of these nutrients, and cytocompatibility. The diffusion of nutrients is mainly limited by the pore sizes found in ECM-mimicking materials and can then lead to apoptosis if the cells are undersupplied [275]. Due to shallow depth of the PCL fiber substrates ( $10\text{-}20\ \mu\text{m}$ ), the diffusion should not be limited. Additionally, we found that the cells rather attach on top of the matrix than inside (**Figure 21**), which lead us to classify the culture as 2.5D (a system between 2D and 3D stem cell cultures [276]), similar to the wrinkled hydrogels (**Paper I**). Although PCL has no cell adhesion sites, in contrast to ELP, both materials are hydrophobic, which means that proteins from serum added to the cell culture medium form hydrophobic interactions with the matrix, slowing their diffusion, and therefore helping the stem cells with nutrient uptake [277] and attachment. Lastly, PCL has shown biocompatibility and is a Food and Drug Administration (FDA) approved material for the use in humans as a contraceptive barrier [277].



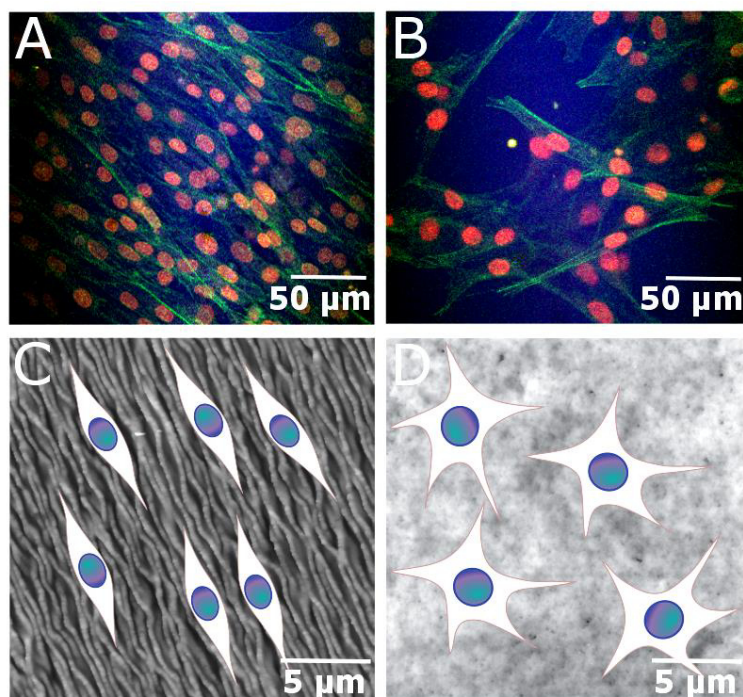


**Figure 20. Alignment of rADSC.** Stem cells align on (A) wrinkles with  $0.60 \mu\text{m}$  in wavelength with  $130 \pm 40 \text{ nm}$  height, but not on (B) with  $0.37 \mu\text{m}$  wavelength with  $50 \pm 40 \text{ nm}$  height. Hydrated ELP (blue, CARS,  $2930 \text{ cm}^{-1}$ ), nuclei (red, MPEF, Hoescht34580), F-Actin (green, MPEF, Alexa488-Phalloidin). (C, D) Schematics of the typical cell shape on these patterns (dry ELP, grey, AFM). Cells are not in scale. Scale bars: 40 and  $5 \mu\text{m}$ .

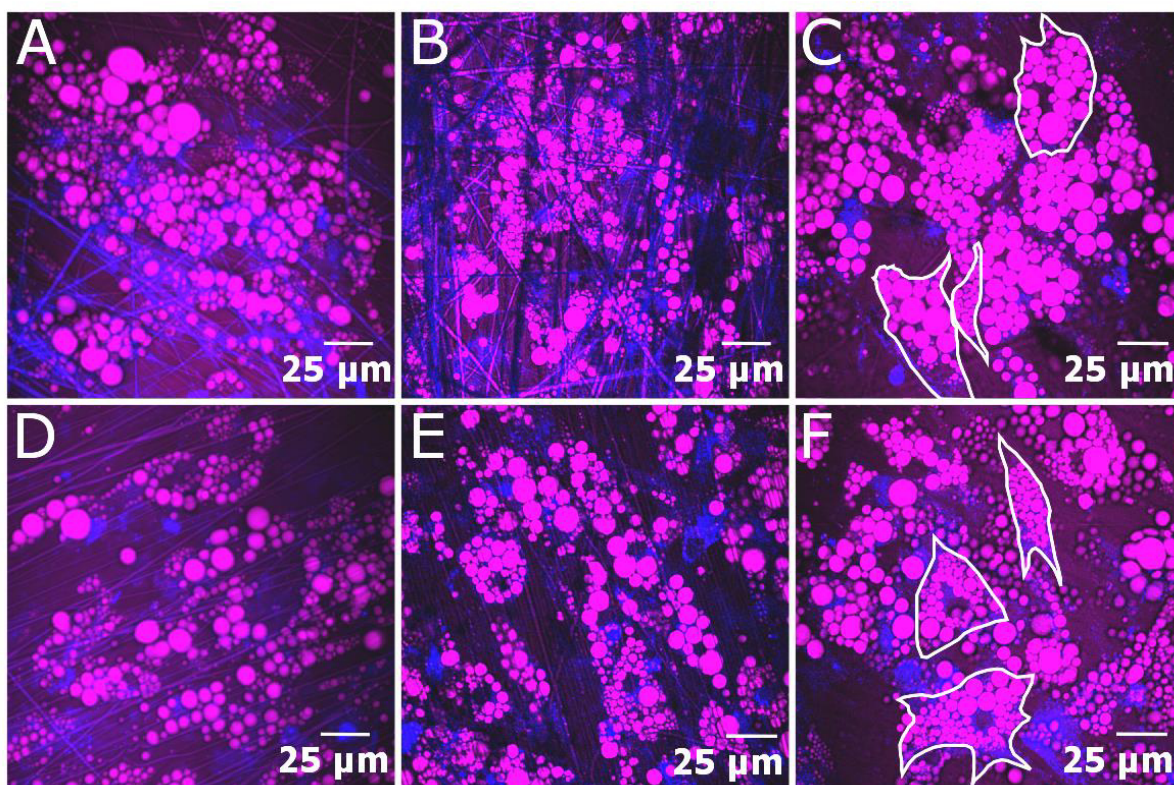


**Figure 21. hADSC differentiated for 14 days on PCL.** (A-C) Unaligned PCL fibers: (A) sum over full thickness of the z-stack. (B) Some cells are between the fibers, (C) while other cells are on top of the matrix. (D-F) Aligned PCL fibers: (D) sum over full thickness of the z-stack. (E) Some cells are on top of the fibers, (F) and a second layer forms on top of these cells. Lipids (magenta, CARS,  $2845 \text{ cm}^{-1}$ ), intrinsic fluorescence (blue, MPEF), estimated cell outlines (white). Scale bars:  $25 \mu\text{m}$ .

Furthermore, PCL containing matrices have been used to enhance adipogenesis/chondrogenesis [278] and electrospun matrices have been used for adipogenesis of ESC [279].

By using aligned or unaligned PCL fiber matrices we found an effect on maturation during adipogenesis. When comparing lipid accumulation, we found more lipids in cells grown on aligned fibers, while the cells grown on both matrices display larger LDs, than the cell culture plastic control (**Paper II**). However, in all of the evaluated systems, there are multiple LDs per cell, in contrast to the unilocular LDs found in mature adipocytes *in vivo*. Yet more crucial than morphology, is the functionality of the differentiated stem cells. We aimed for a more mature phenotype, and used isolated mature adipocytes as a comparison. Here, we found the dose response curve of insulin-stimulated glucose uptake to be closer to mature adipocytes in both fiber matrices than the 2D control. While the cells on the unaligned fibers showed the highest glucose uptake upon stimulation, they also show a high basal uptake, which does not mimic the behavior of the mature cells. Thus, the aligned fibers produce the cells which resemble the mature adipocytes the most. While we did not find differences in gene expression or lipolysis, we still believe the cells differentiated on the aligned fiber matrix to be one step closer to a functional *in vitro* model of adipogenesis than the 2D control.

Summarizing from the *in vitro* studies in **Paper I & II** and other unpublished results, it can be remarked that the modelling of *in vivo* function is a complex challenge. At the same time, from these *in vitro* studies, new mechanistical insights into and material systems for stem cell differentiation and advanced analysis techniques can be developed for application *in vivo*.

### Genetic perturbations of *in vivo* mouse adipocytes (Paper III)

While *in vitro* cultures allow unique insight into isolated adipocyte function, *in vivo* systems can shed light on mechanisms connecting all the organs involved during the development of obesity and its connected diseases. Already in the 1950s, it was proposed that obesity is not purely linked to positive energy balance cause by behavior alone but that genetic factors also play a role [280]. However, gene expression or mutations are a challenging target for drugs [280], thus cell signaling through, *e.g.*, protein kinases or phosphatases might be a more promising target [281]. Several kinases have been described for the function of WAT [282], BAT [42], and in connection with obesity/insulin resistance [283].

One serine/threonine protein kinase (STK)25, part of the sterile 20 (STE20) kinase superfamily [284], has been identified as a regulator for lipid partitioning, and systemic insulin and glucose homeostasis in mice and humans [285]–[293]. **Paper III** is based on the observation that STK25 mRNA and protein is found both in BAT and WAT [285], [286], [288], and therefore might be involved in the adipocyte dysfunction seen during obesity. To investigate this link, high-fat diet (HFD) fed *Stk25* transgenic and knockout mice [286], [294]



were compared to their corresponding wild-type (WT) littermates. Three AT depots were investigated: interscapular BAT, and inguinal/subcutaneous WAT and (peri)gonadal/epididymal WAT (in the paper referred to as sWAT/eWAT, in this thesis referred to as iWAT/gWAT). In the transgenic (TG) mice overexpressing *Stk25* HFD-induced lipid accumulation, inflammation, and fibrosis are aggravated. Specifically, with a combination of CARS for lipids and MPEF for active mitochondria stained with rhodamine123 (Rho123), we could observe that the cellular mitochondrial activity decreases while the lipid content increases. This is also qualitative visible from more unilocular LDs in BAT and lower Rho123 fluorescence. In iWAT/gWAT the same trends are found. These observations are further confirmed with MitoTracker Red staining (active mitochondria) and ATGL/HSL activity (inverse correlation with lipid content). In the knockout (KO) mice that are depleted of STK25 protein, a protective effect against HFD-induced changes could be observed instead. In the STK25-KO, the mitochondrial activity increased and the lipid content decreased against WT littermates. The depletion of STK25 protein was further simulated using *Stk25* siRNA in brown, HIB-1B, and white, 3T3-L1, adipocyte cell lines. In the transfected HIB-1B cells lipid accumulation was reduced, and  $\beta$ -oxidation and mitochondria area augmented. However, no change in fatty acid influx or storage in TAG was observed. LD size was also reduced in the transfected 3T3-L1 adipocytes. These findings on *in vitro* adipocytes combined with the *in vivo* pathology, leads to the conclusion that altered mitochondrial activity might be central to the role of STK25 in ATs. Interestingly, a downregulation of mitochondrial activity has been found in obese humans with decreased fatty acid oxidation and linked to insulin resistance [295].

## Nutritional perturbations of *in vivo* mouse adipocytes (Paper V)

The regular consumption of certain foods has been linked with an increased risk for obesity and diabetes, *e.g.*, foods/drinks with added sweeteners [296]–[298]. Further, a data analysis study on 48 170 white European adults suggest an impact of total fat consumption, and more so the consumption of saturated fat, on the BMI [299]. In fact, not only the absence of carbon-carbon double bonds in TAGs but also the exact location of existing double bonds seems to play a role on the human metabolic health [300]–[302]. In C57BL/6J mice, obesity can be induced with a HFD [303]. As discussed in **Chapter 2**, there are two pathways for the generation of TAGs: (i) *de novo* lipogenesis or (ii) direct esterification of FAs. The main sites for both processes are liver and AT. While diet induced changes in WAT [304], [305] and liver [306] have been explored extensively, the role of BAT is more elusive. It has been found that BAT mass increases in the early stages of weight gain in mice [307], that BAT is involved in the short-term clearance of TAGs in the postprandial period [53], and that the TAG chemistry in BAT changes upon arousal from hibernation [308].

In **Paper V**, we followed the changes of TAG chemistry after one and four weeks of HFD using the BCARS method established in **Paper IV**. Additionally, we tracked changes on a gene expression level. Already after one week of HFD, mice showed increases in LD size in

BAT, iWAT, gWAT, and liver, compared to littermates fed chow diet (CD) (**Figure 22**). In BAT, this results in a shift from multilocular to unilocular LDs (42.2x increase in volume), an observation that has previously been described as ‘whitening’ of BAT and linked to a loss in function [309]. After four weeks of HFD intervention, the fold increase in LD size is less pronounced (3.3x) while there transition from multilocular to unilocular remains. Along with changes in LD diameter, we also found changes in expression of genes involved in *de novo* lipogenesis after one week in BAT and liver. In iWAT the adaptation of genetic expression becomes only significant after four weeks. The observed changes in gene expression indicate that *do novo* lipogenesis is reduced under HFD. Although similarly to other studies, we find a restoration of the expression of these genes in liver under HFD, which has been previously linked to a remodelling of hepatic fatty acids rather than *de novo* lipogenesis under HFD [310]. Still, the downregulation of these genes indicate that changes in TAG chemistry are more likely to result from uptake of dietary fatty acids. On average, the diet provides more unsaturated fatty acids than the chains found in all the tissues. In both BAT and liver, more unsaturated TAG chains are observed after one week of HFD (**Figure 22**), while for iWAT this increase only occurs after four weeks of HFD. It has been previously found that not all dietary fatty acids are taken up equally, rather there is a preference in monounsaturated and n-6 polyunsaturated fatty acids in human iWAT [311], which could be an behind the increase of unsaturation under HFD. If all data is considered, it can be hypothesized that BAT and liver behave similarly and due to their relatively faster metabolism they are responsible to deal with the initial lipid load, while iWAT has a slower adaptation rate and thus adapts slowly over to increase long term storage of lipids under prolonged HFD. However, if the lipid load from the diet remains high, WAT cannot store all the lipids, which leads to ectopic lipid depositions in liver and muscle [312], and speculatively also BAT. The initial role for lipid buffering as hypothesized for BAT and liver, can be also seen from data which follow lipid accumulation in liver over time and show that the accumulation is not a linear process but rather spikes after short term interventions, decreases intermediately (4 weeks in mice), and then increases again [306].

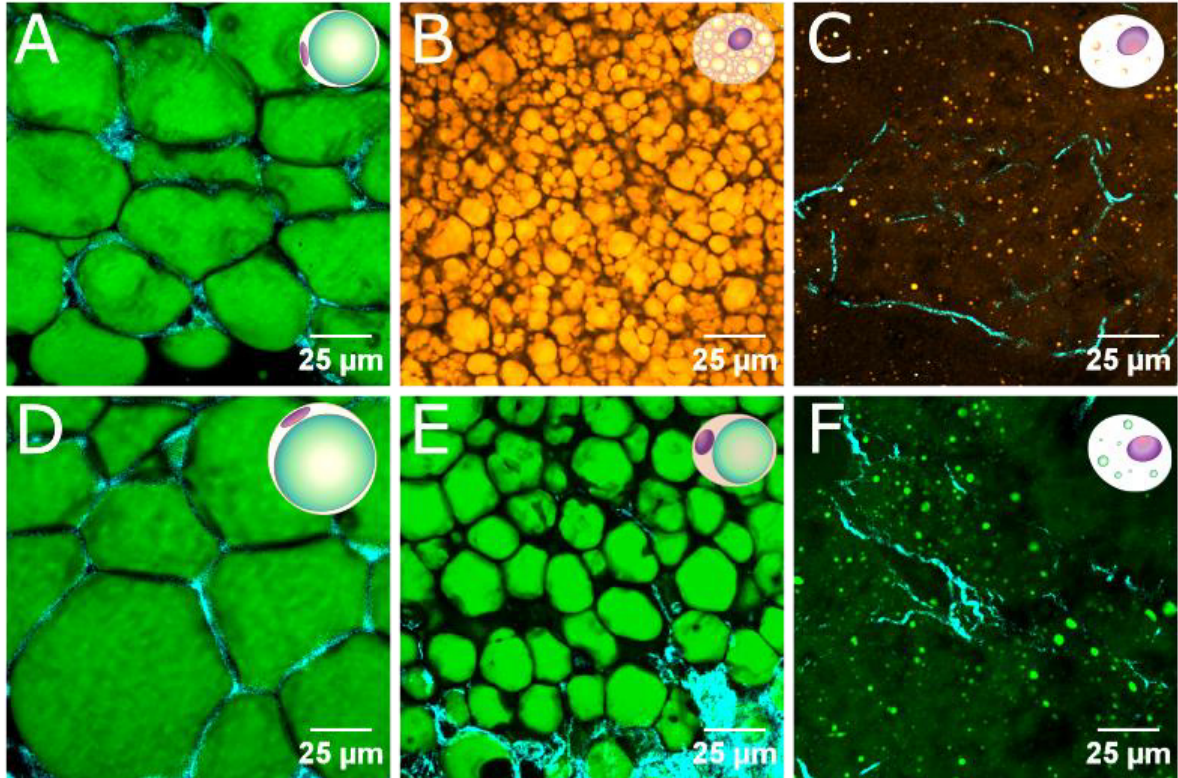


**Figure 22. TAG unsaturation in lipid tissues.** (A, D), iWAT, (B, E) BAT, and (C, F) liver after one week CD (top row) or one week HFD (bottom row). Changes in gWAT are analogous to iWAT. Lipids ( $2845\text{ cm}^{-1}$ , CARS): orange  $\sim 0.5$  double bonds per TAG molecule, green:  $\sim 0.7 - 0.8$ , fibrillar collagen (SHG, cyan). Schematics show LDs inside the cells. Scale bars:  $25\text{ }\mu\text{m}$



## **Chapter 5. Concluding Remarks**



# 5 Concluding Remarks

The focus on AT function in health and disease has increased due to the rise in rates of obese individuals. Especially with the discovery of brown and beige adipocytes in adult humans, the field has received increased traction and interest. However, with growing understanding of AT function, the number of unaddressed questions seems to increase and the need for new analytical techniques has expanded. The research presented in this thesis, focuses on the gap of chemical biology analytical techniques for investigating of AT and cells in various contexts as related to development and pathology *in situ*.

## Methods development

In **Paper I & II**, single frequency CARS microscopy is applied both to study living ADSC in interaction with soft and hydrated ECM-mimicking. Furthermore, the accumulation of LDs in individual cells on top of an analytical interfering matrix has been demonstrated in **Paper II**. This application can then be extended to living adipocytes in *ex vivo* tissue in **Paper III**. Since single frequency CARS microscopy does not require thin slices, the lipids in the adipocytes remain unperturbed in contrast to many other methods. Especially in white adipocytes with small cytosolic volume, a bursting of the cells will also result in a displacement of other organelles, which hinders the study of *in vivo* cell morphology. With the LDs contained inside the adipocytes, a mitochondrial activity staining was also added to simultaneously monitor the primary organelles involved in energy storage and expenditure.

In a next step, we extended the analysis to include information on TAG chemistry in addition to adipocyte morphology. For that purpose, we characterized a method for spectral fitting of Raman-like spectra, collected with BCARS microscopy, from TAGs as demonstrated in **Paper IV**. We could show the acquisition of TAG chain length and number of C=C bonds maps for various model systems. In contrast to most previous studies, we employ a broad spectral range to increase the robustness of the method.

## Biological applications

Spectroscopic methods are often developed as a proof-of-concept, and it takes a long time before they are applied to answer interdisciplinary scientific questions. CARS microscopy has only in the recent years been employed for a broad range of material science, biological, and clinical questions, as a result of the developments of commercial microscopes, increased outreach, and interdisciplinary collaboration. Therefore, it has been of special interest in this thesis work to not only develop methods, but also to apply them within the field of adipocyte biology in model systems with different complexity.

**Paper I** follows the initial attachment ADSC on a wrinkled hydrogel substrate, where they align their cytoskeleton according to the wrinkle direction. There is a lower size limit for

structures on which the cells align and on matrices where the cells align, their migration direction is not uniaxial. **Paper II** adds to these results by showing that an aligned substrate can induce a more mature functional phenotype in adipogenic-differentiated ADSC. These findings are in line with other studies showing that ADSC are mechanosensitive and might be of relevance to the changes in ECM that occur during obesity. Moreover, studying stem cell differentiation *in vitro* and *in vivo* might add to the understanding of AT expansion during weight gain

While certain questions can be fully answered using isolated cultures of adipocytes, in **Paper III & V** we focused on mouse whole body adjustments to genetic or nutritional perturbations, respectively. The increased or decreased expression of *Stk25* can cause whole-body disruptions upon high-fat feeding and in AT specifically, we observed an effect on mitochondrial activity and cellular lipid content (**Paper III**). The presented data leads to the conclusion the *Stk25* might act *via* interference with the mitochondrial  $\beta$ -oxidation. While these findings indicate a possible target to decrease the effects of HFD feeding, we also aimed to further the understanding how HFD feeding affects lipid containing tissue. Therefore, in **Paper V** we follow the changes of TAG chain length and saturation in the early stages of HFD stimulation. BAT is affected in a similar fashion by HFD as liver, points towards an involvement of both tissues in the initial clearance of increase lipid influx. WAT, which typically stores excess TAGs, adapts at a slower rate to the HFD feeding.

### Future directions

In summary, this thesis situated at the interface of physics, material science, and biology, demonstrates the application of advanced microscopy techniques to current biological challenges. As obvious from the number of papers not included in this thesis work, there is a multitude of scientific questions that can be addressed, especially in a collaborative research environment. Since research is a dynamic progress, there have been unfinished projects and a number of new questions along the way.

In a continuation of the work presented in this thesis, the most scientifically relevant and interesting direction would be towards *in vivo* experiments with samples from humans. However, they are limited in availability and require both strict ethical considerations and experimental planning. An interesting method to consider in this context might be coherent Raman endoscopy [313]. Further, since the BCARS method used in **Paper IV & V** needs only small amounts of sample, it would be possible to work with human AT biopsy samples. An interesting experimental outline would be the comparison of TAG chemistry, adipocyte morphology, and gene expression of BAT and WAT in metabolically healthy obese, obese with metabolic syndrome, and a lean control group. If the samples could be collected in a hospital close to a CARS microscope, it would additionally be possible to employ the mitochondrial activity staining as shown in **Paper III**. However, while such an experiment would certainly unravel details about human AT physiology, the groups would at the same time be difficult to match and patient-to-patient variability might outweigh changes induced by metabolic health.



Thus, in a more practical context it would be exciting to take the *in vitro* results from **Paper I & II** into 3D. Especially, beige/brown adipogenesis has not been extensively mimicked in cell cultures, although there is some indication that hydrogel encapsulation can enhance ESC differentiation towards brown/beige adipocytes [314]. Considering, that obesity leads to an ECM-remodeling, a matrix with tunability of biological properties allows for increased control over experimental factors. This increased control, along with ethical considerations about the use of animals, is the main advantage of *in vitro* systems, while *in vivo* experiments reveal interactions and pathological changes. Along the course of my PhD project, I have worked with several promising 3D matrices, which could be used for adipogenesis (**Figure 23**): porous ELP hydrogels, collagen hydrogels with different fiber morphology, and decellularized AT. The latter has successfully been used to drive white adipogenesis of hADSC [253], [315]. The main challenges in 3D matrices are the perfusion of nutrients and possibly a low number of cells that are encapsulated in the matrix. Due to the 3D nature of the system, nonlinear microscopy as evaluation tool can be of increased use and provide value in combination with studies on cellular function.

Personally, I find the latter aspect the most intriguing, *i.e.*, to advance the developed methods so they can be applied to functional studies. One example of a functional study would be the observation of lipolysis in real time from either cultured cells or intact tissue samples. Further, it might be possible to follow ‘browning’ of cultured white adipocytes over time, *i.e.*, follow changes in lipid morphology and mitochondrial activity. An additional project, which I personally would like to pursue, is the uptake of fatty acids in cultured white and beige/brown adipocytes to see if our *in vivo* findings can be replicated *in vitro* where added clues about the role of BAT in lipid clearance could be established.

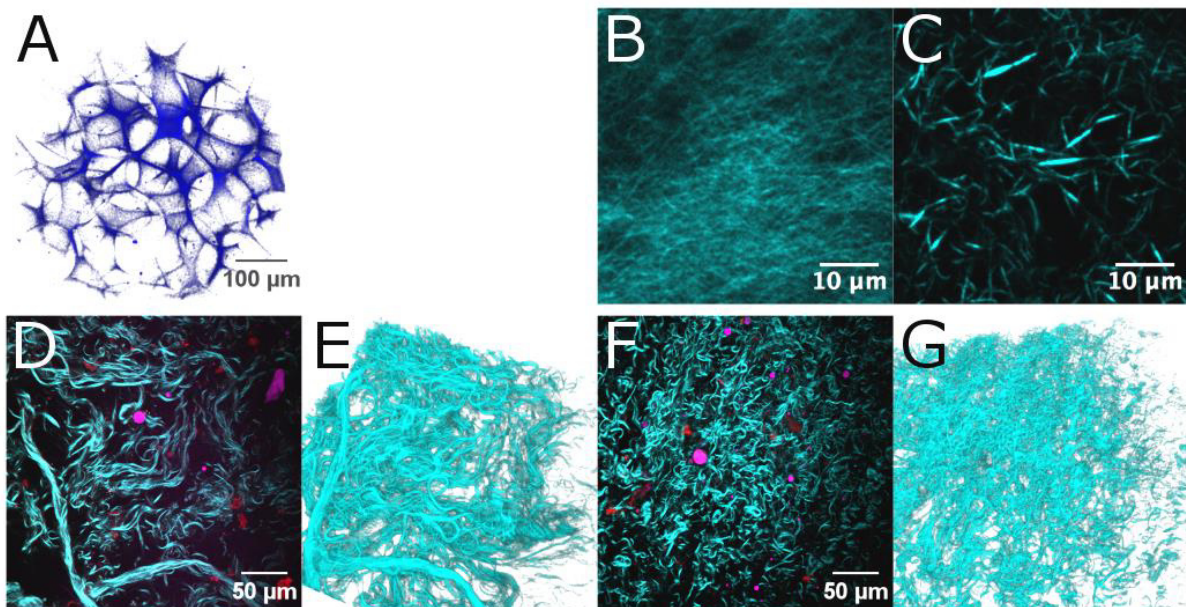


**Figure 23. 3D matrices.** (A) Microporous ELP, (B, C) collagen hydrogels formed at 20°C (B) or 37°C (C), (D-G) decellularized WAT (D, E) or BAT (F, G) from rat. Hydrated ELP (blue, CARS, 2930  $\text{cm}^{-1}$ ), fibrillar collagen (cyan, SHG), lipids (magenta, CARS, 2845  $\text{cm}^{-1}$ ), intrinsic fluorescence (red, MPEF). (A, E, G) 3D renderings. Scale bars: 100, 10, and 50  $\mu\text{m}$ .



# **Acknowledgements**



# Acknowledgements

*"In the end, we will all be judged by the courage of our hearts." – Sense8*

*My heart is with all the brave women who fight for their rights every day, all the children crossing oceans to find a better future, all that do not have equal opportunities in their lives, all struggling with oppression, gender norms, or mental health, and all who are brave enough to take on every day.  
You are not alone.*

First, I want to thank my amazing supervisors: **Cecilia**, you were there for me throughout my project and supported me to become an independent scientist. You were also there to pick me up, when times seemed the hardest and to celebrate each and every single step forward. You are a great role model! **Sapun**, I am really thankful that you welcomed me fully into your lab even when you might have not known what you are getting into. You included me right away in your group and I always had a place to come back to. You taught me how to think critical and I truly enjoy discussing science with you. Your group meetings are a great place to test and defend ideas and to grow as a scientist. **Pernilla**: thank you for supporting me on my way to PhD. This might have not been your typical supervision, but you trusted me that I would be able to get there. At the same time you made sure to clear my way and that I was not left alone at Chalmers.

I also want to thank all the students who walked this way with me. Without you, this would not have been possible. First, our **FINON group**: **Diana, Michael, Juris, Xiao, Amala, Naya, Attilio, Alberto, Carolina, Marie, Siyuan, Vitalis** and **Steffi**. You gave me a lot of strength! The adventures with you made it worth to attend all the FINON meetings. And especially with **Xiao** (凌霄), I always had someone to share PhD and life troubles. 由衷的謝謝你! Luckily, we usually could get some tasty Asian food with **Amala** and **Steffi** to then start forgetting all the troubles. **Michael, Juris**, and **Diana**, you were always there in Sweden and we went through so much. It is still hard to think about it all and to see that not all of us made it out. **Juris**: I miss fikas and discussions with you. **Michael**: thanks for keeping me company during lunch. **Diana**: without your support in these hard times, I would not have made it. You are so understanding and supportive and you shower me with cat pictures (**Tiger** as best model) that make me happy again. Then there was the group at Chalmers, **Duong, Mahesh, Juan Carlos. Duong**: thank you for all the help and support during the beginning of my PhD project. Thank you and **Sebastian** for including us in your Swedish country life. There were of course also the fantastic students in our lab that brought fresh ideas and questions: **Maria, Robin, Jannek, Arsalan, Akanksha**, and **Erik**. Stay curious! I also want to thank **Pernilla's group** and the **ChemBio division** who made sure I did not have to sit alone in an office,

## Acknowledgements

---

supported me, and turned the research environment by 180°. And, of course **Sapun's fantastic group** in Mainz, who guaranteed I had friends at the department in Mainz: **Yu-Jen, Frederik, Mischa, Samet, Sabine, and Xiao** (again). Thanks **Yu-Jen** (王裕仁) for helping me procrastinate with good food, good talks, and everything else. 真心的謝謝妳 Then I am happy about the people I met through the student council, which were there also during hard times, especially **Linnea** and **Gaowa**. You are two amazingly strong women! **Linnea**, alla besök hos dig och **Bosse** var fylld med feminism och bubbel. Så många bra tjejer på ett och samma ställe hjälpte mig att slappna av en stund och glömma allt som hände. **Benjamin**, you will do a great job in the future.

I also want to thank the people who taught me so much about science and inspired me on my way: **John Frostad, Thorsten Wohland, Werner Huppert, Dagmar Auerbach**, and especially **Gregor Jung**, who always has an open ear for my ideas and plans. Danke für Deine selbstlose und andauernde Unterstützung, **Gregor. Daggi**, auch wenn ein gebrochenes Bein in den Weg kam, bin ich froh Dich getroffen zu haben und wünsche Dir und Deiner tollen Familie alles Gute für die Zukunft.

My PhD work would have also not been possible without all my collaborators: **Ingrid Wernsted-Asterholm, Eduard Peris, Peter Micallef, Belén Chancón, Charlotta Olofsson, Margit Mahlapuu, Emmelie Cansby, Silva Sütt, John Grünberg, Johannes Elvin, Kristi Kiick, Hang Kuen Lau, Sarah Heilshorn, Huiyuan Wang, Sharon Chen. Ingrid**: thank you for always being there with new and exciting ideas and to discuss science. **Lotta**: thank you for providing me with lab space and all the support I needed. **Margit**: thank you for the pleasant, constructive, and fun collaboration. **Huiyuan**: we had an amazing time during your summer at Chalmers and it is always a pleasure to do science with you. You inspire me. 由衷的謝謝你

Natürlich wäre ich nicht hier, hätten wir nicht so viele Stunden im Foyer zusammen verbracht: **Pui, Tobi, Tanja, Nadine, Jessi H., Jessi B., Tim Sch., Tim B., Roland, Fabian, Aljosha, Oli, Dennis, Andi, Kai, Alex**. Wir wären vermutlich alle durchgedreht wenn wir nicht ab und zu (so circa ein bis zwei mal) abgeschaltet hätten mit Laborparties, Nächten im Blau, Tagen im Europapark oder einfach in der Sonne. Es ist toll zu sehen wie wir alle unseren Weg finden. Ich glaub noch immer an unser Chemiker Dorf ;). **Alex**, ohne deine Hilfe mit OC hätte ich es sicher nicht so weit geschafft. Danke für all den Kaffee, den du getrunken hast, und all den Kuchen, den du dir von meiner Ma hast „aufzwingen“ lassen.

During my undergrad, I also met the amazing **CISEI summer students** at UCSB. We were a great team, had the best road trips, 'whale' sightings, and especially **Victor** and **Caroline** made my start at Chalmers so much easier. 8

Dann muss ich mich natürlich bei meiner **Familie** bedanken, die mich unterstützt haben als ich von Land zu Land gezogen bin, wenn ich so müde war nach der Uni dass ich nicht mal reden wollte, und die all die Feiertage/Geburtstage die ich verpasst habe, akzeptieren. Danke **Mama** für all die Lernhilfe und deine Unterstützung auf meinem Weg zu einer starken

unabhängigen Frau. Du bist mein Vorbild. Danke **Papa**, dass du immer da bist und du immer einen Weg findest mir zu helfen. Danke **Oma** für all die Stunden zusammen und dass du akzeptiert das ich nicht immer in der Nähe bin. Danke **Opa** dass du mir von klein auf geglaubt hast, dass ich Wissenschaftlerin werden kann. **Pascal**, ich bin stolz auf dich und es macht Spaß zu sehen wohin dein Weg geht. Danke an all meine Familie für die Unterstützung: **Karin, Helmut, Arthur, Brigitte, Victor, Laura, Stephan, Manfred H., Jacqueline, Manfred D., Lisa, Martin, Flo, Dani, Zoe, Sophie, Julia, Manu, Paul, Eva.**

Sist men inte minst måste jag tacka **Leo**. Du är min styrka. Tack att du accepterade all övertid jag lade in för att driva mitt projekt. Du stöttade mig och förstod när jag behövde resa till Tyskland igen och igen. Du fanns alltid hemma och det stöd som du givit mig uppskattar jag otroligt mycket. Du är min familj i Sverige, du är mitt hem, och du är mitt hjärta. Tack.





## References



# References

- [1] WHO, “Obesity and overweight fact sheet,” 2016. [Online]. Available: [www.who.int/mediacentre/factsheets/fs311/en/](http://www.who.int/mediacentre/factsheets/fs311/en/). [Accessed: 21-Jan-2018].
- [2] S. Furukawa, T. Fujita, M. Shimabukuro, M. Iwaki, Y. Yamada, Y. Nakajima, O. Nakayama, M. Makishima, M. Matsuda, and I. Shimomura, “Increased oxidative stress in obesity and its impact on metabolic syndrome,” *J. Clin. Invest.*, vol. 114, no. 12, pp. 1752–1761, 2004.
- [3] J. Wu, P. Boström, L. M. Sparks, L. Ye, J. H. Choi, A.-H. Giang, M. Khandekar, K. A. Virtanen, P. Nuutila, G. Schaart, K. Huang, H. Tu, W. D. Van Marken Lichtenbelt, J. Hoeks, S. Enerbäck, P. Schrauwen, and B. M. Spiegelman, “Beige adipocytes are a distinct type of thermogenic fat cell in mouse and human,” *Cell*, vol. 150, no. 2, pp. 366–376, 2012.
- [4] M. J. Betz and S. Enerbäck, “Human brown adipose tissue: What we have learned so far,” *Diabetes*, vol. 64, no. 7, pp. 2352–2360, 2015.
- [5] D. Wang and S. Bodovitz, “Single cell analysis: The new frontier in ‘omics,’” *Trends Biotechnol.*, vol. 28, no. 6, pp. 281–290, 2010.
- [6] T. S. Church, D. M. Thomas, C. Tudor-Locke, P. T. Katzmarzyk, C. P. Earnest, R. Q. Rodarte, C. K. Martin, S. N. Blair, and C. Bouchard, “Trends over 5 decades in U.S. occupation-related physical activity and their associations with obesity,” *PLoS One*, vol. 6, no. 5, pp. 1–7, 2011.
- [7] D. M. Cutler, E. L. Glaeser, and J. M. Shapiro, “Why Have Americans Become More Obese?,” *J. Econ. Perspect.*, vol. 17, no. 3, pp. 93–118, 2003.
- [8] J. O. Hill, “Understanding and addressing the epidemic of obesity: An energy balance perspective,” *Endocr. Rev.*, vol. 27, no. 7, pp. 750–761, 2006.
- [9] J. Rosenblum and R. D. Venkatesh, “Obesity,” in *The MassGeneral Hospital for Children Adolescent Medicine Handbook*, P. Jackson, A. Yule, and T. Wilens, Eds. Springer, 2017, pp. 67–76.
- [10] OECD, “Obesity Update 2017,” 2017. [Online]. Available: <https://www.oecd.org/els/health-systems/Obesity-Update-2017.pdf>. [Accessed: 21-Jan-2018].
- [11] V. S. Malik, W. C. Willett, and F. B. Hu, “Global obesity: trends, risk factors and policy implications,” *Nat. Rev. Endocrinol.*, vol. 9, no. 1, pp. 13–27, 2013.
- [12] AACE/ACE Obesity Task Force, “AACE/ACE position statement on the prevention, diagnosis, and treatment of obesity (1998 Revision),” *Endocr. Pract.*, vol. 4, no. 5, pp. 297–350, 1998.
- [13] D. O. Okorodudu, M. F. Jumeau, V. M. Montori, A. Romero-Corral, V. K. Somers, P. J. Erwin, and F. Lopez-Jimenez, “Diagnostic performance of body mass index to identify obesity as defined by body adiposity: A systematic review and meta-analysis,” *Int. J. Obes.*, vol. 34, no. 5, pp. 791–799, 2010.
- [14] A. Romero-Corral, V. K. Somers, J. Sierra-Johnson, R. J. Thomas, M. L. Collazo-Clavell, J. Korinek, T. G. Allison, J. A. Batsis, F. H. Sert-Kuniyoshi, and F. Lopez-Jimenez, “Accuracy of body mass index in diagnosing obesity in the adult general population,” *Int. J. Obes.*, vol. 32, no. 6, pp. 959–966, 2008.
- [15] E. Oliveros, V. K. Somers, O. Sochor, K. Goel, and F. Lopez-Jimenez, “The Concept of Normal Weight Obesity,” *Prog. Cardiovasc. Dis.*, vol. 56, no. 4, pp. 426–433, 2014.
- [16] J. Kaur, “A Comprehensive Review on Metabolic Syndrome,” *Cardiol. Res. Pract.*, p. 943162, 2014.
- [17] H. Buchwald, R. Estok, K. Fahrbach, D. Banel, M. Jensen, W. Pories, J. Bantle, and I. Sledge, “Weight and Type 2 Diabetes after Bariatric Surgery: Systematic Review and Meta-analysis,” *Am. J. Med.*, vol. 122, no. 3, pp. 248–256, 2009.
- [18] D. Hofsø, N. Nordstrand, L. K. Johnson, T. I. Karlsen, H. Hager, T. Jenssen, J. Bollerslev, K. Godang, R. Sandbu, J. Røislien, and J. Hjelmæsæth, “Obesity-related cardiovascular risk factors after weight loss: A clinical trial comparing gastric bypass surgery and intensive lifestyle intervention,” *Eur. J. Endocrinol.*, vol. 163, no. 5, pp. 735–745, 2010.
- [19] L. Sjöström, A.-K. Lindroos, M. Peltonen, J. Torgerson, C. Bouchard, B. Carlsson, S. Dahlgren, B. Larsson, K. Narbro, C. D. Sjöström, M. Sullivan, and H. Wedel, “Lifestyle, Diabetes, and Cardiovascular Risk Factors 10 Years after Bariatric Surgery,” *N. Engl. J. Med.*, vol. 351, no. 26, pp. 2683–93, 2004.
- [20] F. Rubino, A. Forgione, D. E. Cummings, M. Vix, D. Gnuli, G. Mingrone, M. Castagneto, and J.

- Marescaux, "The Mechanism of Diabetes Control After Gastrointestinal Bypass Surgery Reveals a Role of the Proximal Small Intestine in the Pathophysiology of Type 2 Diabetes," *Ann. Surg.*, vol. 244, no. 5, pp. 741–749, 2006.
- [21] F. Rubino and M. Gagner, "Potential of surgery for curing type 2 diabetes mellitus," *Ann. Surg.*, vol. 236, no. 5, pp. 554–559, 2002.
- [22] W. J. Pories, M. S. Swanson, K. G. MacDonald, S. B. Long, P. G. Morris, B. M. Brown, H. A. Barakat, R. A. DeRamon, G. Israel, J. M. Dolezal, and et al., "Who would have thought it? An operation proves to be the most effective therapy for adult-onset diabetes mellitus," *Ann. Surg.*, vol. 222, no. 3, pp. 332–339, 1995.
- [23] A. Bartelt and J. Heeren, "Adipose tissue browning and metabolic health.," *Nat. Rev. Endocrinol.*, vol. 10, no. 1, pp. 24–36, 2014.
- [24] S. Rayalam and C. A. Baile, "Adipocyte Growth and Factors Influencing Adipocyte Life Cycle," in *Adipose Tissue Biology*, 1st ed., M. Symonds, Ed. Springer, 2012, pp. 195–226.
- [25] J. Kopecky, "Adipose Tissue and Fat Cell Biology," in *Lipids and Skin Health*, A. Pappas, Ed. Springer, 2015, pp. 201–224.
- [26] S. Cinti, "The adipose organ at a glance," *Dis. Model. Mech.*, vol. 5, pp. 588–594, 2012.
- [27] D. E. Chusyd, D. Wang, D. M. Huffman, and T. R. Nagy, "Relationships between Rodent White Adipose Fat Pads and Human White Adipose Fat Depots," *Front. Nutr.*, vol. 3, no. 10, 2016.
- [28] J.-P. Després and I. Lemieux, "Abdominal obesity and metabolic syndrome," *Nature*, vol. 444, no. 14, pp. 881–887, 2006.
- [29] C. Dani and N. Billon, "Adipocyte Precursors: Developmental Origins, Self-Renewal, and Plasticity," in *Adipose Tissue Biology*, 1st ed., M. E. Symonds, Ed. Springer, 2012, pp. 1–16.
- [30] J. S. Choi, Y. C. Choi, J. D. Kim, E. J. Kim, H. Y. Lee, I. C. Kwon, and Y. W. Cho, "Adipose tissue: A valuable resource of biomaterials for soft tissue engineering," *Macromol. Res.*, vol. 22, no. 9, pp. 932–947, 2014.
- [31] B. A. Bunnell, M. Flaatt, C. Gagliardi, B. Patel, and C. Ripoll, "Adipose-derived Stem Cells: Isolation, Expansion and Differentiation," *Methods*, vol. 45, no. 2, pp. 115–120, 2008.
- [32] T. Tchkonina, T. Thomou, Y. Zhu, I. Karagiannides, C. Pothoulakis, M. D. Jensen, and J. L. Kirkland, "Mechanisms and Metabolic Implications of Regional Differences among Fat Depots," *Cell Metab.*, vol. 17, no. 5, pp. 644–656, 2013.
- [33] L. L. Listenberger, X. Han, S. E. Lewis, S. Cases, R. V. Farese, D. S. Ory, and J. E. Schaffer, "Triglyceride accumulation protects against fatty acid-induced lipotoxicity," *Proc. Natl. Acad. Sci.*, vol. 100, no. 6, pp. 3077–3082, 2003.
- [34] K. Frayn, "Adipose tissue as a buffer for daily lipid flux," *Diabetologia*, vol. 45, no. 9, pp. 1201–1210, 2002.
- [35] J. E. Schaffer, "Lipotoxicity: When tissues overeat," *Curr. Opin. Lipidol.*, vol. 14, pp. 281–287, 2003.
- [36] R. T. Brookheart, C. I. Michel, and J. E. Schaffer, "As a Matter of Fat," *Cell Metab.*, vol. 10, no. 1, pp. 9–12, 2009.
- [37] E. Zacharewicz, M. K. C. Hesselink, and P. Schrauwen, "Exercise counteracts lipotoxicity by improving lipid turnover and lipid droplet quality," *J. Intern. Med.*, 2018.
- [38] D. C. W. Lau, B. Dhillon, H. Yan, P. E. Szmitko, S. Verma, C. W. David, B. Dhillon, H. Yan, and P. E. Szmitko, "Adipokines : molecular links between obesity and atherosclerosis," *Am. J. Physiol. - Hear. Circ. Physiology*, vol. 288, pp. H2031–H2041, 2005.
- [39] P. Trayhurn, N. J. Temple, and J. Van Aerde, "Evidence from immunoblotting studies on uncoupling protein that brown adipose tissue is not present in the domestic pig.," *Can. J. Physiol. Pharmacol.*, vol. 67, no. 12, pp. 1480–1485, 1989.
- [40] M. Jastroch and L. Andersson, "When pigs fly, UCP1 makes heat," *Mol. Metab.*, vol. 4, no. 5, pp. 359–362, 2015.
- [41] J. S. Hayward and P. A. Lisson, "Evolution of brown fat: its absence in marsupials and monotremes," *Can. J. Zool.*, vol. 70, pp. 171–179, 1992.
- [42] B. Cannon and J. Nedergaard, "Brown adipose tissue: function and physiological significance.," *Physiol. Rev.*, vol. 84, pp. 277–359, 2004.
- [43] J. Nedergaard, T. Bengtsson, and B. Cannon, "Unexpected evidence for active brown adipose tissue in adult humans," *Am. J. Physiol. Endocrinol. Metab.*, vol. 293, pp. 444–452, 2007.
- [44] A. M. Cypess, S. Lehman, G. Williams, I. Tal, D. Rodman, A. B. Goldfine, F. C. Kuo, E. L. Palmer, Y. -

- H. Tseng, A. Doria, G. M. Kolodny, and C. R. Kahn, "Identification and Importance of Brown Adipose Tissue in Adult Humans," *N. Engl. J. Med.*, vol. 360, no. 15, pp. 1509–1517, 2009.
- [45] W. D. Van Marken Lichtenbelt, J. W. Vanhommerig, N. M. Smulders, J. M. A. F. L. Drossaerts, G. J. Kemerink, N. D. Bouvy, P. Schrauwen, and G. J. J. Teule, "Cold-Activated Brown Adipose Tissue in Healthy Men," *new Engl. J. Med. Orig.*, vol. 360, no. 15, pp. 1500–1508, 2009.
- [46] K. A. Virtanen, M. E. Lidell, J. Orava, M. Heglind, R. Westergren, T. Niemi, M. Taittonen, J. Laine, N.-J. Savisto, S. Enerbäck, and P. Nuutila, "Functional Brown Adipose Tissue in Healthy Adults," *N. Engl. J. Med.*, vol. 360, pp. 1518–1525, 2009.
- [47] M. Saito, Y. Okamatsu-Ogura, M. Matsushita, K. Watanabe, T. Yoneshiro, J. Nio-Kobayashi, T. Iwanaga, M. Miyagawa, T. Kameya, K. Nakada, Y. Kawai, and M. Tsujisaki, "High Incidence of Metabolically Active Brown Adipose Effects of Cold Exposure and Adiposity," *Diabetes*, vol. 58, pp. 1526–1531, 2009.
- [48] J. Orava, P. Nuutila, M. E. Lidell, V. Oikonen, T. Noponen, T. Viljanen, M. Scheinin, M. Taittonen, T. Niemi, S. Enerbäck, and K. A. Virtanen, "Different metabolic responses of human brown adipose tissue to activation by cold and insulin," *Cell Metab.*, vol. 14, no. 2, pp. 272–279, 2011.
- [49] M. R. Mirbolooki, C. C. Constantinescu, M.-L. Pan, and J. Mukherjee, "Quantitative assessment of brown adipose tissue metabolic activity and volume using 18F-FDG PET/CT and  $\beta$ 3-adrenergic receptor activation," *EJNMMI*, vol. 1, no. 1, p. 30, 2011.
- [50] J. Nedergaard, T. Bengtsson, and B. Cannon, "Three years with adult human brown adipose tissue.," *Ann. N. Y. Acad. Sci.*, vol. 1212, pp. 20–36, 2010.
- [51] L. Sidossis and S. Kajimura, "Brown and beige fat in humans: Thermogenic adipocytes that control energy and glucose homeostasis," *J. Clin. Invest.*, vol. 125, no. 2, pp. 478–486, 2015.
- [52] J. Villarroya, R. Cereijo, and F. Villarroya, "An endocrine role for brown adipose tissue?," *AJP Endocrinol. Metab.*, vol. 305, no. 5, pp. E567–E572, 2013.
- [53] A. Bartelt, O. T. Bruns, R. Reimer, H. Hohenberg, H. Ittrich, K. Peldschus, M. G. Kaul, U. I. Tromsdorf, H. Weller, C. Waurisch, A. Eychmüller, P. L. S. M. Gordts, F. Rinninger, K. Bruegelmann, B. Freund, P. Nielsen, M. Merkel, and J. Heeren, "Brown adipose tissue activity controls triglyceride clearance," *Nat. Med.*, vol. 17, no. 2, pp. 200–205, 2011.
- [54] D. W. Fawcett, "A comparison of the histological organization and cytochemical reactions of brown and white adipose tissues," *J. Morphol.*, vol. 90, no. 2, pp. 363–405, 1952.
- [55] M. Harms and P. Seale, "Brown and beige fat: development, function and therapeutic potential.," *Nat. Med.*, vol. 19, no. 10, pp. 1252–63, 2013.
- [56] J. A. Timmons, K. Wennmalm, O. Larsson, T. B. Walden, T. Lassmann, N. Petrovic, D. L. Hamilton, R. E. Gimeno, C. Wahlestedt, K. Baar, J. Nedergaard, and B. Cannon, "Myogenic gene expression signature establishes that brown and white adipocytes originate from distinct cell lineages," *Proc. Natl. Acad. Sci.*, vol. 104, no. 11, pp. 4401–4406, 2007.
- [57] F. Forner, C. Kumar, C. A. Luber, T. Fromme, M. Klingenspor, and M. Mann, "Proteome Differences between Brown and White Fat Mitochondria Reveal Specialized Metabolic Functions," *Cell Metab.*, vol. 10, no. 4, pp. 324–335, 2009.
- [58] S. Krief, F. Ltnqvist, S. Raimbault, B. Baude, A. Van Spronsen, P. Amer, A. D. Strosberg, D. Ricquier, and L. J. Emorine, "Tissue Distribution of  $\beta$ 3-adrenergic Receptor mRNA in Man," *J. Clin. Invest.*, vol. 91, pp. 344–349, 1993.
- [59] C. de Souza and B. Burkey, "Beta 3-adrenoceptor agonists as anti-diabetic and anti-obesity drugs in humans.," *Curr. Pharm. Des.*, vol. 7, no. 14, pp. 1433–1449, 2001.
- [60] M. R. Candelore, L. Deng, L. M. Tota, L. J. Kelly, M. A. Cascieri, and C. D. Strader, "Pharmacological characterization of a recently described human beta 3-adrenergic receptor mutant.," *Endocrinology*, vol. 137, no. 6, pp. 2638–41, 1996.
- [61] A. M. Cypess, L. S. Weiner, C. Roberts-Toler, E. F. Elía, S. H. Kessler, P. A. Kahn, J. English, K. Chatman, S. A. Trauger, A. Doria, and G. M. Kolodny, "Activation of Human Brown Adipose Tissue by a  $\beta$ 3-Adrenergic Receptor Agonist," *Cell Metab.*, vol. 21, no. 1, pp. 33–38, 2015.
- [62] H. Liang and W. F. Ward, "PGC-1  $\alpha$ : a key regulator of energy metabolism," *Adv. Physiol. Educ.*, vol. 30, pp. 145–151, 2006.
- [63] I. T. H. Au-Yong, N. Thorn, R. Ganatra, A. C. Perkins, and M. E. Symonds, "Brown Adipose Tissue and Seasonal Variation in Humans," *Diabetes*, vol. 58, pp. 2583–2587, 2009.
- [64] G. Barbatelli, I. Murano, L. Madsen, Q. Hao, M. Jimenez, K. Kristiansen, J. P. Giacobino, R. De Matteis, and S. Cinti, "The emergence of cold-induced brown adipocytes in mouse white fat depots is

- determined predominantly by white to brown adipocyte transdifferentiation,” *AJP Endocrinol. Metab.*, vol. 298, no. 6, pp. E1244–E1253, 2010.
- [65] N. Petrovic, T. B. Walden, I. G. Shabalina, J. A. Timmons, B. Cannon, and J. Nedergaard, “Chronic peroxisome proliferator-activated receptor  $\gamma$  (PPAR $\gamma$ ) activation of epididymally derived white adipocyte cultures reveals a population of thermogenically competent, UCP1-containing adipocytes molecularly distinct from classic brown adipocytes,” *J. Biol. Chem.*, vol. 285, no. 10, pp. 7153–7164, 2010.
- [66] P. Lee, C. D. Werner, E. Kebebew, and F. S. Celi, “Functional thermogenic beige adipogenesis is inducible in human neck fat,” *Int. J. Obes.*, vol. 38, no. 2, pp. 170–176, 2014.
- [67] B. Gustafson, S. Hedjazifar, S. Gogg, A. Hammarstedt, and U. Smith, “Insulin resistance and impaired adipogenesis,” *Trends Endocrinol. Metab.*, vol. 26, no. 4, pp. 193–200, 2015.
- [68] W. Wang and P. Seale, “Control of brown and beige fat development,” *Nat. Rev. Mol. Cell Biol.*, vol. 17, no. 11, pp. 691–702, 2016.
- [69] P. Seale, B. Bjork, W. Yang, S. Kajimura, S. Chin, S. Kuang, A. Scimè, S. Devarakonda, H. M. Conroe, H. Erdjument-Bromage, P. Tempst, M. A. Rudnicki, D. R. Beier, and B. M. Spiegelman, “PRDM16 controls a brown fat/skeletal muscle switch,” *Nature*, vol. 454, no. 7207, pp. 961–967, 2008.
- [70] M. E. Lidell, M. J. Betz, O. D. Leinhard, M. Heglind, L. Elander, M. Slawik, T. Mussack, D. Nilsson, T. Romu, P. Nuutila, K. A. Virtanen, F. Beuschlein, A. Persson, M. Borga, and S. Enerbäck, “Evidence for two types of brown adipose tissue in humans,” *Nat. Med.*, vol. 19, no. 5, pp. 631–634, 2013.
- [71] S. Cinti, “Anatomy of the adipose organ,” *Eat Weight Disord.*, vol. 5, no. 2, pp. 132–142, 2000.
- [72] A. Vitali, I. Murano, M. C. Zingaretti, A. Frontini, D. Ricquier, and S. Cinti, “The adipose organ of obesity-prone C57BL/6J mice is composed of mixed white and brown adipocytes,” *J. Lipid Res.*, vol. 53, no. 4, pp. 619–629, 2012.
- [73] X. R. Peng, P. Gennemark, G. O’Mahony, and S. Bartsaghi, “Unlock the thermogenic potential of adipose tissue: Pharmacological modulation and implications for treatment of diabetes and obesity,” *Front. Endocrinol. (Lausanne)*, vol. 6, p. 174, 2015.
- [74] M. Ghorbani and J. Himms-Hagen, “Appearance of brown adipocytes in white adipose tissue during CL 316,243-induced reversal of obesity and diabetes in Zucker fa/fa rats,” *Int. J. Obes.*, vol. 21, no. 6, pp. 465–475, 1997.
- [75] J. Himms-Hagen, A. Melnyk, M. C. Zingaretti, E. Ceresi, G. Barbatelli, and S. Cinti, “Multilocular fat cells in WAT of CL-316243-treated rats derive directly from white adipocytes,” *Am. J. Physiol. Cell Physiol.*, vol. 279, no. 3, pp. C670–C681, 2000.
- [76] L. Z. Sharp, K. Shinoda, H. Ohno, D. W. Scheel, E. Tomoda, L. Ruiz, H. Hu, L. Wang, Z. Pavlova, V. Gilsanz, and S. Kajimura, “Human BAT Possesses Molecular Signatures That Resemble Beige / Brite Cells,” *PLoS One*, vol. 7, no. 11, p. e49452, 2012.
- [77] P. Lee, S. Smith, J. Linderman, A. B. Courville, and R. J. Brychta, “Temperature-Acclimated Brown Adipose Tissue Modulates Insulin Sensitivity in Humans,” *Diabetes*, vol. 63, pp. 3686–3698, 2014.
- [78] A. A. J. J. Van Der Lans, J. Hoeks, B. Brans, G. H. E. J. Vijgen, M. G. W. Visser, M. J. Vosselman, J. Hansen, J. A. Jørgensen, J. Wu, F. M. Mottaghy, P. Schrauwen, and W. D. Van Marken Lichtenbelt, “Cold acclimation recruits human brown fat and increases nonshivering thermogenesis,” *J. Clin. Invest.*, vol. 123, no. 8, pp. 3395–3403, 2013.
- [79] T. Yoneshiro, S. Aita, M. Matsushita, T. Kayahara, T. Kameya, Y. Kawai, T. Iwanaga, and M. Saito, “Recruited brown adipose tissue as an antiobesity agent in humans,” *J. Clin. Invest.*, vol. 123, no. 8, pp. 3404–3408, 2013.
- [80] R. P. Kühnlein, “Lipid droplet-based storage fat metabolism in Drosophila,” *J. Lipid Res.*, vol. 53, pp. 1430–1436, 2012.
- [81] B. C. Mullaney and K. Ashrafi, “C. elegans Fat Storage and Metabolic Regulation,” *Biochim. Biophys. Acta*, vol. 1791, no. 6, pp. 474–478, 2009.
- [82] M. Radulovic, O. Knittelfelder, A. Cristobal-Sarramian, D. Kolb, H. Wolinski, and S. D. Kohlwein, “The emergence of lipid droplets in yeast: Current status and experimental approaches,” *Curr. Genet.*, vol. 59, no. 4, pp. 231–242, 2013.
- [83] T. C. Walther and R. V. Farese Jr., “Lipid Droplets And Cellular Lipid Metabolism,” *Annu. Rev. Biochem.*, vol. 81, pp. 687–714, 2012.
- [84] D. J. Murphy, “The biogenesis and functions of lipid bodies in animals, plants and microorganisms,” *Prog. Lipid Res.*, vol. 40, no. 5, pp. 325–438, 2001.
- [85] S. Murphy, S. Martin, and R. G. Parton, “Lipid droplet-organelle interactions; sharing the fats,”

- Biochim. Biophys. Acta - Mol. Cell Biol. Lipids*, vol. 1791, no. 6, pp. 441–447, 2009.
- [86] T. Fujimoto, Y. Ohsaki, J. Cheng, M. Suzuki, and Y. Shinohara, “Lipid droplets : a classic organelle with new outfits,” *Histochem. Cell Biol.*, vol. 130, pp. 263–279, 2008.
  - [87] Y. Lee, H. Hirose, M. Ohneda, J. H. Johnson, D. J. McGarry, and R. H. Unger, “Beta-cell lipotoxicity in the pathogenesis of non-insulin-dependent diabetes mellitus of obese rats: impairment in adipocyte-beta-cell relationships,” *Proc. Natl. Acad. Sci.*, vol. 91, no. 23, pp. 10878–10882, 1994.
  - [88] M. Shimabukuro, M. Higa, Y. Zhou, M. Wang, C. B. Newgard, and R. H. Unger, “Lipoapoptosis in Beta-cells of Obese Prediabetic fa / fa Rats,” *J. Biol. Chem.*, vol. 273, no. 49, pp. 32487–32490, 1998.
  - [89] D. T. Stein, B. E. Stevenson, M. W. Chester, M. Basit, M. B. Daniels, S. D. Turley, and J. D. McGarry, “The insulinotropic potency of fatty acids is influenced profoundly by their chain length and degree of saturation,” *J. Clin. Invest.*, vol. 100, no. 2, pp. 398–403, 1997.
  - [90] M. P. Corcoran, S. Lamon-Fava, and R. A. Fielding, “Skeletal muscle lipid deposition and insulin resistance : effect of dietary fatty acids and exercise,” *Am. J. Clin. Nutr.*, vol. 85, pp. 662–677, 2007.
  - [91] A. Herms, M. Bosch, N. Ariotti, B. J. N. Reddy, A. Fajardo, A. Fernández-Vidal, A. Alvarez-Guaita, M. A. Fernández-Rojo, C. Rentero, F. Tebar, C. Enrich, M. I. Geli, R. G. Parton, S. P. Gross, and A. Pol, “Cell-to-cell heterogeneity in lipid droplets suggests a mechanism to reduce lipotoxicity,” *Curr. Biol.*, vol. 23, no. 15, pp. 1489–1496, 2013.
  - [92] K. Hsieh, Y. K. Lee, C. Londos, B. M. Raaka, K. T. Dalen, and A. R. Kimmel, “Perilipin family members preferentially sequester to either triacylglycerol-specific or cholesteryl-ester-specific intracellular lipid storage droplets,” *J. Cell Sci.*, vol. 125, no. 17, pp. 4067–4076, 2012.
  - [93] T. C. Walther and R. V. Farese, “Lipid Droplets and Cellular Lipid Metabolism,” *Annu. Rev. Biochem.*, vol. 81, no. 1, pp. 687–714, 2012.
  - [94] S. D. Kohlwein, M. Veenhuis, and I. J. Van Der Klei, “Lipid Droplets and Peroxisomes : Key Players in Cellular Lipid Homeostasis or A Matter,” *Genetics*, vol. 193, pp. 1–50, 2013.
  - [95] A. R. Thiam and M. Beller, “The why, when and how of lipid droplet diversity,” *J. Cell Sci.*, vol. 130, pp. 315–324, 2017.
  - [96] A. R. Thiam, R. V. Farese Jr., and T. C. Walther, “The Biophysics and Cell Biology of Lipid Droplets,” *Nat Rev Mol Cell Biol.*, vol. 14, no. 12, p. 775–786., 2013.
  - [97] C. Chascione, D. E. Elwyn, M. Davila, K. M. Gil, J. Askanazi, and J. M. Kinney, “Effect of carbohydrate intake on de novo lipogenesis in human adipose tissue,” *Am. J. Physiol. - Endocrinol. Metab.*, vol. 253, no. 6, pp. E664–669, 1987.
  - [98] L. Sjöström, “Fatty Acid Synthesis De Novo in Adipose Tissue from Obese Subjects on a Hypercaloric High-Carbohydrate Diet,” *Scand. J. Clin. Lab. Invest.*, vol. 32, no. 4, pp. 339–349, 1973.
  - [99] P. Björntorp and L. Sjöström, “Carbohydrate Storage in Man : Speculations and Some Quantitative Considerations,” *Metabolism*, vol. 27, no. 12, pp. 1853–1865, 1978.
  - [100] A. Strawford, F. Antelo, M. Christiansen, and M. K. Hellerstein, “Adipose tissue triglyceride turnover, de novo lipogenesis, and cell proliferation in humans measured with 2H2O,” *Am. J. Physiol. - Endocrinol. Metab.*, vol. 286, no. 4, pp. E577–E588, 2004.
  - [101] F. Q. Nuttall, A. Ngo, and M. C. Gannon, “Regulation of hepatic glucose production and the role of gluconeogenesis in humans: is the rate of gluconeogenesis constant?,” *Diabetes. Metab. Res. Rev.*, vol. 24, pp. 438–458, 2008.
  - [102] C. A. Millward, D. DeSantis, C.-W. Hsieh, J. D. Heaney, S. Pisano, Y. Olswang, L. Reshef, M. Beidelschies, M. Puchowicz, and C. M. Croniger, “Phosphoenolpyruvate carboxykinase ( Pck1 ) helps regulate the triglyceride / fatty acid cycle and development of insulin resistance in mice,” *J. Lipid Res.*, vol. 51, pp. 1452–1463, 2010.
  - [103] J. B. Kim, P. Sarraf, M. Wright, K. M. Yao, E. Mueller, G. Solanes, B. B. Lowell, and B. M. Spiegelman, “Nutritional and insulin regulation of fatty acid synthetase and leptin gene expression through ADD1/SREBP1,” *J. Clin. Invest.*, vol. 101, no. 1, pp. 1–9, 1998.
  - [104] D. Eberlé, B. Hegarty, P. Bossard, P. Ferré, and F. Foufelle, “SREBP transcription factors : master regulators of lipid homeostasis,” *Biochimie*, vol. 86, pp. 839–848, 2004.
  - [105] S. E. Gale, A. Frolov, X. Han, P. E. Bickel, L. Cao, A. Bowcock, J. E. Schaffer, and D. S. Ory, “A Regulatory Role for AGPAT2 in Adipocyte Differentiation,” *J. Biol. Chem.*, vol. 281, pp. 11082–11089, 2006.
  - [106] S. Gesta and C. R. Kahn, “White Adipose Tissue,” in *Adipose Tissue Biology*, 1st ed., M. Symonds, Ed. Springer, 2012, pp. 71–121.
  - [107] C. Nye, J. Kim, S. C. Kalhan, and R. W. Hanson, “Reassessing triglyceride synthesis in adipose tissue,”

- Trends Endocrinol. Metab.*, vol. 19, no. 10, pp. 356–361, 2008.
- [108] P. Flachs, M. Rossmeisl, O. Kuda, and J. Kopecky, “Stimulation of mitochondrial oxidative capacity in white fat independent of UCP1: A key to lean phenotype,” *BBA - Mol. Cell Biol. Lipids*, vol. 1831, no. 5, pp. 986–1003, 2013.
  - [109] W. T. . Festuccia, R. Guerra-Sá, N. H. Kawashita, M. A. . Garófalo, E. A. Evengelista, V. Rodrigues, I. C. Kettelhut, and R. H. Migliorini, “Expression of glycerokinase in brown adipose tissue is stimulated by the sympathetic nervous system,” *Am. J. Physiol. - Regul. Integr. Comparative Physiol.*, vol. 284, no. 6, pp. R1536–1541, 2003.
  - [110] J. Borén, M.-R. Askenen, S.-O. Olofsson, and M. Levin, “Ectopic lipid storage and insulin resistance : a harmful relationship,” *J. Intern. Med.*, vol. 274, no. 1, pp. 25–40, 2013.
  - [111] L. Kuerschner, C. Moessinger, and C. Thiele, “Imaging of lipid biosynthesis: How a neutral lipid enters lipid droplets,” *Traffic*, vol. 9, no. 3, pp. 338–352, 2008.
  - [112] S. J. Stone, M. C. Levin, P. Zhou, J. Han, T. C. Walther, and R. V. Farese, “The endoplasmic reticulum enzyme DGAT2 is found in mitochondria-associated membranes and has a mitochondrial targeting signal that promotes its association with mitochondria,” *J. Biol. Chem.*, vol. 284, no. 8, pp. 5352–5361, 2009.
  - [113] P. Oelkers, A. Behari, D. Cromley, J. T. Billheimer, and S. L. Sturley, “Characterization of Two Human Genes Encoding Acyl Coenzyme A : Cholesterol Acyltransferase-related Enzymes,” *J. Biol. Chem.*, vol. 273, no. 41, pp. 26765–26771, 1998.
  - [114] S. Cases, S. J. Smith, Y.-W. Zheng, H. M. Myers, S. R. Lear, E. Sande, S. Novak, C. Collins, C. B. Welch, A. J. Lusis, S. K. Erickson, and R. V. Farese Jr., “Identification of a gene encoding an acyl CoA : diacylglycerol acyltransferase , a key enzyme in triacylglycerol synthesis,” *Proc. Natl. Acad. Sci.*, vol. 95, pp. 13018–13023, 1998.
  - [115] D. M. Grant, R. J. Pugmire, E. P. Black, and K. A. Christensen, “Rotational Diffusion in Near Ellipsoid Molecules,” *J. Am. Chem. Soc.*, pp. 8465–8467, 1973.
  - [116] M. Ahmadian, R. E. Duncan, and H. S. Sul, “Skinny on Fat Metabolism: Lipolysis and Fatty Acid Utilization,” *Trends Endocrinol. Metab.*, vol. 20, no. 9, pp. 424–428, 2009.
  - [117] A. S. Rambold, S. Cohen, and J. Lippincott-Schwartz, “Fatty acid trafficking in starved cells: regulation by lipid droplet lipolysis, autophagy and mitochondrial fusion dynamics,” *Dev. Cell*, vol. 32, no. 6, pp. 678–692, 2015.
  - [118] K. Jaworski, M. Ahmadian, R. E. Duncan, E. Sarkadi-Nagy, K. A. Varady, M. K. Hellerstein, H. Y. Lee, V. T. Samuel, G. I. Shulman, K. H. Kim, S. De Val, C. Kang, and H. S. Sul, “AdPLA ablation increases lipolysis and prevents obesity induced by high-fat feeding or leptin deficiency,” *Nat. Med.*, vol. 15, no. 2, pp. 159–168, 2009.
  - [119] M. Ahmadian, R. E. Duncan, K. A. Varady, D. Frasson, M. K. Hellerstein, A. L. Birkenfeld, V. T. Samuel, G. I. Shulman, Y. Wang, C. Kang, and H. S. Sul, “Adipose overexpression of desnutrin promotes fatty acid use and attenuates diet-induced obesity,” *Diabetes*, vol. 58, no. 4, pp. 855–866, 2009.
  - [120] S. B. Pruisner, B. Cannon, and O. Lindberg, “Oxidative Metabolism in Cells Isolated horn Brown Adipose Tissue 1 . Catecholamine and Fatty Acid Stimulation of Respiration,” *Eur. J. Biochem.*, vol. 6, pp. 15–22, 1968.
  - [121] N. Reed and J. N. Fain, “Potassium-dependent Stimulation of Respiration in Brown Fat Cells by Fatty Acids and Lipolytic Agents,” *J. Biol. Chem.*, vol. 243, no. 23, pp. 6077–6083, 1968.
  - [122] A. Matthias, K. B. E. Ohlson, J. M. Fredriksson, A. Jacobsson, J. Nedergaard, and B. Cannon, “Thermogenic responses in brown fat cells are fully UCP1-dependent. UCP2 or UCP3 do not substitute for UCP1 in adrenergically or fatty acid-induced thermogenesis,” *J. Biol. Chem.*, vol. 275, no. 33, pp. 25073–25081, 2000.
  - [123] M. D. Jensen, K. Ekberg, and B. R. Landau, “Lipid metabolism during fasting.,” *Am. J. Physiol. Endocrinol. Metab.*, vol. 281, no. 4, pp. E789–93, 2001.
  - [124] K. N. Frayn, P. Arner, and H. Yki-Jarvinen, “Fatty acid metabolism in adipose tissue, muscle and liver in health and disease,” *Essays Biochem.*, vol. 42, pp. 89–103, 2006.
  - [125] S. W. Coppack, R. M. Fisher, G. F. Gibbons, S. M. Humphreys, M. J. McDonough, J. L. Potts, and K. N. Frayn, “Postprandial substrate deposition in human forearm and adipose tissues in vivo,” *Clin. Sci.*, vol. 79, pp. 339–348, 1990.
  - [126] M. W. Radomski and T. Orme, “Response of lipoprotein lipase in various tissues to cold exposure,” *Am. J. Physiol.*, vol. 220, no. 6, pp. 1852–1856, 1971.



- 
- [127] C. Carneheim, J. A. N. Nedergaard, and B. Cannon, "Beta-Adrenergic stimulation of lipoprotein lipase in rat brown adipose tissue during acclimation to cold," *Am. J. Physiol.*, vol. 246, no. 4, pp. E327-333, 1984.
  - [128] T. I. A. Sørensen, S. Virtue, and A. Vidal-Puig, "Obesity as a clinical and public health problem: Is there a need for a new definition based on lipotoxicity effects?," *Biochim. Biophys. Acta - Mol. Cell Biol. Lipids*, vol. 1801, no. 3, pp. 400-404, 2010.
  - [129] Q. A. Wang, C. Tao, R. K. Gupta, and P. E. Scherer, "Tracking adipogenesis during white adipose tissue development, expansion and regeneration," *Nat. Med.*, vol. 19, no. 10, pp. 1338-1344, 2013.
  - [130] K. N. Manolopoulos, F. Karpe, and K. N. Frayn, "Gluteofemoral body fat as a determinant of metabolic health," *Int. J. Obes.*, vol. 34, no. 6, pp. 949-959, 2010.
  - [131] S. E. Kahn, R. L. Prigeon, R. S. Schwartz, W. Y. Fujimoto, R. H. Knopp, J. D. Brunzell, and D. Porte, "Obesity, Body Fat Distribution, Insulin Sensitivity and Islet beta-Cell Function as Explanations for Metabolic Diversity," *J Nutr.*, vol. 131, no. 2, p. 354S-360S, 2001.
  - [132] D. Medrikova, Z. M. Jilkova, K. Bardova, P. Janovska, M. Rossmeisl, and J. Kopecky, "Sex differences during the course of diet-induced obesity in mice: Adipose tissue expandability and glycemic control," *Int. J. Obes.*, vol. 36, no. 2, pp. 262-272, 2012.
  - [133] C. Weyer, J. E. Foley, C. Bogardus, P. A. Tataranni, and R. E. Pratley, "Enlarged subcutaneous abdominal adipocyte size, but not obesity itself, predicts Type II diabetes independent of insulin resistance," *Diabetologia*, vol. 43, pp. 1498-1506, 2000.
  - [134] E. E. Kershaw and J. S. Flier, "Adipose Tissue as an Endocrine Organ," *J. Clin. Endocrinol. Metab.*, vol. 89, no. 6, pp. 2548-2556, 2004.
  - [135] M. Qatanani and M. A. Lazar, "Mechanisms of obesity-associated insulin resistance : many choices on the menu," *Genes Dev.*, vol. 21, pp. 1443-1455, 2007.
  - [136] H. Xu, G. T. Barnes, Q. Yang, G. Tan, D. Yang, C. J. Chou, J. Sole, A. Nichols, J. S. Ross, L. A. Tartaglia, and H. Chen, "Chronic inflammation in fat plays a crucial role in the development of obesity-related insulin resistance," *J. Clin. Invest.*, vol. 112, no. 12, pp. 1821-1830, 2003.
  - [137] C. A. Curat, A. Miranville, C. Sengene, M. Diehl, C. Tonus, R. Busse, and A. Bouloumie, "From Blood Monocytes to Adipose Tissue-Resident Macrophages," *Diabetes*, vol. 53, pp. 1285-1292, 2004.
  - [138] A. Guilherme, J. V. Virbasius, V. Puri, and M. P. Czech, "Adipocyte dysfunctions linking obesity to insulin resistance and type 2 diabetes," *Nat. Rev. Mol. Cell Biol.*, vol. 9, no. 5, pp. 367-77, 2008.
  - [139] I. Wernstedt Asterholm, C. Tao, T. S. Morley, Q. A. Wang, F. Delgado-Lopez, Z. V. Wang, and P. E. Scherer, "Adipocyte inflammation is essential for healthy adipose tissue expansion and remodeling," *Cell Metab.*, vol. 20, pp. 103-118, 2014.
  - [140] F. J. Ruiz-Ojeda, A. I. Rupérez, C. Gomez-Llorrente, A. Gil, and C. M. Aguilera, "Cell Models and Their Application for Studying Adipogenic Differentiation in Relation to Obesity : A Review," *Int. J. Mol. Sci.*, vol. 17, p. 1040, 2016.
  - [141] S. Bartsaghi, S. Hallen, L. Huang, P. Svensson, R. A. Momo, S. Wallin, E. K. Carlsson, A. Forslöw, and P. Seale, "Thermogenic Activity of UCP1 in Human White Fat- Derived Beige Adipocytes," *Mol. Endocrinol.*, vol. 29, pp. 130-139, 2015.
  - [142] F. M. Watt and W. T. S. Huck, "Role of the extracellular matrix in regulating stem cell fate.," *Nat. Rev. Mol. Cell Biol.*, vol. 14, no. 8, pp. 467-73, 2013.
  - [143] N. Shoham and A. Gefen, "Mechanotransduction in adipocytes," *J. Biomech.*, vol. 45, pp. 1-8, 2012.
  - [144] Y. H. Lee, E. P. Mottillo, and J. G. Granneman, "Adipose tissue plasticity from WAT to BAT and in between," *Biochim. Biophys. Acta - Mol. Basis Dis.*, vol. 1842, no. 3, pp. 358-369, 2014.
  - [145] S. J. Morrison and A. C. Spradling, "Stem Cells and Niches: Mechanisms That Promote Stem Cell Maintenance throughout Life," *Cell*, vol. 132, no. 4, pp. 598-611, 2008.
  - [146] I. Nakajima, H. Aso, T. Yamaguchi, and K. Ozutsumi, "Adipose tissue extracellular matrix : newly organized by adipocytes during differentiation," *Differentiation*, vol. 63, no. 4, pp. 193-200, 1998.
  - [147] A. Wronska and Z. Kmiec, "Structural and biochemical characteristics of various white adipose tissue depots," *Acta Physiol.*, vol. 205, no. 2, pp. 194-208, 2012.
  - [148] K. Sun, C. M. Kusminski, and P. E. Scherer, "Adipose tissue remodeling and obesity," *J. Clin. Invest.*, vol. 121, no. 6, pp. 2094-2101, 2011.
  - [149] E. D. Rosen and O. A. MacDougald, "Adipocyte differentiation from the inside out.," *Nat. Rev. Mol. Cell Biol.*, vol. 7, no. 12, pp. 885-96, Dec. 2006.
  - [150] A. G. Cristancho and M. A. Lazar, "Forming functional fat: a growing understanding of adipocyte

- p>differentiation,”
- Nat. Rev. Mol. Cell Biol.*
- , vol. 12, no. 11, pp. 722–734, 2011.
- [151] J. B. Kim and B. M. Spiegelman, “ADD 1 / SREBP1 promotes adipocyte differentiation and gene expression linked to fatty acid metabolism,” *Genes Dev.*, vol. 10, pp. 1096–1107, 1996.
  - [152] H. Shimano, I. Shimomura, R. E. Hammer, J. Herz, J. L. Goldstein, M. S. Brown, and J. D. Horton, “Elevated Levels of SREBP-2 and Cholesterol Synthesis in Livers of Mice Homozygous for a Targeted Disruption of the SREBP-1 Gene,” *J. Clin. Invest.*, vol. 100, no. 8, pp. 2115–2124, 1997.
  - [153] J. M. Lehmann, L. B. Moore, T. A. Smith-Oliver, W. O. Wilkison, T. M. Willson, and S. A. Kliewer, “An antidiabetic thiazolidinedione is a high affinity ligand for peroxisome proliferator-activated receptor gamma (PPAR gamma).,” *The Journal of biological chemistry*, vol. 270, no. 22, pp. 12953–12956, 1995.
  - [154] X. M. Shi, H. C. Blair, X. Yang, J. M. McDonald, and X. Cao, “Tandem repeat of C/EBP binding sites mediates PPARgamma2 gene transcription in glucocorticoid-induced adipocyte differentiation.,” *J. Cell. Biochem.*, vol. 76, no. 3, pp. 518–527, 2000.
  - [155] D. M. Essayan, “Cyclic nucleotide phosphodiesterases,” *J Allergy Clin Immunol*, vol. 108, no. 5, pp. 671–680, 2001.
  - [156] A.-M. Rodriguez, C. Elabd, F. Delteil, J. Astier, C. Vernochet, P. Saint-Marc, J. Guesnet, A. Guezennec, E.-Z. Amri, C. Dani, and G. Ailhaud, “Adipocyte differentiation of multipotent cells established from human adipose tissue,” *Biochem. Biophys. Res. Commun.*, vol. 315, no. 2, pp. 255–263, 2004.
  - [157] A. Dicker, K. Le Blanc, G. Åström, V. Van Harmelen, C. Götherström, L. Blomqvist, P. Arner, and M. Rydén, “Functional studies of mesenchymal stem cells derived from adult human adipose tissue,” *Exp. Cell Res.*, vol. 308, no. 2, pp. 283–290, 2005.
  - [158] M. J. Lee, Y. Wu, and S. K. Fried, “A modified protocol to maximize differentiation of human preadipocytes and improve metabolic phenotypes,” *Obesity*, vol. 20, no. 12, pp. 2334–2340, 2012.
  - [159] D. Langin, A. Dicker, G. Tavernier, J. Hoffstedt, A. Mairal, M. Rydén, E. Arner, A. Sicard, C. M. Jenkins, N. Viguerie, V. Van Harmelen, R. W. Gross, C. Holm, and P. Arner, “Adipocyte lipases and defect of lipolysis in human obesity,” *Diabetes*, vol. 54, no. 11, pp. 3190–3197, 2005.
  - [160] S. P. Blaber, Rebecca A Webster, C. J. Hill, E. J. Breen, D. Kuah, G. Vesey, and B. R. Herbert, “Analysis of in vitro secretion profiles from adipose-derived cell populations,” *Transl. Med.*, vol. 10, p. 172, 2012.
  - [161] H. Stoll and J. Y. Lim, “Role of Mechanical Stimulations in Directing Mesenchymal Stem Cell Adipogenesis,” in *The Mechanobiology of Obesity and Related Diseases*, 16th ed., A. Gefen and D. Benayahu, Eds. Springer, 2014, pp. 63–87.
  - [162] Y. Ohsaki, M. Suzuki, and T. Fujimoto, “Open questions in lipid droplet biology,” *Chem. Biol.*, vol. 21, pp. 86–96, 2014.
  - [163] T. Fujimoto, Y. Ohsaki, M. Suzuki, and J. Cheng, *Imaging Lipid Droplets by Electron Microscopy*, 1st ed., vol. 116. Elsevier Inc., 2013.
  - [164] K. Tauchi-Sato, S. Ozeki, T. Houjou, R. Taguchi, and T. Fujimoto, “The surface of lipid droplets is a phospholipid monolayer with a unique fatty acid composition,” *J. Biol. Chem.*, vol. 277, no. 46, pp. 44507–44512, 2002.
  - [165] H. Robenek, M. J. Robenek, and D. Troyer, “PAT family proteins pervade lipid droplet cores.,” *J. Lipid Res.*, vol. 46, no. 6, pp. 1331–1338, 2005.
  - [166] R. Erni, M. D. Rossell, C. Kisielowski, and U. Dahmen, “Atomic Resolution Imaging with a sub-50 pm Electron Probe,” *Phys. Rev. Lett.*, vol. 102, no. 9, pp. 96–101, 2009.
  - [167] N. Fischer, P. Neumann, A. L. Konevega, L. V. Bock, R. Ficner, M. V. Rodnina, and H. Stark, “Structure of the E. coli ribosome-EF-Tu complex at <3 Å resolution by Cs-corrected cryo-EM,” *Nature*, vol. 520, no. 7548, pp. 567–570, 2015.
  - [168] X. Zheng, W. Zhu, F. Ni, H. Ai, and C. Yang, “A specific bioprobe for super-resolution fluorescence imaging of lipid droplets,” *Sensors Actuators, B Chem.*, vol. 255, pp. 3148–3154, 2018.
  - [169] S. W. Hell, S. J. Sahl, M. Bates, X. Zhuang, R. Heintzmann, M. J. Booth, J. Bewersdorf, G. Shtengel, H. Hess, P. Tinnefeld, A. Honigsmann, S. Jakobs, I. Testa, L. Cognet, B. Lounis, H. Ewers, S. J. Davis, C. Eggeling, D. Klennerman, K. I. Willig, G. Vicidomini, M. Castello, A. Diaspro, and T. Cordes, “The 2015 super-resolution microscopy roadmap,” *J. Phys. D. Appl. Phys.*, vol. 48, no. 44, 2015.
  - [170] S. Daemen, M. A. M. J. van Zandvoort, S. H. Parekh, and M. K. C. Hesselink, “Microscopy tools for the investigation of intracellular lipid storage and dynamics,” *Mol. Metab.*, vol. 5, no. 3, pp. 153–163, 2016.
  - [171] M. Paar, C. Jüngst, N. A. Steiner, C. Magnes, F. Sinner, D. Kolb, A. Lass, R. Zimmermann, A.

- Zumbusch, S. D. Kohlwein, and H. Wolinski, "Remodeling of lipid droplets during lipolysis and growth in adipocytes," *J. Biol. Chem.*, vol. 287, no. 14, pp. 11164–73, 2012.
- [172] I. Ivnitcki-Steele, A. R. Holmes, E. Lamping, B. C. Monk, R. D. Cannon, and L. A. Sklar, "Identification of Nile red as a fluorescent substrate of the *Candida albicans* ATP-binding cassette transporters Cdr1p and Cdr2p and the major facilitator superfamily transporter Mdr1p," *Anal. Biochem.*, vol. 394, no. 1, pp. 87–91, 2009.
- [173] I. Gregor, M. Spiecker, R. Petrovsky, J. Großhans, R. Ros, and J. Enderlein, "Rapid nonlinear image scanning microscopy," *Nat. Methods*, vol. 14, no. 11, pp. 1087–1089, 2017.
- [174] A. Zumbusch, G. R. Holtom, and X. S. Xie, "Three-Dimensional Vibrational Imaging by Coherent Anti-Stokes Raman Scattering," *Phys. Rev. Lett.*, vol. 82, no. 20, pp. 4142–4145, 1999.
- [175] M. Göppert-Mayer, "Über Elementarakte mit zwei Quantensprüngen," *Ann. Phys.*, vol. 9, pp. 273–295, 1931.
- [176] B. R. Masters, "English Translations of and Translator's Notes on Maria Göppert-Mayer's Theory of Two-Quantum Processes," in *Handbook of Biomedical Nonlinear Microscopy*, B. R. Masters and P. So, Eds. Oxford University Press, 2008, pp. 42–84.
- [177] C. J. R. Sheppard, J. N. Gannaway, R. Kompfner, and D. Walsh, "The scanning harmonic optical microscope," *IEEE J. Quantum Electron.*, vol. 13, no. 9, p. 912, 1977.
- [178] R. W. Boyd, *Nonlinear Optics*, vol. 0, no. 1941. Elsevier Science, 2003.
- [179] J.-X. Cheng and X. S. Xie, *Coherent Raman Scattering Microscopy*. CRC Press, 2013.
- [180] C. N. Banwell, "Raman Spectroscopy," in *Fundamentals of Molecular Spectroscopy*, 1983, pp. 124–154.
- [181] E. J. Woodbury and W. K. Ng, "Ruby Laser Operation in the Near IR," *Proc. Inst. Radio Eng*, vol. 50, p. 2367, 1962.
- [182] C. Freudiger, W. Min, B. Saar, S. Lu, G. Holtom, C. He, J. C. Tsai, J. X. Kang, and S. Xie, "Label-free biomedical imaging with high sensitivity by stimulated Raman scattering microscopy," *Science (80-. )*, vol. 322, pp. 1857–61, 2008.
- [183] J. C. Mansfield, G. R. Littlejohn, M. P. Seymour, R. J. Lind, S. Perfect, and J. Moger, "Label-free chemically specific imaging in planta with stimulated Raman scattering microscopy," *Anal. Chem.*, vol. 85, no. 10, pp. 5055–63, May 2013.
- [184] C. H. Camp Jr. and M. T. Cicerone, "Chemically sensitive bioimaging with coherent Raman scattering," *Nat. Photonics*, vol. 9, no. 5, pp. 295–305, 2015.
- [185] P. D. Maker and R. W. Terhune, "Study of Optical Effects Due to an Induced Polarization Third Order in the Electric Field Strength," *Phys. Rev.*, vol. 137, no. 3, pp. A801–A818, 1964.
- [186] M. D. Duncan, J. Reintjes, and T. J. Manuccia, "Scanning coherent anti-Stokes Raman microscope," *Opt. Lett.*, vol. 7, no. 8, pp. 350–2, 1982.
- [187] C. L. Evans and X. S. Xie, "Coherent anti-stokes Raman scattering microscopy: chemical imaging for biology and medicine," *Annu. Rev. Anal. Chem. (Palo Alto. Calif.)*, vol. 1, pp. 883–909, 2008.
- [188] F. Ganikhanov, C. L. Evans, B. G. Saar, and X. S. Xie, "High-sensitivity vibrational imaging with frequency modulation coherent anti-Stokes Raman scattering (FM CARS) microscopy," *Opt. Lett.*, vol. 31, no. 12, pp. 1872–4, 2006.
- [189] J. Cheng, A. Volkmer, L. D. Book, and X. S. Xie, "An Epi-Detected Coherent Anti-Stokes Raman Scattering (E-CARS) Microscope with High Spectral Resolution and High Sensitivity," *J. Phys. Chem. B*, vol. 105, no. 7, pp. 1277–1280, 2001.
- [190] E. O. Potma, C. L. Evans, and X. S. Xie, "Heterodyne coherent anti-Stokes Raman scattering (CARS) imaging," *Opt. Lett.*, vol. 31, no. 2, pp. 241–243, 2006.
- [191] A. Volkmer, L. D. Book, and X. S. Xie, "Time-resolved coherent anti-Stokes Raman scattering microscopy: Imaging based on Raman free induction decay," *Appl. Phys. Lett.*, vol. 80, no. 9, pp. 1505–1507, 2002.
- [192] C. L. Evans, E. O. Potma, M. Puoris'haag, D. Côté, C. P. Lin, and X. S. Xie, "Chemical imaging of tissue in vivo with video-rate coherent anti-Stokes Raman scattering microscopy," *Proc. Natl. Acad. Sci. U. S. A.*, vol. 102, no. 46, pp. 16807–12, 2005.
- [193] Y. Fu, H. Wang, R. Shi, and J.-X. Cheng, "Characterization of photodamage in coherent anti-Stokes Raman scattering microscopy," *Opt. Express*, vol. 14, no. 9, pp. 3942–3951, 2006.
- [194] J.-X. Cheng, A. Volkmer, and X. S. Xie, "Theoretical and experimental characterization of coherent anti-Stokes Raman scattering microscopy," *J. Opt. Soc. Am. B*, vol. 19, no. 6, pp. 1363–75, 2002.

- [195] P. J. Campagnola and L. M. Loew, "Second-harmonic imaging microscopy for visualizing biomolecular arrays in cells, tissues and organisms.," *Nat. Biotechnol.*, vol. 21, no. 11, pp. 1356–60, 2003.
- [196] D. Yelin and Y. Silberberg, "Laser scanning third-harmonic-generation microscopy in biology," *Opt. Express*, vol. 5, no. 8, pp. 169–175, 1999.
- [197] D. Débarre, W. Supatto, A.-M. Pena, A. Fabre, T. Tordjmann, L. Combettes, M.-C. Schanne-Klein, and E. Beaurepaire, "Imaging lipid bodies in cells and tissues using third-harmonic generation microscopy," *Nat. Methods*, vol. 3, no. 1, pp. 47–53, 2006.
- [198] P. T. C. So, C. Y. Dong, B. R. Masters, and K. M. Berland, "Two-Photon Excitation Fluorescence Microscopy," *Annu. Rev. Biomed. Eng.*, vol. 2, pp. 399–429, 2000.
- [199] B. R. Masters and P. T. C. So, *Handbook of Biomedical Nonlinear Microscopy*. Oxford University Press, 2008.
- [200] W. R. Zipfel, R. M. Williams, R. Christie, A. Y. Nikitin, B. T. Hyman, and W. W. Webb, "Live tissue intrinsic emission microscopy using multiphoton-excited native fluorescence and second harmonic generation.," *Proc. Natl. Acad. Sci. U. S. A.*, vol. 100, no. 12, pp. 7075–80, 2003.
- [201] G. Wurfel, H. Rinia, and M. Müller, "Imaging orientational order and lipid density in multilamellar vesicles with multiplex CARS microscopy," *J. Microsc.*, vol. 218, no. 1, pp. 37–45, 2005.
- [202] E. O. Potma and X. S. Xie, "Direct visualization of lipid phase segregation in single lipid bilayers with coherent anti-Stokes Raman scattering microscopy.," *Chemphyschem*, vol. 6, no. 1, pp. 77–9, 2005.
- [203] E. O. Potma and X. S. Xie, "Detection of single lipid bilayers with coherent anti-Stokes Raman scattering (CARS) microscopy," *J. Raman Spectrosc.*, vol. 34, no. 9, pp. 642–650, 2003.
- [204] Y. Zeng, B. G. Saar, M. G. Friedrich, F. Chen, Y.-S. Liu, R. a. Dixon, M. E. Himmel, X. S. Xie, and S.-Y. Ding, "Imaging Lignin-Downregulated Alfalfa Using Coherent Anti-Stokes Raman Scattering Microscopy," *BioEnergy Res.*, vol. 3, no. 3, pp. 272–277, 2010.
- [205] N. A. Belsey, N. L. Garrett, L. R. Contreras-rojas, A. J. Pickup-gerlaugh, G. J. Price, J. Moger, and R. H. Guy, "Evaluation of drug delivery to intact and porated skin by coherent Raman scattering and fluorescence microscopies," *J. Control. Release*, vol. 174, pp. 37–42, 2014.
- [206] A. D. G. Nunn, T. Scopigno, N. Pediconi, M. Levrero, H. Hagman, J. Kiskis, and A. Enejder, "The histone deacetylase inhibiting drug Entinostat induces lipid accumulation in differentiated HepaRG cells," *Sci. Rep.*, vol. 6, pp. 1–11, 2016.
- [207] T. Hellerer, C. Axäng, C. Brackmann, P. Hillertz, M. Pilon, and A. Enejder, "Monitoring of lipid storage in *Caenorhabditis elegans* using coherent anti-Stokes Raman scattering (CARS) microscopy.," *Proc. Natl. Acad. Sci. U. S. A.*, vol. 104, no. 37, pp. 14658–63, 2007.
- [208] R. K. Lyn, D. C. Kennedy, S. M. Sagan, D. R. Blais, Y. Rouleau, A. F. Pegoraro, X. S. Xie, A. Stelow, and J. P. Pezacki, "Direct imaging of the disruption of hepatitis C virus replication complexes by inhibitors of lipid metabolism.," *Virology*, vol. 394, no. 1, pp. 130–42, 2009.
- [209] J. P. Smus, C. Costa Moura, E. McMorro, R. S. Tare, R. O. C. Oreffo, and S. Mahajan, "Tracking adipogenic differentiation of skeletal stem cells by label-free chemically selective imaging," *Chem. Sci.*, vol. 6, no. 12, pp. 7089–7096, 2015.
- [210] R. Mouras, P. Bagnaninchi, A. Downes, and A. Elfick, "Multimodal, label-free nonlinear optical imaging for applications in biology and biomedical science," *J. Raman Spectrosc.*, vol. 44, no. 10, pp. 1373–1378, 2013.
- [211] M. E. Trujillo and P. E. Scherer, "Adipose tissue-derived factors: impact on health and disease.," *Endocr. Rev.*, vol. 27, no. 7, pp. 762–78, 2006.
- [212] A. Baracca, G. Sgarbi, G. Solaini, and G. Lenaz, "Rhodamine 123 as a probe of mitochondrial membrane potential : evaluation of proton flux through F<sub>0</sub> during ATP synthesis," *Biochim. Biophys. Acta*, vol. 1606, pp. 137–146, 2003.
- [213] F. Miao, W. Zhang, Y. Sun, R. Zhang, Y. Liu, F. Guo, G. Song, M. Tian, and X. Yu, "Novel fluorescent probes for highly selective two-photon imaging of mitochondria in living cells.," *Biosens. Bioelectron.*, vol. 55, pp. 423–9, 2014.
- [214] T. Seppänen-Laakso, I. Laakso, and R. Hiltunen, "Analysis of fatty acids by gas chromatography, and its relevance to research on health and nutrition," *Anal. Chim. Acta*, vol. 465, no. 1–2, pp. 39–62, 2002.
- [215] L. Borisjuk, H. Rolletschek, and T. Neuberger, "Nuclear magnetic resonance imaging of lipid in living plants," *Prog. Lipid Res.*, vol. 52, no. 4, pp. 465–487, 2013.
- [216] S. B. Heymsfield, H. H. Hu, W. Shen, and O. Carmichael, "Emerging Technologies and their Applications in Lipid Compartment Measurement," *Trends Endocrinol. Metab.*, vol. 26, no. 12, pp. 688–698, 2015.

- 
- [217] G. Hamilton, T. Yokoo, M. Bydder, I. Cruite, M. E. Schroeder, C. B. Sirlin, and M. S. Middleton, "In vivo characterization of the liver fat 1 H MR spectrum," *NMR Biomed*, vol. 24, no. 7, pp. 784–790, 2011.
  - [218] M. Kompauer, S. Heiles, and B. Spengler, "Atmospheric pressure MALDI mass spectrometry imaging of tissues and cells at 1.4- $\mu$ m lateral resolution," *Nat. Methods*, vol. 14, no. 1, pp. 90–96, 2016.
  - [219] H. Kano and H. Hamaguchi, "Ultrabroadband multiplex coherent anti-Stokes Raman scattering microspectroscopy using a supercontinuum generated from a photonic crystal fiber Ultrabroadband ,, > 2500 cm<sup>-1</sup> ... multiplex coherent anti-Stokes Raman scattering microspectroscopy using a supe," *Appl. Phys. Lett.*, vol. 86, p. 121113, 2005.
  - [220] T. W. Kee and M. T. Cicerone, "Simple approach to one-laser , broadband coherent anti-Stokes Raman scattering microscopy," *Opt. Lett.*, vol. 29, no. 23, pp. 2701–2703, 2004.
  - [221] M. Müller and J. M. Schins, "Imaging the Thermodynamic State of Lipid Membranes with Multiplex CARS Microscopy," *J. Phys. Chem. B*, vol. 106, pp. 3715–3723, 2002.
  - [222] J. Cheng, A. Volkmer, L. D. Book, and X. S. Xie, "Multiplex Coherent Anti-Stokes Raman Scattering Microspectroscopy and Study of Lipid Vesicles," *J. Phys. Chem. B*, vol. 106, no. 34, pp. 8493–8498, 2002.
  - [223] A. C. Sekhar Talari, Z. Movasaghi, S. Rehman, and I. Ur Rehman, "Raman Spectroscopy of Biological Tissues," *Appl. Spectrosc. Rev.*, vol. 50, pp. 46–111, 2015.
  - [224] K. Czamara, K. Majzner, M. Z. Pacia, K. Kochan, A. Kaczor, and M. Baranska, "Raman spectroscopy of lipids: A review," *J. Raman Spectrosc.*, vol. 46, no. 1, pp. 4–20, 2015.
  - [225] Y. J. Lee, Y. Liu, and M. T. Cicerone, "Characterization of three-color CARS in a two-pulse broadband CARS spectrum," *Opt. Lett.*, vol. 32, no. 22, pp. 3370–3372, 2007.
  - [226] Y. J. Lee, S. H. Parekh, Y. H. Kim, and M. T. Cicerone, "Optimized continuum from a photonic crystal fiber for broadband time-resolved coherent anti-Stokes Raman scattering," *Opt. Express*, vol. 18, no. 5, pp. 4371–4379, 2010.
  - [227] H. A. Rinia, M. Bonn, and M. Mu, "Quantitative Multiplex CARS Spectroscopy in Congested Spectral Regions," *J. Phys. Chem. B*, vol. 110, no. 9, pp. 4472–4479, 2006.
  - [228] D. Y. Smith, "Dispersion relations for complex reflectivities," *J. Opt. Soc. Am.*, vol. 67, no. 4, pp. 570–571, 1977.
  - [229] Y. Liu, Y. J. Lee, and M. T. Cicerone, "Broadband CARS spectral phase retrieval using a time-domain Kramers-Kronig transform.," *Opt. Lett.*, vol. 34, no. 9, pp. 1363–1365, 2009.
  - [230] J. Zhao, H. Lui, D. I. Mclean, and H. Zeng, "Automated autofluorescence background subtraction algorithm for biomedical raman spectroscopy," *Appl. Spectrosc.*, vol. 61, no. 11, pp. 1225–1232, 2007.
  - [231] N. Billecke, M. Bosma, W. Rock, F. Fleissner, G. Best, P. Schrauwen, S. Kersten, M. Bonn, M. K. C. Hesselink, and S. H. Parekh, "Perilipin 5 mediated lipid droplet remodelling revealed by coherent Raman imaging," *Integr. Biol.*, vol. 7, no. 4, pp. 467–476, 2015.
  - [232] H. A. Rinia, K. N. J. Burger, M. Bonn, and M. Müller, "Quantitative label-free imaging of lipid composition and packing of individual cellular lipid droplets using multiplex CARS microscopy.," *Biophys. J.*, vol. 95, no. 10, pp. 4908–4914, 2008.
  - [233] C. Di Napoli, I. Pope, F. Masia, P. Watson, W. Langbein, and P. Borri, "Hyperspectral and differential CARS microscopy for quantitative chemical imaging in human adipocytes," *Biomed. Opt. Express*, vol. 5, no. 5, pp. 1378–1390, 2014.
  - [234] C. Di Napoli, I. Pope, F. Masia, W. Langbein, P. Watson, and P. Borri, "Quantitative Spatiotemporal Chemical Profiling of Individual Lipid Droplets by Hyperspectral CARS Microscopy in Living Human Adipose-Derived Stem Cells," *Anal. Chem.*, vol. 88, no. 7, pp. 3677–3685, 2016.
  - [235] H. Wu, J. V Volponi, A. E. Oliver, A. N. Parikh, B. A. Simmons, and S. Singh, "In vivo lipidomics using single-cell Raman spectroscopy.," *Proc. Natl. Acad. Sci. U. S. A.*, vol. 108, no. 9, pp. 3809–14, 2011.
  - [236] I. W. Schie, L. Nolte, T. L. Pedersen, Z. Smith, J. Wu, I. Yahiatène, J. W. Newman, and T. Huser, "Direct comparison of fatty acid ratios in single cellular lipid droplets as determined by comparative Raman spectroscopy and gas chromatography.," *Analyst*, vol. 138, no. 21, pp. 6662–6670, 2013.
  - [237] C. Yew Tan, S. Virtue, S. Murfitt, L. D. Robert, Y. H. Phua, M. Dale, J. L. Griffin, F. Tinahones, P. E. Scherer, and A. Vidal-Puig, "Adipose tissue fatty acid chain length and mono-unsaturation increases with obesity and insulin resistance.," *Sci. Rep.*, vol. 5, no. November, p. 18366, 2015.
  - [238] N. Djaker, D. Gachet, N. Sandeau, P.-F. Lenne, and H. Rigneault, "Refractive effects in coherent anti-Stokes Raman scattering microscopy.," *Appl. Opt.*, vol. 45, no. 27, pp. 7005–7011, 2006.

- [239] E. Fuchs, T. Tumber, and G. Guasch, "Socializing with the neighbors: stem cells and their niche.," *Cell*, vol. 116, no. 6, pp. 769–778, Mar. 2004.
- [240] A. W. Lund, B. Yener, J. P. Stegemann, and G. E. Plopper, "The natural and engineered 3D microenvironment as a regulatory cue during stem cell fate determination.," *Tissue Eng. Part B. Rev.*, vol. 15, no. 3, pp. 371–380, 2009.
- [241] E. Dawson, G. Mapili, K. Erickson, S. Taqvi, and K. Roy, "Biomaterials for stem cell differentiation," *Adv. Drug Deliv. Rev.*, vol. 60, no. 2, pp. 215–228, 2008.
- [242] J. M. Curran, R. Chen, and J. A. Hunt, "The guidance of human mesenchymal stem cell differentiation in vitro by controlled modifications to the cell substrate," *Biomaterials*, vol. 27, no. 27, pp. 4783–4793, 2006.
- [243] J. E. Phillips, T. A. Petrie, F. P. Creighton, and A. J. Garcia, "Human mesenchymal stem cell differentiation on self-assembled monolayers presenting different surface chemistries," *Acta Biomater.*, vol. 6, no. 1, pp. 12–20, 2010.
- [244] D. S. W. Benoit, M. P. Schwartz, A. R. Durney, and K. S. Anseth, "Small functional groups for controlled differentiation of hydrogel-encapsulated human mesenchymal stem cells.," *Nat. Mater.*, vol. 7, no. 10, pp. 816–23, Oct. 2008.
- [245] A. J. Engler, S. Sen, H. L. Sweeney, and D. E. Discher, "Matrix elasticity directs stem cell lineage specification.," *Cell*, vol. 126, no. 4, pp. 677–689, Aug. 2006.
- [246] B. D. Boyan, T. W. Hummert, D. D. Dean, and Z. Schwartz, "Role of material surfaces in regulating bone and cartilage cell response," *Biomaterials*, vol. 17, no. 2, pp. 137–146, 1996.
- [247] D. D. Deligianni, N. D. Katsala, P. G. Koutsoukos, and Y. F. Missirlis, "Effect of surface roughness of hydroxyapatite on human bone marrow cell adhesion, proliferation, differentiation and detachment strength," *Biomaterials*, vol. 22, no. 1, pp. 87–96, 2000.
- [248] M. J. Dalby, N. Gadegaard, R. Tare, A. Andar, M. O. Riehle, P. Herzyk, C. D. W. Wilkinson, and R. O. Oreffo, "The control of human mesenchymal cell differentiation using nanoscale symmetry and disorder.," *Nat. Mater.*, vol. 6, pp. 997–1003, 2007.
- [249] K. A. Kilian, B. Bugarija, B. T. Lahn, and M. Mrksich, "Geometric cues for directing the differentiation of mesenchymal stem cells.," *Proc. Natl. Acad. Sci. U. S. A.*, vol. 107, no. 11, pp. 4872–4877, 2010.
- [250] E. Martínez, E. Engel, J. A. Planell, and J. Samitier, "Effects of artificial micro- and nano-structured surfaces on cell behaviour," *Ann. Anat.*, vol. 191, no. 1, pp. 126–135, 2009.
- [251] C. J. Bettinger, R. Langer, and J. T. Borenstein, "Engineering substrate topography at the Micro- and nanoscale to control cell function," *Angew. Chemie - Int. Ed.*, vol. 48, no. 30, pp. 5406–5415, 2009.
- [252] C. Brännmark, A. Paul, D. Ribeiro, B. Magnusson, G. Brolén, A. Enejder, and A. Forslöv, "Increased adipogenesis of human adipose-derived stem cells on polycaprolactone fiber matrices," *PLoS One*, vol. 9, no. 11, p. e0113620, 2014.
- [253] L. E. Flynn, "The use of decellularized adipose tissue to provide an inductive microenvironment for the adipogenic differentiation of human adipose-derived stem cells," *Biomaterials*, vol. 31, no. 17, pp. 4715–4724, 2010.
- [254] E. Bellas, K. G. Marra, and D. L. Kaplan, "Sustainable three-dimensional tissue model of human adipose tissue.," *Tissue Eng. Part C. Methods*, vol. 19, no. 10, pp. 745–754, 2013.
- [255] D. H. Stacey, S. E. Hanson, G. Lahvis, K. a Gutowski, and K. S. Masters, "In vitro adipogenic differentiation of preadipocytes varies with differentiation stimulus, culture dimensionality, and scaffold composition.," *Tissue Eng. Part A*, vol. 15, no. 11, pp. 3389–3399, 2009.
- [256] J.-S. Lee, J. M. Hong, J. W. Jung, J.-H. Shim, J.-H. Oh, and D.-W. Cho, "3D printing of composite tissue with complex shape applied to ear regeneration.," *Biofabrication*, vol. 6, no. 2, p. 24103, 2014.
- [257] M. Spencer, R. Unal, B. Zhu, N. Rasouli, R. E. McGehee, C. A. Peterson, and P. A. Kern, "Adipose Tissue Extracellular Matrix and Vascular Abnormalities in Obesity and Insulin Resistance," *J. Clin. Endocrinol. Metab.*, vol. 96, no. 12, pp. E1990–E1998, 2011.
- [258] K. S. Straley and S. C. Heilshorn, "Dynamic, 3d-pattern formation within enzyme-responsive hydrogels," *Adv. Mater.*, vol. 21, no. 41, pp. 4148–4152, 2009.
- [259] K. S. Straley and S. C. Heilshorn, "Independent tuning of multiple biomaterial properties using protein engineering," *Soft Matter*, vol. 5, no. 1, p. 114, 2009.
- [260] E. Ruoslahti, "RGD and Other Recognition Sequences for Integrins," *Annu Rev Cell Dev Biol*, vol. 12, pp. 697–715, 1996.
- [261] K. J. Lampe, A. L. Antaris, and S. C. Heilshorn, "Design of three-dimensional engineered protein hydrogels for tailored control of neurite growth.," *Acta Biomater.*, vol. 9, no. 3, pp. 5590–5599, Mar.

- 2013.
- [262] M. K. Hale, L. A. Setton, and A. Chilkoti, "Synthesis and in Vitro Evaluation of Enzymatically Cross-Linked Elastin-Like Polypeptide Gels for Cartilaginous Tissue Repair," *Tissue Eng.*, vol. 11, no. 11, pp. 1768–1779, 2005.
  - [263] N. Annabi, S. M. Mithieux, E. A. Boughton, A. J. Ruys, A. S. Weiss, and F. Dehghani, "Synthesis of highly porous crosslinked elastin hydrogels and their interaction with fibroblasts in vitro," *Biomaterials*, vol. 30, no. 27, pp. 4550–4557, 2009.
  - [264] H. Betre, S. R. Ong, F. Guilak, A. Chilkoti, B. Fermor, and L. A. Setton, "Chondrocytic differentiation of human adipose-derived adult stem cells in elastin-like polypeptide," *Biomaterials*, vol. 27, no. 1, pp. 91–99, 2006.
  - [265] C. Chung, K. J. Lampe, and S. C. Heilshorn, "Tetrakis(hydroxymethyl) phosphonium chloride as a covalent cross-linking agent for cell encapsulation within protein-based hydrogels," *Biomacromolecules*, vol. 13, no. 12, pp. 3912–3916, Dec. 2012.
  - [266] M. D. Huntington, C. J. Engel, A. J. Hryn, and T. W. Odom, "Polymer nanowrinkles with continuously tunable wavelengths," *ACS Appl. Mater. Interfaces*, vol. 5, no. 13, pp. 6438–6442, 2013.
  - [267] Z. Wang, A. A. Volinsky, and N. D. Gallant, "Crosslinking effect on polydimethylsiloxane elastic modulus measured by custom-built compression instrument," *J. Appl. Polym. Sci.*, vol. 41050, 2014.
  - [268] A. G. Clark and D. M. Vignjevic, "Modes of cancer cell invasion and the role of the microenvironment," *Curr. Opin. Cell Biol.*, vol. 36, pp. 13–22, 2015.
  - [269] A. L. Bauer, T. L. Jackson, and Y. Jiang, "Topography of extracellular matrix mediates vascular morphogenesis and migration speeds in angiogenesis," *PLoS Comput. Biol.*, vol. 5, no. 7, p. e1000445, 2009.
  - [270] M. P. Lutolf, P. M. Gilbert, and H. M. Blau, "Designing materials to direct stem-cell fate.," *Nature*, vol. 462, no. 7272, pp. 433–441, 2009.
  - [271] A. S. Mao, J. Shin, and D. J. Mooney, "Effects of substrate stiffness and cell-cell contact on mesenchymal stem cell differentiation," *Biomaterials*, vol. 98, pp. 184–191, 2016.
  - [272] J. Tang, R. Peng, and J. Ding, "The regulation of stem cell differentiation by cell-cell contact on micropatterned material surfaces," *Biomaterials*, vol. 31, no. 9, pp. 2470–2476, 2010.
  - [273] A. Chen, E. Lee, R. Tu, K. Santiago, A. Grosberg, C. Fowlkes, and M. Khine, "Integrated platform for functional monitoring of biomimetic heart sheets derived from human pluripotent stem cells," *Biomaterials*, vol. 35, no. 2, pp. 675–683, 2014.
  - [274] J. S. Choi, Y. Piao, and T. S. Seo, "Generation of hierarchical nano- and microwrinkle structure for smooth muscle cell alignment," *Biotechnol. Bioprocess Eng.*, vol. 19, no. 2, pp. 269–275, 2014.
  - [275] D. E. Discher, D. J. Mooney, and P. W. Zandstra, "Growth factors, matrices, and forces combine and control stem cells.," *Science (80-. )*, vol. 324, no. 5935, pp. 1673–1677, 2009.
  - [276] M. P. Lutolf, P. M. Gilbert, and H. M. Blau, "Designing materials to direct stem-cell fate.," *Nature*, vol. 462, no. 7272, pp. 433–41, 2009.
  - [277] C. J. Wilson, R. E. Clegg, D. I. Leavesley, and M. J. Pearcy, "Mediation of Biomaterial – Cell Interactions by Adsorbed Proteins : A Review," *Tissue Eng.*, vol. 11, no. 1/2, pp. 1–18, 2005.
  - [278] J.-S. Lee, J. M. Hong, J. W. Jung, J.-H. Shim, J.-H. Oh, and D.-W. Cho, "3D printing of composite tissue with complex shape applied to ear regeneration," *Biofabrication*, vol. 6, p. 24103, 2014.
  - [279] X. Kang, Y. Xie, H. M. Powell, L. James Lee, M. A. Belury, J. J. Lannutti, and D. A. Kniss, "Adipogenesis of murine embryonic stem cells in a three-dimensional culture system using electrospun polymer scaffolds.," *Biomaterials*, vol. 28, no. 3, pp. 450–8, 2007.
  - [280] C. Jou, "The Biology and Genetics of Obesity - A Century of Inquiries," *N. Engl. J. Med.*, vol. 370, no. 20, pp. 1874–1877, 2014.
  - [281] P. Cohen, "Protein kinases - the major drug targets of the twenty-first century?," *Nat. Rev. Drug Discov.*, vol. 1, pp. 309–315, 2002.
  - [282] R. B. Ceddia, "The role of AMP-activated protein kinase in regulating white adipose tissue metabolism," *Mol. Cell. Endocrinol.*, vol. 366, no. 2, pp. 194–203, 2013.
  - [283] A. Engin, "Human Protein Kinases and Obesity," in *Obesity and Lipotoxicity - Advances in Experimental Medicine and Biology*, vol. 960, A. B. Engin and A. Engin, Eds. 2017, pp. 111–134.
  - [284] B. J. Thompson and E. Sahai, "MST kinases in development and disease," *J. Cell Biol.*, vol. 210, no. 6, pp. 871–882, 2015.
  - [285] A. Nerstedt, E. Cansby, C. X. Andersson, M. Laakso, A. Staněáková, M. Blüher, U. Smith, and M.

- Mahlapuu, "Serine/threonine protein kinase 25 (STK25): A novel negative regulator of lipid and glucose metabolism in rodent and human skeletal muscle," *Diabetologia*, vol. 55, no. 6, pp. 1797–1807, 2012.
- [286] E. Cansby, M. Amrutkar, L. M. Holm, A. Nerstedt, A. Reyahi, E. Stenfeldt, J. Borén, P. Carlsson, U. Smith, J. R. Zierath, and M. Mahlapuu, "Increased expression of STK25 leads to impaired glucose utilization and insulin sensitivity in mice challenged with a high-fat diet," *FASEB J.*, vol. 27, no. 9, pp. 3660–3671, 2013.
- [287] M. Amrutkar, E. Cansby, E. Nuñez-Durán, C. Pirazzi, M. Ståhlman, E. Stenfeldt, U. Smith, J. Borén, and M. Mahlapuu, "Protein kinase STK25 regulates hepatic lipid partitioning and progression of liver steatosis and NASH," *FASEB J.*, vol. 29, no. 4, pp. 1564–1576, 2015.
- [288] M. Amrutkar, E. Cansby, U. Chursa, E. Nuñez-Durán, B. Chanclón, M. Ståhlman, V. Fridén, L. Mannerås-Holm, A. Wickman, U. Smith, F. Bäckhed, J. Borén, B. W. Howell, and M. Mahlapuu, "Genetic disruption of protein kinase STK25 ameliorates metabolic defects in a diet-induced type 2 diabetes model," *Diabetes*, vol. 64, no. 8, pp. 2791–2804, 2015.
- [289] M. Amrutkar, U. Chursa, M. Kern, E. Nuñez-Durán, M. Ståhlman, S. Sutt, J. Boren, B. R. Johansson, H. U. Marschall, M. Bluher, and M. Mahlapuu, "STK25 is a critical determinant in nonalcoholic steatohepatitis," *FASEB J.*, vol. 30, no. 10, pp. 3628–3643, 2016.
- [290] M. Amrutkar, M. Kern, E. Nuñez-Durán, M. Ståhlman, E. Cansby, U. Chursa, E. Stenfeldt, J. Borén, M. Bluher, and M. Mahlapuu, "Protein kinase STK25 controls lipid partitioning in hepatocytes and correlates with liver fat content in humans," *Diabetologia*, vol. 59, no. 2, pp. 341–353, 2016.
- [291] U. Chursa, E. Nuñez-Durán, E. Cansby, M. Amrutkar, S. Sutt, M. Ståhlman, B. M. Olsson, J. Borén, M. E. Johansson, F. Bäckhed, B. R. Johansson, C. Sihlbom, and M. Mahlapuu, "Overexpression of protein kinase STK25 in mice exacerbates ectopic lipid accumulation, mitochondrial dysfunction and insulin resistance in skeletal muscle," *Diabetologia*, vol. 60, no. 3, pp. 553–567, 2017.
- [292] E. Nuñez-Durán, B. Chanclón, S. Sutt, J. Real, H. U. Marschall, I. W. Asterholm, E. Cansby, and M. Mahlapuu, "Protein kinase STK25 aggravates the severity of non-alcoholic fatty pancreas disease in mice," *J. Endocrinol.*, vol. 234, no. 1, pp. 15–27, 2017.
- [293] E. Nuñez-Durán, M. Aghajan, M. Amrutkar, S. Sutt, E. Cansby, S. L. Booten, A. Watt, M. Ståhlman, N. Stefan, H.-U. Häring, H. Staiger, J. Borén, H.-U. Marschall, and M. Mahlapuu, "Serine/threonine protein kinase 25 antisense oligonucleotide treatment reverses glucose intolerance, insulin resistance, and nonalcoholic fatty liver disease in mice," *Hepatol. Commun.*, vol. 2, no. 1, pp. 69–83, 2018.
- [294] T. Matsuki, J. Chen, and B. W. Howell, "Acute inactivation of the serine-threonine kinase Stk25 disrupts neuronal migration," *Neural Dev.*, vol. 8, no. 1, p. 21, 2013.
- [295] S. Heinonen, J. Buzkova, M. Muniandy, R. Kaksonen, M. Ollikainen, K. Ismail, A. Hakkarainen, J. Lundbom, N. Lundbom, K. Vuolteenaho, E. Moilanen, J. Kaprio, A. Rissanen, A. Suomalainen, and K. H. Pietiläinen, "Impaired mitochondrial biogenesis in adipose tissue in acquired obesity," *Diabetes*, vol. 64, no. 9, pp. 3135–3145, 2015.
- [296] K. L. Stanhope, "Sugar consumption, metabolic disease and obesity: The state of the controversy," *Crit. Rev. Clin. Lab. Sci.*, vol. 53, no. 1, pp. 52–67, 2016.
- [297] G. A. Bray and B. M. Popkin, "Dietary sugar and body weight: Have we reached a crisis in the epidemic of obesity and diabetes? - We have but the pox on sugar is overwrought and overworked," *Diabetes Care*, vol. 37, no. 4, pp. 950–956, 2014.
- [298] Y. Wang, Y. Ali, C.-Y. Lim, W. Hong, Z. P. Pang, and W. Han, "Insulin-stimulated leptin secretion requires calcium and PI3K/Akt activation," *Biochem. J.*, vol. 458, no. 3, pp. 491–498, 2014.
- [299] C. A. Celis-Morales, D. M. Lyall, S. Gray, L. Steell, J. Anderson, S. Iliodromiti, P. Welsh, Y. Guo, F. Petermann, D. F. Mackay, M. E. S. Bailey, J. Pell, J. M. R. Gill, and N. Sattar, "Dietary fat and total energy intake modifies the effect of genetic profile risk score on obesity: Evidence from 48 170 UK Biobank participants," *Int. J. Obes.*, vol. 41, no. 12, pp. 1761–1768, 2017.
- [300] F. Imamura, R. Micha, J. H. Y. Wu, M. C. de Oliveira Otto, F. O. Otite, A. I. Abioye, and D. Mozaffarian, "Effects of Saturated Fat, Polyunsaturated Fat, Monounsaturated Fat, and Carbohydrate on Glucose-Insulin Homeostasis: A Systematic Review and Meta-analysis of Randomised Controlled Feeding Trials," *PLoS Med.*, vol. 13, no. 7, pp. 1–18, 2016.
- [301] J. Kim, Y. Li, and B. A. Watkins, "Fat to treat fat: Emerging relationship between dietary PUFA, endocannabinoids, and obesity," *Prostaglandins Other Lipid Mediat.*, vol. 104–105, pp. 32–41, 2013.
- [302] A. P. Simopoulos, "An increase in the Omega-6/Omega-3 fatty acid ratio increases the risk for obesity," *Nutrients*, vol. 8, no. 3, pp. 1–17, 2016.
- [303] C. Wang and J. K. Liao, "A Mouse Model of Diet-Induced Obesity and Insulin Resistance," *Methods*



- Mol Biol*, vol. 821, pp. 421–433, 2012.
- [304] J. Field and T. Clandinin, “Relationship of diet to the fatty acid composition of human adipose tissue structural and stored lipids,” *Am. J. Clin. Nutr.*, vol. 42, pp. 1206–1220, 1985.
  - [305] D. R. Body, “The Lipid Composition of Adipose Tissue,” *Prog. Lipid Res.*, vol. 27, pp. 39–60, 1988.
  - [306] I. W. Asterholm and P. E. Scherer, “Enhanced metabolic flexibility associated with elevated adiponectin levels,” *Am. J. Pathol.*, vol. 176, no. 3, pp. 1364–1376, 2010.
  - [307] M. Clerte, D. M. Baron, P. Brouckaert, L. Ernande, M. J. Raher, A. W. Flynn, M. H. Picard, K. D. Bloch, E. S. Buys, and M. Scherrer-Crosbie, “Brown adipose tissue blood flow and mass in obesity: A contrast ultrasound study in mice,” *J. Am. Soc. Echocardiogr.*, vol. 26, no. 12, pp. 1465–1473, 2013.
  - [308] C. Carneheim, B. Cannon, and J. Nedergaard, “Rare fatty acids in brown fat are substrates for thermogenesis during arousal from hibernation,” *Am. J. Physiol. - Regul. Integr. Comperative Physiol.*, vol. 256, no. 1, pp. R146-154, 1989.
  - [309] I. Shimizu, T. Aprahamian, R. Kikuchi, A. Shimizu, K. N. Papanicolaou, S. MacLauchlan, S. Maruyama, and K. Walsh, “Vascular rarefaction mediates whitening of brown fat in obesity,” *J. Clin. Invest.*, vol. 124, no. 5, pp. 2099–2112, 2014.
  - [310] M. H. Oosterveer, T. H. van Dijk, U. J. F. Tietge, T. Boer, R. Havinga, F. Stellaard, A. K. Groen, F. Kuipers, and D. J. Reijngoud, “High fat feeding induces hepatic fatty acid elongation in mice,” *PLoS One*, vol. 4, no. 6, 2009.
  - [311] L. K. M. Summers, S. C. Barnes, B. A. Fielding, C. Beysen, V. Ilic, S. M. Humphreys, and K. N. Frayn, “Uptake of individual fatty acids into adipose tissue in relation to their presence in the diet,” *Am. J. Clin. Nutr.*, vol. 71, no. 6, pp. 1470–1477, 2000.
  - [312] H. Roger, “Lipotoxic disease,” *Annu. Rev. Med.*, vol. 53, pp. 319–336, 2002.
  - [313] A. Lombardini, V. Mytskaniuk, S. Sivankutty, E. R. Andresen, X. Chen, J. Wenger, M. Fabert, N. Joly, F. Louradour, A. Kudlinski, and H. Rigneault, “High-resolution multimodal flexible coherent Raman endoscope,” *arXiv:1708.04149 [physics.med-ph]*, 2017.
  - [314] A. M. Unser, B. Mooney, D. T. Corr, Y. H. Tseng, and Y. Xie, “3D brown adipogenesis to create ‘Brown-Fat-in-Microstrands,’” *Biomaterials*, vol. 75, pp. 123–134, 2016.
  - [315] L. E. Flynn, G. D. Prestwich, J. L. Semple, and K. a. Woodhouse, “Proliferation and differentiation of adipose-derived stem cells on naturally derived scaffolds,” *Biomaterials*, vol. 29, pp. 1862–1871, 2008.